

Fibrous scaffolds of polymer/graphene oxide for antimicrobial biomedical applications

Sofia Ferreira Melo

Integrated Masters in Bioengineering - Molecular Biotechnology

Supervisor: Dr Inês C. Gonçalves (i3S)
Co-supervisors: Dr Fernão Magalhães (LEPABE), Dr Sara Neves (i3S)

Porto, September 2018

The work described in this thesis was conducted at:

I3S/INEB - Instituto de Investigação e Inovação em Saúde; Universidade do Porto



LEPABE/FEUP - Laboratório de Engenharia de Processos, Ambiente, Biotecnologia e Energia; Universidade do Porto



The work described in this thesis was financially supported by:

Project POCI-01-0145-FEDER-007274 (Institute for Research and Innovation in Health Sciences); Project POCI-01-0145-FEDER-006939 (Laboratory for Process Engineering, Environment, Biotechnology and Energy - LEPABE) and NORTE-01-0145-FEDER-000012 - Structured Program on Bioengineered Therapies for Infectious Diseases and Tissue Regeneration, funded by FEDER funds through COMPETE2020 - Programa Operacional Competitividade e Internacionalização (POCI), Programa Operacional Regional do Norte (NORTE2020), and by national funds through FCT (Fundação para a Ciência e Tecnologia); and Project PTDC/CTM-Bio/4033/2014 (NewCat - New biomaterials to prevent infection associated with dialysis catheters), funded by FEDER funds through COMPETE2020 - Programa Operacional Competitividade e Internacionalização (POCI) - and by national funds through FCT - Fundação para a Ciência e Tecnologia.



“Somewhere, something incredible is waiting to be known.”

Carl Sagan

Acknowledgements

I would like to express my gratitude to my supervisor, Inês Gonçalves, who welcomed me in her team and allowed me to conduct this study. Thank you for your enormous availability, help, valuable suggestions and for being so understanding during these six months. I have a profound admiration for you.

To my co-supervisors, Fernão Magalhães and Sara Neves, for clarifying my doubts. Thank you Fernão, for your inputs and constructive vision. Thank you, Sara, for sharing your knowledge about this 3D printing world. You taught me every detail and trick I needed to know.

To Cristina Martins and Bioengineered Surfaces group, for whom I have a deep feeling of appreciation. To my closest companions, Andreia, Inês and Patrícia, for teaching me so many things, being so generous and patient. You made me feel I was home and I learnt a lot with each one of you.

To Natacha, from FEUP, for her help with spray coatings and SEM. To Rúben, from Biomaterials for Multistage Drug & Cell Delivery group, for his persistence. To María, Ricardo and Dalila, from i3s, for their help and guidance.

To all my friends, the ones I grew up with and the ones I made at the University. Julianas, for making these last years so joyful and for lightening all the stress we shared. Miguel, for making me laugh 24/7. To my oldest and best friends, Catarina, Cristiana, Luísa, Luís, Mariana, Maria, Tozé, for your kindness and true friendship. To Miradouro's staff, for working harder this summer and making double shifts, so I could work on this thesis.

To my family, which is huge but still very close, but specially to my parents, who are my cornerstone since I can remember. Thank you for all the encouragement, support and love that we share. To my sister, Verinha, for motivating and inspiring me beyond imagination.

Abstract

Implantable medical devices-associated infections and consequent failure is a worldwide public health issue. Device-associated infections can result from bacterial adhesion and subsequent biofilm formation at the implantation site, often causing loss of the implanted devices and even sepsis.

Graphene-based materials (GBMs), namely graphene oxide (GO), have been described as potential antibacterial compounds when immobilized and exposed in a composite polymeric matrix, but also when incorporated in a stable coating. These findings led to an increasing interest in the development of GBMs-containing surfaces, when searching for antimicrobial properties and fighting infection.

The main goal of this thesis was the development of novel antibacterial and biocompatible fibrous materials. For that, GO was incorporated in polymeric scaffolds, creating two different 3D structures: i) 3D organized scaffolds with GO/polymer composite fibers; and ii) randomly organized polymeric fibrous meshes with GO-coated fibers. These biomaterials were designed to prevent bacteria-related infection while allowing human cells culture.

Poly(ϵ -caprolactone) - PCL - or poly(ethylene terephthalate) - PET - scaffolds were produced, with and without incorporated GO, using wet-spinning combined with additive manufacturing (AM) to produce polymer/GO composite scaffolds, and spray coating to produce GO-coated polymeric meshes. The first approach enabled the successful fabrication of PCL/GO composite fibrous scaffolds, although not allowing PET/GO composite fibers production. Spray coating over commercially available PET meshes was therefore used to develop PET/GO fibrous scaffolds.

Scaffolds with different GO loadings were evaluated regarding their physical-chemical characterization (namely GO sheets exposure), antibacterial properties and ability to support human cells adhesion. Scanning electron microscopy confirmed GO exposure at the fibers surface both in the 3D-printed PCL/GO composite fibrous scaffolds and in GO-coated PET meshes.

Antimicrobial properties were evaluated through live/dead assays performed with *Staphylococcus epidermidis*, a bacterial species that is commonly found in infected devices and represents an important fraction of implant failure-causing and biofilm-producing microorganisms.

The 2-hour and 24-hour adhesion assays to PCL/GO composite scaffolds revealed a time-dependent bactericidal effect when GO was present, with death rates of adherent bacteria reaching 90% with a GO concentration of 5% w/w, after 24 hours.

For GO-coated PET fibers, 24-hour adhesion assays performed showed a combination of antifouling and bactericidal behavior. Total number of adherent bacteria decreased when GO was present, and percentages of death were between 40% and 60%, depending on the solvent used to prepare the coating solutions.

In vitro biocompatibility of the produced scaffolds towards fibroblasts (HFF-1) was shown by filamentous actin spreading of adherent cells.

Regarding PCL/GO scaffolds, the presence of both 5% w/w GO and 7.5% w/w GO concentrations did not seem to induce any decrease in the fiber area occupied by cells, after 7 days. The obtained results were in fact similar when compared to the PCL scaffolds without GO, given that in all cases cell adhesion and spreading along the fibers was observed during 7 days of culture.

As for PET scaffolds, uncoated and GO-coated samples showed same levels of cell adhesion and spreading after 7 days, suggesting coating's cytocompatibility.

Overall, this work demonstrates the potential of the developed GO-containing fibrous scaffolds to be used as biomaterials that hinder bacteria-caused infection, while stimulating human cells adhesion.

Table of contents

Acknowledgements	vii
Abstract.....	ix
Table of contents	xi
List of figures	xv
List of tables	xviii
Abbreviations and Symbols	xix
Chapter I: Aim and Structure	1
1. Motivation.....	1
2. Aim	3
2.1. Specific objectives.....	3
2.1.1. GBM selection and production	3
2.1.2. Polymer/GO composite scaffolds production.....	3
2.1.3. GO-coated PET scaffolds production	4
2.1.4. Antimicrobial performance of the fibrous scaffolds.....	4
2.1.5. Biocompatibility of the fibrous scaffolds	5
3. Structure of the Dissertation	6
Chapter II: Literature Review	7
1. Device-associated infection as a worldwide public health issue	7
1.1. Infection associated with polymeric fibrous medical devices	8
1.2. <i>Staphylococcus epidermidis</i>	9
2. Polymeric fiber-based biomaterials	10
2.1. PCL: a biodegradable polymer	10
2.1.1. PCL properties	10
2.1.2. PCL applications as fiber-based biomaterials	12
2.2. PET: a non-degradable polymer	13
2.2.1. PET properties	13
2.2.2. PET applications as fiber-based biomaterials	14
3. Modification of polymers: incorporation of GBMs	15
3.1. Graphene and GBMs	15
3.2. Fibrous polymeric composites production techniques.....	18
3.2.1. Solvent mixing	18
3.2.1.1. Electrospinning.....	19
3.2.1.2. Dry-spinning and wet-spinning	20
3.2.2. Melt blending.....	22
3.2.2.1. Melt-electrospinning.....	23
3.2.2.2. Melt-spinning	23
3.3. Fibrous polymeric scaffolds coating techniques.....	25
4. Antimicrobial and biocompatible properties of GBMs	27

4.1. GBMs as antimicrobial materials.....	27
4.1.1. Antimicrobial mechanisms of immobilized GBMs	28
4.1.1.1. Antimicrobial effect of GO in composites	29
4.1.1.2. Antimicrobial effect of GO in coatings	31
4.2. GBMs as biocompatible materials	33
Chapter III: Materials and Methods	35
1. Materials production.....	35
1.1. Graphene Oxide	35
1.1.1. Graphene Oxide production.....	35
1.1.2. Graphene Oxide dispersions stability	37
1.2. GO-containing fibrous scaffolds	38
1.2.1. PCL/GO fibrous scaffolds	38
1.2.1.1. Wet-spinning combined with additive manufacturing	38
1.2.2. PET/GO fibrous scaffolds.....	40
1.2.2.1. Wet-spinning combined with additive manufacturing	40
1.2.2.2. Spray coating	41
2. Materials characterization	43
2.1. GO characterization	43
2.1.1. X-ray photoelectron spectroscopy (XPS)	43
2.2. PCL/GO composite scaffolds characterization	43
2.2.1. Optical microscopy.....	43
2.2.2. Scanning electron microscopy (SEM).....	43
2.3. GO-coated PET scaffolds characterization	44
2.3.1. Optical microscopy.....	44
2.3.2. Coating stability test.....	44
2.3.3. Scanning electron microscopy (SEM).....	44
3. Antibacterial effect assessment	45
3.1. Bacteria strain and growth conditions	45
3.2. Bacterial adhesion assays.....	45
3.2.1. PCL/GO composite scaffolds: drop assay	46
3.2.2. GO-coated PET scaffolds: immersion assay.....	46
3.3. Visualization of adherent bacteria	47
3.3.1. Live/Dead staining	47
3.3.2. Confocal microscopy	47
3.3.3. Adherent bacteria quantification: ImageJ/Fiji.....	49
4. <i>In vitro</i> biocompatibility assessment.....	50
4.1. HFF-1 cell line and culture conditions	50
4.2. Adhesion and proliferation assay	50
4.3. Visualization of adherent cells.....	51
4.3.1. Nuclei/F-actin staining	51
4.3.2. Confocal microscopy and LAS X software	52
5. Statistical analysis	53
Chapter IV: Results and Discussion	55
1. Graphene Oxide	55
2. PCL/GO fibrous scaffolds	57
2.1. Wet-spinning combined with additive manufacturing	57
2.2. Antibacterial effect of PCL/GO scaffolds	65
2.3. <i>In vitro</i> biocompatibility of PCL/GO scaffolds.....	71
3. PET/GO fibrous scaffolds	73

3.1. Wet-spinning combined with additive manufacturing	73
3.1.1. Parameters optimization	73
3.2. Spray coating	77
3.3. Antibacterial effect of GO-coated PET scaffolds.....	80
3.4. <i>In vitro</i> biocompatibility of GO-coated PET scaffolds	83
Chapter V: Conclusion and Future Considerations	85
1. Conclusion.....	85
2. Future Considerations	87
2.1. Exploring different GBMs	88
2.2. Testing on different bacteria	88
2.3. Melt-Electro-Writing to produce PET/GO fibrous scaffolds.....	88
References	89
Annexes.....	99

List of figures

Figure 1. PCL synthesis by ring-opening polymerization of ϵ -caprolactone, using a catalyst (such as stannous octoate).	10
Figure 2. PET synthesis: polycondensation of dimethyl terephthalate with ethylene glycol.	13
Figure 3. Scanning electron micrographs of the surface structure of several PET fiber-based commercial products (30x). Adapted from Metzger A, <i>Biomed Eng.</i> ⁴⁰	14
Figure 4. Graphene properties and applications.	15
Figure 5. GBMs and their production methods: top-down strategies. Adapted from Henriques, A.P. <i>et al</i> , <i>Carbon</i> (2018). ¹⁵	16
Figure 6. Electrospinning basic set-up: spinneret, Taylor cone (zoomed on the right), spun liquid jet, power supplier and collector (target). Adapted from Ghorani <i>et al</i> . <i>Food Hydrocoll.</i> (2015). ¹²³	19
Figure 7. Polymer solution (a)/GBMs dispersion (b) (solvent mixed) are extruded by wet-spinning combined with AM. Fibers deposition in the coagulation bath is software-controlled (xyz).	20
Figure 8. Melt compounding - procedure and equipment.	22
Figure 9. FDM printing technique: a 3D object is fabricated by extruding a stream of heated or melted thermoplastic.	24
Figure 10. Antibacterial mechanisms of action of GBMs-containing surfaces, depending on basal planes/sharp edges exposure.	29
Figure 11. Modified Hummer's Method for GO production using commercial graphite.	36
Figure 12. Wet-spinning+AM technique schematics. Asterisks represent optimizable parameters for a successful 3D printing. Adapted from Sara C Neves <i>et al.</i> , <i>Biofabrication</i> (2016). ¹³³	39
Figure 13. Solution printability comparison between PET/GO mixtures (left) and PCL/GO mixtures (right).	41
Figure 14. Spray coating set-up with a (A) magnetic stirrer, an (B) airbrush, (C) target polymeric mesh fixed to the hotte wall and (D) compressed air flux control valve.	42
Figure 15. Bacterial adhesion assay schematics for PCL/GO composite scaffolds. ...	46
Figure 16. Bacterial adhesion assay schematics for GO-coated PET scaffolds.	46

Figure 17. Confocal microscopy user interface (LAS AF software) screenshots. A: z-stack volume and step size, sequential scanning preferences and laser power can be adjusted, among several other parameters. B: Image acquisition, switching channels between frames.	48
Figure 18. Cell adhesion assay schematics, showing a 1-hour seeding step and subsequent culturing conditions.	51
Figure 19. Image processing software (LAS X) screenshot. z-projections, orthogonal views decompositions and channel's color level tunings can be performed.....	52
Figure 20. XPS analysis of GO. A: Differences in atomic percentages (at %) of Carbon 1s and Oxygen 1s between GO and commercial graphite. *XPS results for graphite were published by Pinto A <i>et. al.</i> (2013) ¹⁹⁴ ; B: Carbon 1s high-resolution spectrum of GO; C: Contents of chemical groups resulting of C 1s spectra fitting.	55
Figure 21. GO dispersions in: Chloroform, THF, Acetone and TFA/DCM (1:2).	56
Figure 22. Screening for PCL solvents (acetone and THF) and non-solvents (ethanol and isopropanol). Left: stereomicroscope imaging; Right: SEM analysis (scale bar: 100 μm).	57
Figure 23. SEM images of the fiber surface of PCL and PCL/GO scaffolds, with different amounts of PCL and GO. Scale bar: 8 μm	58
Figure 24. Flow rate and plotting speed adjustments for PCL/GO scaffolds prepared with 10% w/w GO (on the left) and 7.5% w/w GO (on the right). Images displayed were obtained by Stereomicroscopy (scale bar: 1mm).	60
Figure 25. x, y and z distances adjustment for PCL/GO scaffolds prepared with 5% (w/w) GO . Images displayed were obtained by Stereomicroscopy (scale bar: 1mm).	61
Figure 26. 3D model of the produced scaffolds, showing a top view, a cross-section view and x, y and z-axis distances.	62
Figure 27. Stereomicroscope images of final optimized 3D printed PCL scaffolds with and without GO (scale bar: 1cm).	62
Figure 28. SEM analysis of the top views and cross-section views of final PCL scaffolds, with and without GO. Each row represents a different GO concentration. Scale bar, from left to right: 400 μm , 50 μm , 10 μm).	64
Figure 29. <i>S. epidermidis</i> adhesion to PCL/GO scaffolds after 2h incubation in plasma-free TSB (A) and 10% plasma supplemented TSB (C). Live and dead bacteria are stained in green and red, respectively. Scale bar: 100 μm . B, D: Grouped graphs with number of live bacteria per μm^2 of fiber displayed in green and number of dead bacteria per μm^2 of fiber displayed in red. Statistically significant differences are indicated with */# ($p \leq 0.05$), **/## ($p \leq 0.01$), ***/### ($p \leq 0.001$) and ****/#### ($p \leq 0.0001$).	66
Figure 30. <i>S. epidermidis</i> adhesion to PCL/GO scaffolds after 24h incubation in plasma-free TSB (A) and 10% plasma supplemented TSB (C). Live and dead	

bacteria are stained in green and red, respectively. Scale bar: 100µm. B, D: Grouped graphs with number of live bacteria per µm ² of fiber displayed in green and number of dead bacteria per µm ² of fiber displayed in red. Statistically significant differences are indicated with */# (p ≤ 0.05), **/## (p≤0.01), ***/### (p≤0.001) and ****/#### (p≤0.0001).....	68
Figure 31. HFF-1 adhesion and growth in PCL scaffolds after 1 day and 7 days. DNA was stained with DAPI (3µg/mL) and F-actin was stained with Phalloidin (1:100). Images represent a 150µm volume z-stack projection. Scale bar: 50µm.....	71
Figure 32. Printing trial of the 3% w/v PET and 10% w/w GO solution using TFA/water (1:3) as coagulation bath, a 410µm dispensing tip and a flow rate of 0.5mL/h.	76
Figure 33. SEM images of commercially available electrospun PET meshes. Top: PET203; Bottom: PET305. Scale bar: 100 µm (on the left) and 50 µm (on the right).....	77
Figure 34. Stereomicroscope images of commercially available electrospun PET meshes before (left) and after spray coating with 0.5mg/mL of GO dispersed in acetone and THF. Row A: PET203; row B: PET305. Scale bar: 1cm.	78
Figure 35. SEM images of PET without GO and GO-coated PET fibers before and after washing. Top panel A: PET203; bottom panel B: PET305. Scale bar: 10µm.....	79
Figure 36. <i>S. epidermidis</i> adhesion to PET and GO-coated PET scaffolds (PET203 - A; PET305 - C) after 24h incubation in 10% plasma supplemented TSB. Live and dead bacteria are stained in green and red, respectively. Scale bar: 100µm. B, D: Grouped graphs with number of live bacteria per µm ² of fiber displayed in green and number of dead bacteria per µm ² of fiber displayed in red.	81
Figure 37. HFF-1 adhesion and growth in PET203 fibers after 1 day and 7 days. DNA was stained with DAPI (3µg/mL) and F-actin was stained with Phalloidin (1:100). Images represent a 150µm volume z-stack projection. Scale bar: 50µm.....	83
Figure 38. Detailed top and cross section views of different produced materials. GO exposure is visible in all cases (top view, last column - scale bar: 8µm). Effects in porosity are observed for all concentrations (cross section, last column - scale bar: 8µm).	100
Figure 39. SEM images of PET203 control and GO in water-coated (0.5mg/mL-2mg/mL) fibers before and after washing. Scale bar: 10µm.	100
Figure 40. SEM images of PET305 control and GO in water-coated fibers before washing. Scale bar: 10µm.....	100

List of tables

Table 1. PCL-containing scaffolds: biomedical applications and production methods.	12
Table 2. Randomly orientated GBMs-containing coatings production methods: features, advantages and disadvantages. Adapted from Henriques A P <i>et al.</i> , <i>Carbon</i> (2018). ¹⁵	26
Table 3. Antibacterial effect of non-functionalized GO-containing polymeric composites.	30
Table 4. Antibacterial effect of non-functionalized GO-coated polymers.	32
Table 5. Solvent screening for PET. Solubility was scored between (-), which represents total lack of solubility, and (++) , which represents fast solubility. The solvents with best performances are displayed in green.	73
Table 6. Injectability assessment for PET/GO dispersions with increasing amounts of PET. First column, without PET: a solution of 5 mg/mL GO was used. Last 5 columns: [GO]=10% w/w. Green boxes represent continuous flow; yellow boxes mean occasional clogging events; red boxes report total clogging.	74
Table 7. Coagulation bath screening for PET. Light grey boxes (-): described behavior was not observed; grey boxes (+/-): described behavior was occasionally observed; dark grey (+) boxes: described behavior was frequently observed.	75
Table 8. XPS analysis: effects on the oxidation degree of graphene oxide caused by TFA and TFA+DCM (1:2), unusually found as chosen solvents for GO dispersion.	99

Abbreviations and Symbols

AM	Additive manufacturing
CAD	Computer aided design
CFUs	Colony forming units
CO ₂	Carbon dioxide
CS	Chitosan
DCM	Dichloromethane
dH ₂ O	Distilled water
DMEM	Dulbecco's modified Eagle medium
DMF	Dimethylformamide
EDS	Energy-dispersive X-ray spectroscopy
EO	Ethylene oxide
FBS	Fetal bovine serum
FDA	Food and Drug Administration
FDM	Fused deposition modeling
FFF	Fused filament fabrication
FLG	Few-layer graphene
FTIR	Fourier-transform infrared spectroscopy
G	Graphene
GBM	Graphene-based material
GNP	Graphene nanoplatelet
GNP-ox	Oxidized graphene nanoplatelet
GO	Graphene oxide
Gt	Graphite
GtO	Graphite oxide
HD	Hemodialysis
HFF-1	Human foreskin fibroblasts
ID	Internal diameter
MEW	Melt-electrospinning-writing
MHM	Modified Hummer's method
MRSA	Methicillin-resistant <i>S. aureus</i>
MRSE	Methicillin-resistant <i>S. epidermidis</i>
OD	Optical density

OD ₆₀₀	Optical density at 600 nm
PBS	Phosphate-buffered saline
PCL	Poly(ϵ -caprolactone)
PCU	Polycarbonate urethane
PD	Peritoneal dialysis
Pen/Strep	Penicillin-Streptomycin
PET	Poly(ethylene terephthalate)
pHEMA	Poly(2-hydroxyethyl-methacrylate)
PI	Propidium iodide
PLA	Poly(lactic acid)
PS	Polystyrene
PU	Polyurethane
PVDF	Polyvinylidene fluoride
PVP	Polyvinylpyrrolidone
RAD	Robotic assisted deposition
rGO	Reduced graphene oxide
ROS	Reactive Oxygen species
Rpm	Revolutions <i>per</i> minute
RT	Room temperature
SEM	Scanning electron microscopy
SF	Silk fibroin
SLA	Stereolithography
TFA	Trifluoroacetic acid
THF	Tetrahydrofuran
TPU	Thermoplastic polyurethane
TSA	Trypticase soy agar
TSB	Trypticase soy broth
XPS	X-ray photoelectron spectroscopy
d	Diameter
λ	Wavelength

Chapter I: Aim and Structure

1. Motivation

One of the main challenges associated with polymeric fibrous scaffolds as implantable devices is to find strategies to face bacterial adhesion and consequent infection. This has been subject of extensive research, but the desirable successful prevention or effective solution were not yet achieved. Several alternatives are currently being adopted, but most of them are still far from being able to eliminate infection and antibiotic resistance crisis worldwide.

Fiber meshes used in biomedical applications are commonly intended to have the ability to promote cellular adhesion, which results in tissue integration in substitution/repairing scenarios and in scaffolds' successful colonization when it comes to regeneration. As such, it is important that these properties are not compromised when improving the antimicrobial capacities.

Graphene was first isolated and described in 2004 by Andre Geim and Konstantin Novoselov,¹ and this discovery earned them the Nobel Prize in Physics. Since 2004, graphene derivatives have been developed and investigated, commonly conjugated with polymers to produce composites or used to modify their surface.²⁻⁴

In 2010, the antibacterial properties of graphene-based materials (GBMs) were explored for the first time, instigating a growing number of reports that describe GBMs as antimicrobial nanomaterials. However, most of the work that combines GBMs and polymers is directed towards an improvement of physical characteristics or mechanical/electrical properties.

The interaction between GBMs and biological systems is already being studied,⁵⁻⁸ beginning to give insights on their effects on bacteria, mammalian cells or plants. Nevertheless, these interactions need to be deeper explored regarding GBMs which are immobilized in polymeric matrices or in stable coatings, since their features may vary. Antimicrobial properties, for instance, are known to be different for GBMs in suspension versus GBMs immobilized on a surface.⁹⁻¹¹

Representing low cost raw materials, with proved low cytotoxicity for mammalian cells and described antimicrobial capacity, GBMs may be the ideal material for biomedical applications, namely in medical devices and implants fabrication.

2. Aim

This investigation aimed to infer if GBMs represent a step forward in the antimicrobial biomaterials field, similarly to what has been verified for these materials in so many distinct areas. In order to do so, this work's goals included the production of GO-containing 3D polymeric fibrous scaffolds and the assessment of their antimicrobial and biocompatibility properties. The incorporation of GO intended an improvement in antimicrobial properties, simultaneously ensuring cell adhesion and proliferation. PCL and PET were the selected polymers, given their vast medical applications history, suitability to allow the production of 3D fibrous scaffolds, and availability.

2.1. Specific objectives

2.1.1. GBM selection and production

The selection and subsequent production of GBMs was the first step in this study. In this work, graphene oxide (GO) was chosen among GBMs to be produced and incorporated in polymeric matrices and coatings, since smaller and more oxidized forms of GBMs have been associated with higher biocompatibility.¹² Furthermore, stronger bactericidal properties have been associated to oxidized forms of graphite and graphene nanoplatelets.^{10,13,14}

2.1.2. Polymer/GO composite scaffolds production

It is well described that the orientation and exposure of GO sheets on the fibers' surface is an important parameter, being an essential factor for antibacterial properties.¹⁵ Thereby, the fibrous scaffolds production methods were selected to potentiate the exposure of GO on the polymeric composite fibers' surface.

In one hand, fibers needed to be large enough to incorporate GO sheets (with diameters of 2 - 10 μm), which disregarded nanometric fibers production techniques, such as electrospinning.¹⁶ On the other hand, GO exposure in melt-spun composites (produced from blendings) is hardly seen, once millimeter-range fibers are typically produced¹⁵ and therefore GO sheets are usually mostly covered by the polymer.

In some cases, a diameter of several hundred micrometers is possible to obtain,^{17,18} but this dimension is still far from the desired 50-150 μm fiber diameter, thought to be adequate for the fabrication of 3D scaffolds with incorporated and exposed GO. Bearing in mind this limitation, techniques such as fused deposition modeling were also excluded.

Albeit the diameter of solid-based additive manufacturing (AM) produced fibers was not suitable, a combination of AM with wet-spinning, which allows liquid-based micrometer-range fibers production,¹⁹ appeared as a promising technique. GO exposure was expected to be achieved in wet-spun PCL fibers. Besides, the complementation of wet-spinning with precise fibers spatial deposition (AM) presents the additional advantage of 3D-organized scaffolds fabrication. This process had been previously described for the manufacturing of PCL scaffolds used for bone tissue engineering.¹⁹⁻²¹ Therefore, wet-spinning combined with AM was selected to produce PCL/GO and PET/GO fibrous scaffolds.

2.1.3. GO-coated PET scaffolds production

Besides wet-spinning combined with AM as an approach for PET/GO scaffolds fabrication, GO-coated PET fibers were developed in parallel. Since GO is considered antimicrobial when immobilized both in composite stable matrixes or in coatings, readily acting and killing bacteria, comparing these two different approaches revealed interesting. Moreover, the spray coating technique allowed to modify commercially available medical grade PET meshes, which may facilitate the production scale-up process.

2.1.4. Antimicrobial performance of the fibrous scaffolds

After materials production, an assessment of the antimicrobial properties was performed, exploring the viability of bacteria that adhere to the fibers. This was performed over different timepoints, namely after 2 hours and 24 hours (to search for a possible time-dependent GO effect), and with different culture conditions, namely with or without supplementing the culture medium with plasma (to understand the influence of surface adsorbed proteins).

2.1.5. Biocompatibility of the fibrous scaffolds

Finally, developed fibrous scaffolds were evaluated regarding cell adhesion. Human fibroblasts (HFF-1 cell line) were selected to be cultured in the scaffolds since this cell type is the major constituent of connective tissue. Although cytocompatibility must be evaluated also towards different cell types, fibroblasts represent a particularly important target, given their frequent direct contact with implanted medical devices.

3. Structure of the Dissertation

This document is divided in five main chapters, presenting a References' section in the end, only followed by Annexes. Chapter I, where this structure section is inserted, also reflects the motivation and aim of this work, further highlighting specific objectives.

Chapter II consists of a literature review and introduces this work. Focused on different topics, it can be divided in four main groups: the problem of infection, polymeric fiber-based biomaterials, modification of polymers and GBMs incorporation, and antimicrobial/biocompatible properties associated with GBMs.

Chapter III focus on the methodology developed and used, during materials production, characterization, antibacterial effect assessment and biocompatibility assessment. This chapter includes a last section describing the performed statistical tests.

Results and further discussion are presented in Chapter IV, regarding GO production and dispersion quality, 3D fibrous structures of PCL/GO fabrication process, PET fibers modification, and microbiological and cellular studies.

Chapter V summarizes the main conclusions of this thesis and suggests future considerations, which can be related to the investigation of different GBMs, the exploration of new scaffold fabrication techniques, and further biological studies.

Chapter II: Literature Review

1. Device-associated infection as a worldwide public health issue

Medical devices-associated infections can cause major public health concerns and consequent economic sequelae. In hospital settings, these device-related infections are considered one of the most threatful issues to patients, and resistant bacteria play a key role in the spreading of these healthcare-derived complications.²² Colonization of the indwelling device by bacteria can be a prelude to its consequent malfunction.²³ Bacterial adhesion may result in subsequent biofilm formation at the implantation site, being a serious widespread health problem accentuated by growing antibiotic resistance, and causing loss of the implanted device or even sepsis.²⁴

Infections may derive from previously mentioned bacterial adhesion to biomaterials and may suffer aggravation caused by unsuccessful tissue integration and lack of biocompatibility.²⁵ Microorganisms involved in biomaterial-associated infections (BAI) are usually resistant to antibiotics due to their biofilm mode of growth, and infected implants often have to be removed before the infection can be fully eradicated from surrounding tissue.²⁶ However, implantable biomaterials are still indispensable in the restoration of human body functions after severe damage, frequently beyond natural repair.

1.1. Infection associated with polymeric fibrous medical devices

Among hundreds of distinct types of implantable biomaterials, with diverse applications and specific complications, implantable fibrous meshes are a particularly important fraction.²⁷ Ideally, these fiber-based materials should aid cellular colonization, through cells settlement along the fibrous scaffolds, simultaneously avoiding bacterial proliferation and biofilm formation. Textiles and fibrous structures are being brought to play this essential role in the efficiency of implantable medical devices, trying to fulfil both requirements. Other critical aspect is associated with the permeability of the textile structure that allows to regulate exchanges. Fibrous devices can act as a filter or a barrier that can prevent or promote cells, nutrients, fluids, or even bacteria, to pass through.²⁸

Fibrous scaffolds can be divided in two main groups, depending on their ultimate goal: tissue engineering (TE)-applied scaffolds²⁹⁻³¹ and substitution-oriented fabrics³²⁻³⁴. The first group is compatible with the use of biodegradable polymers, while for the last bioinert polymers are more suitable.

A variety of engineered scaffolds have been created for TE, using polymers to generate a local bioactive environment upon implantation to regenerate the damaged or lost tissue.³⁵ Polymer fibrous scaffolds for nerve,³⁶ bone³⁷ or muscle³⁸ regeneration are examples of developed biomaterials that can face infection scenarios.

Concerning the second approach, where biodegradability is not intended, fabrics can be used, among other applications, as dialysis catheter's cuffs,³⁹ abdominal wall repair meshes³², or sutures⁴⁰.

All these materials present severe susceptibility to infection, which reinforces the urgent need to find alternative, with stronger antimicrobial potential, fibrous materials. The usual causative organisms associated with cases of mesh infection are *Staphylococcus* spp.⁴¹

1.2. *Staphylococcus epidermidis*

Gram-positive bacteria are the microorganisms responsible for most of the medical implant-related infections, with *Staphylococcus epidermidis* on the leading positions. *S. epidermidis* is a biofilm-forming bacterium, which produces extracellular polysaccharides (also known as glycocalyx) when proliferating on a surface.⁴² Belonging to the genus of *Staphylococci*, these bacteria are characterized by grape-like cluster-forming cocci.⁴³ As a member of the coagulase-negative *Staphylococci* group, *S. epidermidis* differentiates from other species, such as *S. aureus*, due to its inability to produce the exoenzyme coagulase (enzyme that converts fibrinogen to fibrin and leads to the coagulation of blood plasma).⁴⁴ Coagulase-negative *Staphylococci* are microorganisms naturally present on human skin and mucous membranes, thus representing part of our endogenous flora.⁴⁵

S. epidermidis action is a common cause for many coagulase-negative infections developed outside a hospital environment. Moreover, the most important group of infections caused by these bacteria are infections on foreign bodies, such as implanted devices, including meshes, ceramics or metallic prosthetics.⁴⁶

S. epidermidis has a naturally high resistance to antimicrobials, which generates great concerns when it comes to biofilm-related infections. Adherence of *S. epidermidis* to device's surface is not a one-time phenomenon, but rather an evolving process. Initially, there is a rapid attachment to the surface, mediated either by nonspecific factors (such as surface tension, hydrophobicity, and electrostatic forces) or by specific adhesins.⁴⁷ This initial phase is followed by an accumulative phase, during which bacteria adhere to each other and form the biofilm.⁴⁸

2. Polymeric fiber-based biomaterials

To create 3D structures in the form of fibrous scaffolds, poly(lactic-co-glycolic) acid (PLGA) and poly(ϵ -caprolactone) (PCL) are currently the most popular among synthetic polymers.³⁵ Allowing the formation of 3D biodegradable porous structures, PCL fibers are broadly studied, namely in the scope of TE approaches.^{49,50}

On the other hand, for non-resorbable fibrous materials that have to keep integrity during the whole implantation duration, chemical stability is required. These properties can be achieved with the use of polymers like poly(ethylene terephthalate) (PET).²⁸

2.1. PCL: a biodegradable polymer

2.1.1. PCL properties

PCL, a well-known aliphatic polyester material first synthesized in the 1930s, is widely used for the fabrication of 3D scaffolds for TE applications.⁵¹ PCL is semi-crystalline,⁵² naturally elastic, and consists of nonpolar methylene groups and one semi-polar ester group.³⁵ Two main pathways to produce polycaprolactone have been described in the literature: the polycondensation of a hydroxycarboxylic acid: 6-hydroxyhexanoic acid, and the ring-opening polymerization (ROP) of a lactone: ϵ -caprolactone (ϵ -CL), displayed in Figure 1. Emphasis is given to the ROP pathway due to its prevalence in the literature and the superior polymer that is obtained.⁵²

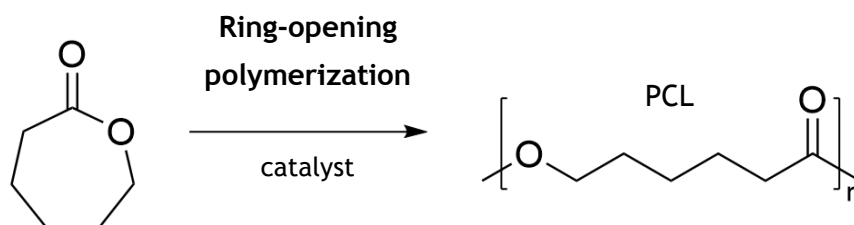


Figure 1. PCL synthesis by ring-opening polymerization of ϵ -caprolactone, using a catalyst (such as stannous octoate).

PCL is highly appealing due to its physical-chemical and mechanical characteristics,⁵³ easy processability due to a relatively low melting temperature (approximately 60 °C),⁵⁴ and non-toxic degradation products. PCL received Food and Drug Administration (FDA) approval and CE Mark registration for a number of drug delivery and medical device applications.⁵³

Besides, this polymer presents additional interesting aspects, namely its availability, relative low cost, suitability for modification,⁵⁵ and a relatively long biodegradation time, which makes PCL widely used in long-term implants.⁵⁶ However, PCL biodegradation rate depends on its molecular weight, degree of crystallinity, and the conditions of degradation. Complete degradation can occur within several months to several years.⁵⁷⁻⁶⁵ PCL undergoes a two-stage degradation process: firstly, the non-enzymatic hydrolytic cleavage of ester groups in physiological conditions;⁴⁹ secondly, when the polymer presents low molecular weight (less than Mn 3000), it is shown to undergo intracellular degradation.⁶⁶

In comparison with other aliphatic polyesters, the superior rheological and viscoelastic properties also render PCL easy to manufacture and manipulate into a wide range of 3D platforms.⁶⁷

2.1.2. PCL applications as fiber-based biomaterials

Being a synthetic thermoplastic polymer with biodegradability and resorption capacity, PCL has attracted considerable attention in recent years, notably in the biomedical areas of controlled-release drug delivery systems, surgical sutures, and 3D scaffolds for TE ^{49,51,68}, as displayed in Table 1.

Table 1. PCL-containing scaffolds: biomedical applications and production methods.

Biomedical application	Production method	References
Bone graft substitutes and customized scaffolds for bone TE	<i>Fused Deposition Modeling, Electrospinning, Additive Manufacturing + Wet-spinning</i>	69 70 19, 71, 29
3D porous scaffolds for Human foreskin fibroblasts (HFF-1) and engineered skin	<i>Fused Deposition Modeling, Electrospinning</i>	72, 71 73, 74
Intervertebral disk (annulus fibrosus) TE	<i>Electrospinning</i>	30
Cartilage TE	<i>Electrospinning</i>	75
Biodegradable sutures, antimicrobial surgical monofilaments	<i>Electrospinning, Melt-spinning.</i>	76 77
TE-intended blood vessels tubular scaffolds	<i>Electrospinning</i>	78, 79
Drug delivery systems (anti-tumoral and antibacterial effects).	<i>Electrospinning</i>	80
Muscle–tendon junction TE	<i>Electrospinning</i>	81
Peripheral nerve regeneration	<i>Electrospinning</i>	31

PCL has been explored for various fiber-based biomedical applications. However, its generally poor cell affinity due to hydrophobicity and lack of cell-binding signals⁸² has become the major obstacle to be an ideal TE material. Further improvements in PCL performance can be accomplished with polymer modifications, through functionalization or new components incorporation in a composite.

2.2. PET: a non-degradable polymer

2.2.1. PET properties

Poly(ethylene terephthalate) (PET) is a highly biocompatible, biostable, and non-degradable polymer.³² From the viewpoint of a well-established implant history as being relatively inert, PET, fluoropolymers (PTFE), polypropylene (PP), polyurethanes (PU) and silicones have played the most important role in the development of polymeric materials.⁸³ PET is a linear, strong but lightweight thermoplastic, belonging to the aromatic polyesters family. The basic building blocks of PET are terephthalic acid/dimethyl terephthalate and ethylene glycol (Figure 2).⁸⁴

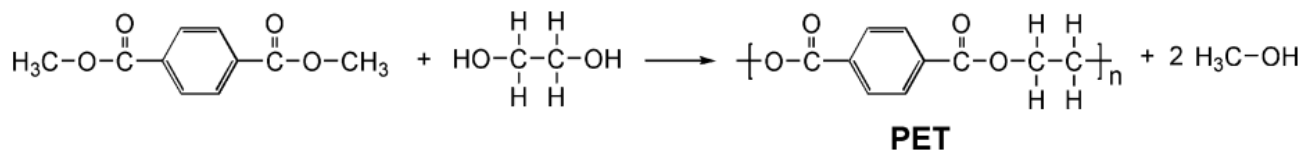


Figure 2. PET synthesis: polycondensation of dimethyl terephthalate with ethylene glycol.

The physical properties of PET are largely determined by the degree of crystallinity. It is a typically strong material, with a tensile strength of 170-180 MPa and a tensile modulus of about 14 GPa in its oriented form.⁸⁵ PET is considered relatively non-reactive to drugs in general.

As such, health-safety agencies around the world (e.g. FDA, Health Canada, EU's European Food Safety Authority) have approved PET as safe, with the extra benefit of being recyclable and highly sustainable.⁸⁶

The notable biological characteristics of PET, which were observed during its long history of human implantation,⁸⁷ are key to fight infection. These features include biostability,⁸⁸ promotion of tissue ingrowth,⁸⁹ and a well characterized fibrotic response.⁹⁰ The biostability of PET is a result of its chemical structure, which promotes resistance to hydrolysis due to hydrophobic aromatic groups.⁴⁰

2.2.2. PET applications as fiber-based biomaterials

PET was first synthesized in the U.S. (1940s) by DuPont chemists,⁹¹ when searching for suitable polymers to fabricate new textile fibers. PET is typically called "polyester" when used in clothing fibers or fabrics, "PET resin" when used for bottles, containers or packaging applications⁸⁶ and "Dacron" in the biomedical context, where its role is largely versatile (Figure 3).⁴⁰

Current medical applications of PET include implantable non-biodegradable sutures,^{92,93} surgical meshes,⁹⁴⁻⁹⁶ vascular grafts,^{97,98} sewing cuffs for heart valves,^{27,99} and components for percutaneous access devices like catheters.¹⁰⁰ These fiber-based materials are produced using electrospinning techniques, originating non-woven meshes or woven fabrics, which can be obtained if braiding or knitting is further performed.

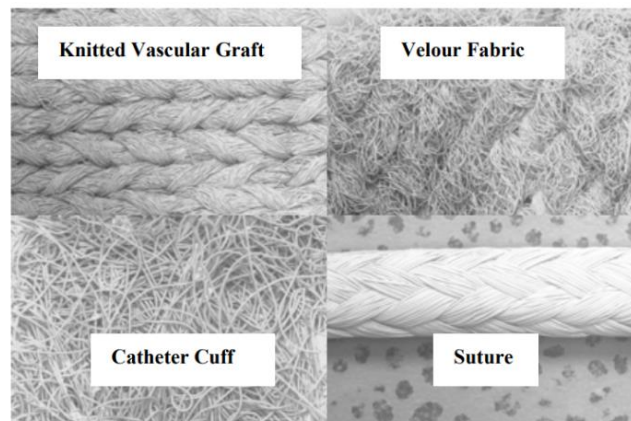


Figure 3. Scanning electron micrographs of the surface structure of several PET fiber-based commercial products (30x). Adapted from Metzger A, *Biomed Eng.*⁴⁰

Counteracting the infection-related problems mentioned before, efficient promotion of tissue ingrowth is often fulfilled with the use of PET, through the creation of a porous matrix that encourages tissue ingrowth, consequently preventing relative motion between the tissue bed and the implant.⁴⁰ This permanent anchoring serves to retain the implanted device and maintain proper function. The biological reaction to PET is characterized by a chronic inflammatory response, fibrous capsule formation, and granulomatous tissue with an intercellular matrix infiltrating the fabric.^{101,102} Fibrous capsule formation is typically complete within 4 weeks.³³ Nevertheless, susceptibility to bacterial infection and biofilm formation is a major problem when PET implants are used.¹⁰³ The adhered bacteria proliferate and develop an irreversible attachment, forming dense microbial communities.¹⁰⁴

3. Modification of polymers: incorporation of GBMs

3.1. Graphene and GBMs

Single-layer graphene (G) is a two-dimensional plane of carbon atoms¹⁰⁵, densely packed in a honeycomb crystal lattice with hybridized sp^2 bonding. It presents unique physical features, namely high area/thickness ratio, mechanical strength and stability, as well as exceptional electric and optical properties¹⁰⁶ (Figure 4).

Recently, graphene has attracted both academic and industrial interest because it can produce a dramatic improvement in other materials' properties at low filler content.⁴ Graphene combines the layered structure of clays with the superior mechanical properties of carbon nanotubes (CNTs), which can provide excellent functional property enhancements.¹⁰⁷ So far, most research work trying to combine polymers and GBMs focuses on the production of composite materials intending to achieve a reinforcement of mechanical, thermal or electrical properties of the base polymeric material.¹⁰⁸

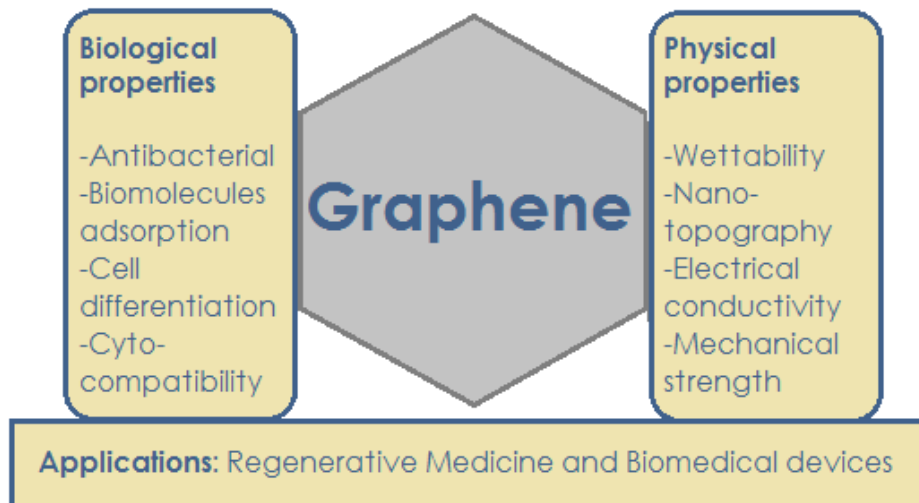


Figure 4. Graphene properties and applications.

There is still lack of consensus regarding GBMs nomenclature. Hence, defining the abbreviations adopted throughout this work reveals necessary: bilayer or trilayer graphene refers to 2 or 3 graphene sheets packed together; few-layer graphene (FLG) refers to 2-5 graphene sheets; multi-layer graphene (MLG) - also called graphene nanoplatelets (GNPs) - refers to stacks of 2-10 graphene sheets packed together. Graphite (Gt) is formed by more than 10 sheets. All these structures can be oxidized and named using the suffix O/ox (e.g. GO, GNP-ox, GtO).

Several GBMs have been developed, differing in terms of morphology, number of layers and lateral dimensions. Different methods have been both explored and modified to obtain high quality GBMs, involving bottom-up approaches (starting from alternative carbon sources), as well as top-down approaches (starting from Gt), displayed in Figure 5.^{15,109,110}

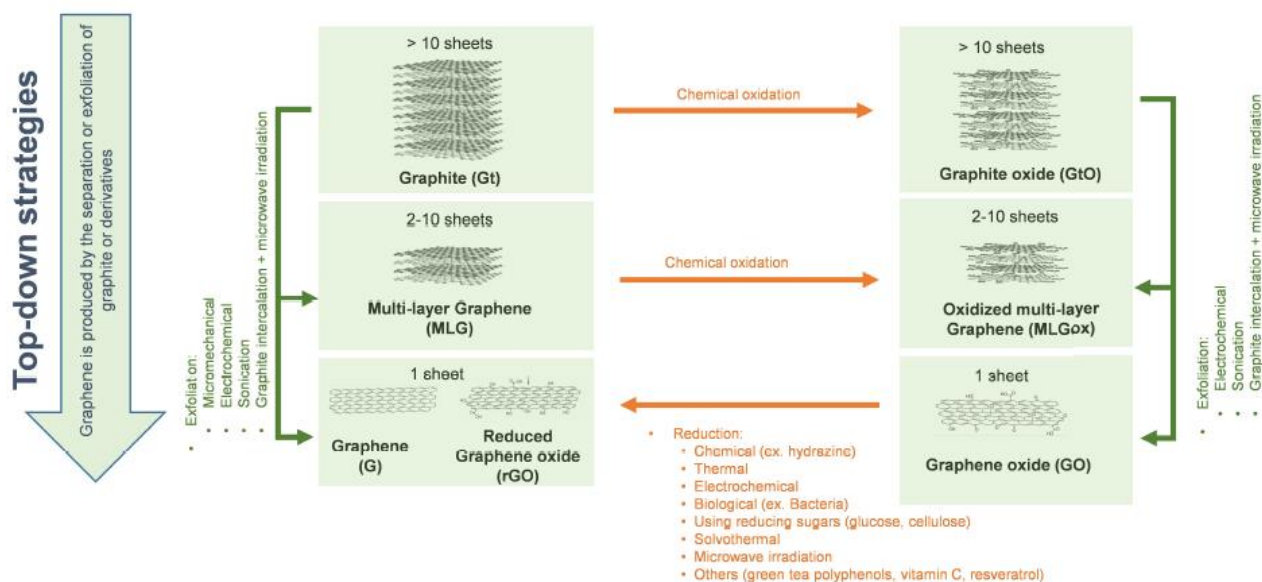


Figure 5. GBMs and their production methods: top-down strategies. Adapted from Henriques, A.P. *et al*, *Carbon* (2018).¹⁵

The chemical oxidation process has been improved with Gt oxidation into GtO having evolved from Brodie's method, to Staudenmaier's¹¹¹, Hofmann's¹¹², Hummers'¹¹³ and, more recently (2010), to Marcano's method¹¹⁴. Hummers' or modified Hummers' methods (MHM) are still the most implemented ones.¹¹⁵

The process of GtO exfoliation into GO may also vary between authors, possibly occurring electrochemically, through sonication or microwave irradiation.¹⁵ GO reduction to rGO has been the step where more improvements have been made. The most common reduction process uses chemical reducing agents, such as anhydrous hydrazine.¹¹⁴

All the described materials can be used *per se* or incorporated as polymer modifiers. Hence, GBMs-containing materials can be divided in three main types: free-standing films (made only of GBMs), coatings (GBMs applied on a substrate), and bulk composites (GBMs dispersed within a polymer matrix).

3.2. Fibrous polymeric composites production techniques

GBMs incorporation into a matrix has been thoroughly explored, specifically as a way to improve mechanical, thermal or electrical properties of a material, even when added in small amounts.^{109,110,116-118}

GBMs composites can be produced via 1) solvent mixing, 2) melt blending, 3) *in situ* polymerization or 4) dispersion into prepolymer solutions.¹⁰⁹ The preparation method depends on the polarity, molecular weight, hydrophobicity and reactive groups present in the polymer.¹¹⁹ For the final composite fiber production step and GBMs exposure at the surface, the most commonly used approaches are the incorporation of GBMs in the bulk polymer either through solvent mixing or melt blending, followed by fiber extrusion.

3.2.1. Solvent mixing

When solvent mixing is performed, GBMs powder is dispersed in a solvent (aqueous/organic) by sonication and the polymer is dissolved in the previous solution. The solid polymer (e.g. pellets) can either be added to the GBMs dispersion or be already in solution using the same solvent. The mixture becomes homogenous after high-speed shear mixing or sonication.¹²⁰ To choose a good solvent, there are three main parameters to take into account, namely: temperature, concentration of the solvent, and total surface area of the polymer. Some disadvantages are associated with solvent mixing, mainly related to the high shear forces induced while sonicating, which may damage GBMs sheets.¹²¹ However, it is a widely-implemented technique to produce GBMs/polymer composites, since good dispersions can easily be obtained without the need for expensive equipment.

The homogeneously mixed polymer/GBMs dispersion obtained can then be casted into a mold, spread as a film, or extruded. Extrusion methods can lead to the production of fibrous scaffolds by spinning into filaments and subsequent fabrication of desirable textile structures. Spinning may be performed through several approaches,⁴⁹ including electrospinning, dry-spinning or wet-spinning. Moreover, these techniques can be combined with a moving collector or a xyz plotter to obtain 3D organized structures.

3.2.1.1. Electrospinning

Electrospinning is a fiber production method which uses electric fields to draw charged threads of polymer solutions up to fiber diameters in the order of hundred nanometers.¹²²

Briefly, according to Figure 6: when a sufficiently high voltage is applied to a liquid droplet and it becomes charged, electrostatic repulsion counteracts surface tension, and the droplet is stretched (slow acceleration zone - Taylor cone).¹²³ At a critical point, a liquid stream erupts from the surface in the spinneret and the evaporation of the solvent while the solution travels towards the collector produces solid polymer fibers¹²⁴ (rapid acceleration zone). In this path, the jet is elongated, until it is finally deposited on the grounded collector, leading to the formation of a non-woven mesh¹²⁵ composed by uniform fibers with nanometer-scale diameter.¹²⁶⁻¹²⁸

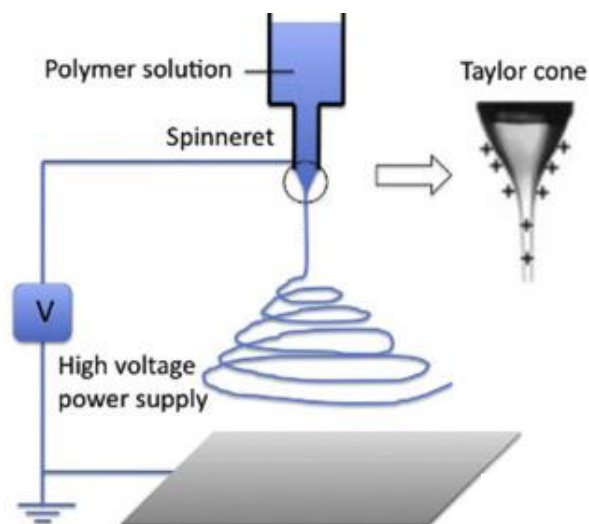


Figure 6. Electrospinning basic set-up: spinneret, Taylor cone (zoomed on the right), spun liquid jet, power supplier and collector (target). Adapted from Ghorani *et al.* *Food Hydrocoll.* (2015).¹²³

In an attempt to better control electrospun fibers deposition, some strategies can be explored, namely collector's patterning or controlled movements. Zhang *et al.* found that structured collectors could greatly affect the resulting structures of the electrospun mats, essentially acting as a patterned template to influence electrospun fiber collection.¹²⁹ Neves *et al.* also patterned solution electrospun meshes with shaped collectors, with specific dimensions and designs, and evaluated the structures of obtained fibers for biomedical applications.¹³⁰

Although structured collectors allow porous electrospun scaffolds, the process in general still relies on a chaotic deposition of fibers, and their accurate placement is limited to the collector used in the experiments.¹²⁵

3.2.1.2. Dry-spinning and wet-spinning

Dry spinning is the fiber formation process that transforms a high vapor pressure polymer solution to a solid fiber by controlled solvent evaporation in the spin line.¹³¹ In this technique, the solution is extruded through a spinneret and a stream of air or inert gas impinges on the emerging jet. Key variables are heat transfer, mass transfer and stress on the filament.¹³¹

Wet-spinning, the oldest among spinning processes, is a non-solvent induced phase separation (NIPS) technique that allows the processing of several natural and synthetic polymers.^{19-21,132-134} Filled with a dissolved polymer, a dispensing tip is submerged in a chemical bath that causes the fibers to precipitate, and then solidify. The process name is due to the use of the "wet" coagulation solution.

Some of the initial wet-spinning studies aimed at the manufacturing of randomly oriented scaffolds, manually deposited in a non-solvent.¹³⁵ In order to precisely control the fiber spatial deposition during fibers formation, recent studies proposed the combination of additive manufacturing (AM) with wet-spinning, in a computer-aided process (Figure 7).^{133,136} As defined by the American Society for Testing and Materials (ASTM), AM refers to "the process of joining materials to make objects from 3D model data, usually layer upon layer".

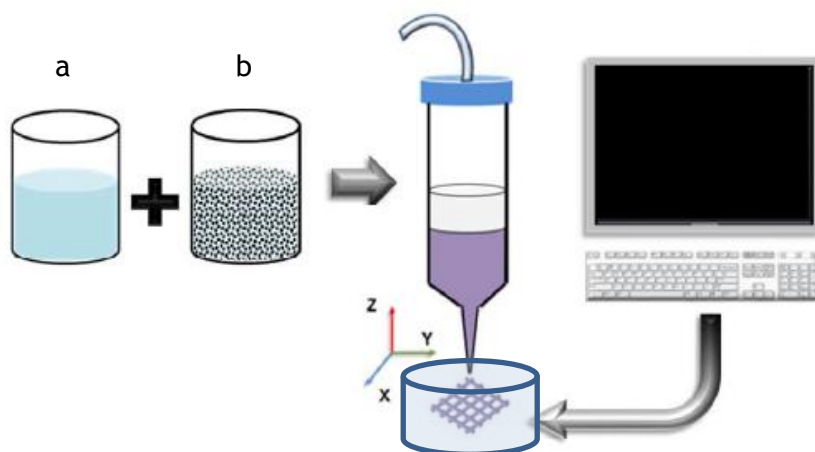


Figure 7. Polymer solution (a)/GBMs dispersion (b) (solvent mixed) are extruded by wet-spinning combined with AM. Fibers deposition in the coagulation bath is software-controlled (xyz).

This process can lead to the production of microvoids that influence the fiber properties, and which arise from the rapidly drawn out solvent. On the other hand, since it is based on a solution processing method, possible material degradation related to thermal treatments is avoided.

Furthermore, advanced computer-aided design and manufacturing enables a high degree of automation, good accuracy and reproducibility for the fabrication of clinically-sized, anatomically-shaped scaffolds with a tailored porous structure characterized by a fully interconnected network of pores with customized size and shape.¹³⁶

3.2.2. Melt blending

Another way to produce fibrous polymeric composites is using melt blending. Considering this alternative approach, GBMs powder can be mixed with the molten polymer at elevated temperatures, preceding composite extrusion. Melt-blending is considered one of the most successful routes for large scale production of polymer composites containing nanofillers.¹⁰⁹ Composite melts are usually produced by mixing GBMs and polymers using a melt compounder (Figure 8) or by adding GBMs to molten polymer while stirring.

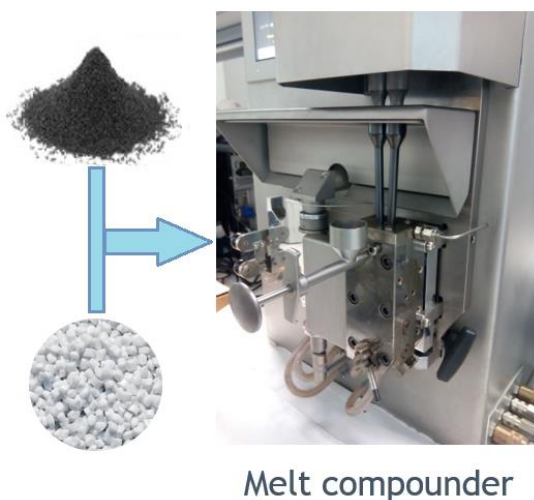


Figure 8. Melt compounding - procedure and equipment.

Melt blending may lead to some degree of GBMs aggregation, with Kim *et al.* reporting that good exfoliation cannot be obtained during the blending procedure.¹²¹

Choosing melt blending to obtain a composite, the final form of the material can be defined by extrusion, injection molding or hot pressing. Extrusion shows competency to allow fibers production in techniques such as melt-spinning, with or without the use of electric fields. On the other hand, injection molding traditionally leads to the formation of molds, such as dog bone-shaped samples, and hot pressing is commonly used to obtain 2D films.

Similarly to what was described above for solution extrusion, melt extrusion techniques can also be coupled with controlled fiber spatial deposition to obtain a 3D-organized structure.

3.2.2.1. Melt-electrospinning

A relatively small number of publications can be found in the literature about the application of melt-electrospinning (MES), compared with classic solution electrospinning.¹³⁷ The use of molten precursors represents an interesting alternative, since electrospinning of polymeric melts eliminates the need for volatile solvents (present in solution-electrospinning), ensuring that no solvent is carried over into the final product.¹³⁷

The setup is similar to that employed in conventional electrospinning and includes the use of a syringe or spinneret, a high voltage supply and a collector.¹³⁸ Due to high viscosity characteristic of polymer melts, the fiber diameters are usually slightly larger than those obtained from solution electrospinning.

Zaiss *et al.* detailed melt-electrospinning of a polymer in a static way onto structured metallic collector substrates to produce open pore morphologies without using AM. Microscale and biocompatible 3D scaffolds with suitable pore sizes and fiber diameters for cell penetration could be obtained.¹³⁹

However, AM can also be coupled with this technique. The electrified molten jet created via melt-electrospinning generally has a somehow predictable path, allowing polymer fibers to be accurately deposited onto the collector. Using a moving computer-controlled collector plate, melt-electrospinning-writing (MEW) is a way to perform AM. 3D constructs are then obtained by repetitive fiber-by-fiber stacking.¹⁴⁰

In this sense, MEW can be seen as an alternative to bridge the gap between solution-electrospinning and additive manufacturing processes.^{140,141} Castilho *et al.* reported the rational design and fabrication of ultra-stretchable microfiber scaffolds with controlled hexagonal microstructures via MEW.¹⁴⁰

3.2.2.2. Melt-spinning

Polymers and GBMs which were previously melted to form a composite are extruded through a spinneret and the melt is drawn from the spinneret hole at a melt temperature. In the draw zone, the extruded filaments are cooled to the solidification temperature.

Melt-spun polymer/GBMs composite melts can be molded into diverse shapes,¹⁴² including a thin filament with few mm.¹⁴³ Such filament can be used to feed a 3D printer, allowing precise fiber's spatial deposition through a technique named fused deposition modeling (FDM).

FDM requires a 3D printer with a heated moving nozzle head, which can melt the thin filament again. Fibers with narrower diameters (hundreds of μm) can be obtained from the dispensing system/tip (Figure 9).

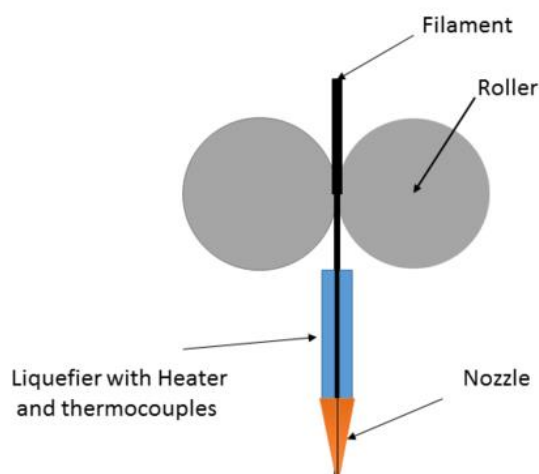


Figure 9. FDM printing technique: a 3D object is fabricated by extruding a stream of heated or melted thermoplastic.

GBMs were already successfully melt compounded in polymeric matrixes using completely solvent-free processes, and then extruded into filaments, suitable for FDM for various applications (namely TE).^{144,145} This procedure implies a thermoresistant equipment, namely using printing syringes and tips that endure high temperatures (250 °C). Drawbacks are associated with the specific equipment required (that may be expensive to acquire) and with the poor dispersion and exposure of the GBMs in the polymer matrix that is usually obtained.¹⁴⁶ Also, high temperatures applied during melting may affect the GBMs thermal stability.¹²¹

Fused Filament Fabrication/Fused Deposition Modeling/Molten Composite Deposition/Molten Polymer Deposition are different designations for the same method.¹⁴⁷ FDM still presents the difficulty of downsizing printed structures to the few-micrometer scale, given that nozzles with increased diameters are used.⁸

3.3. Fibrous polymeric scaffolds coating techniques

Coatings are a layer of material adhered onto the surface of a bulk material (substrate) with the purpose of achieving a surface with intended properties. GBMs-based coatings have been widely explored in different areas, focusing on the protection of metals or biomedical devices from corrosion¹⁴⁸, oxidation^{149,150} or bacterial adhesion and colonization.¹⁵¹

Numerous techniques can be implemented for the production of GBMs-integrating coatings, resulting in GBMs deposition in a well-defined orientation or in a random orientation, in which their GBMs basal planes and sharp edges can be both exposed.

Regarding randomly oriented GBMs coatings, each technique has its proper advantages, requirements and disadvantages, as summarized on Table 2.

Table 2. Randomly orientated GBMs-containing coatings production methods: features, advantages and disadvantages. Adapted from Henriques A P *et al.*, *Carbon* (2018).¹⁵

Technique	Substrate requirement	Advantages	Disadvantages	Refs
<i>Dip coating</i>	Preferably hydrophilic	<ul style="list-style-type: none"> - Low cost - Simple - Deposition at room temperature - Deposition in both sides simultaneously - Large area coverage 	<ul style="list-style-type: none"> - Difficulty in controlling thickness (dependent on several factors, including solution accumulation) - Requires a long drying step - Films with non-uniform thickness (heterogeneous) 	152,153.
<i>Spray coating</i>	---	<ul style="list-style-type: none"> - Low cost - Deposition at room temperature - Large area coverage - Substrates may have different sizes and shapes 	<ul style="list-style-type: none"> - Difficulty in controlling thickness (dependent on several factors) - Requires specific equipment (e.g. airbrush gun) - Difficulty in controlling homogeneity and reproducibility 	154,155,156, 157.
<i>Spin-coating</i>	Flat substrate	<ul style="list-style-type: none"> - Uniformity of the coating - Controllable thickness - Deposition at RT - Very thin films quickly obtained 	<ul style="list-style-type: none"> - Limited substrate dimensions - Coated one side at a time - Requires specific equipment 	110,116,158, 159,160.
<i>Drop casting</i>	Flat substrate	<ul style="list-style-type: none"> - Simple - Low-cost - Deposition at RT - No waste of material 	<ul style="list-style-type: none"> - Difficulty in controlling thickness - Poor uniformity 	115,9,161, 162,163.
<i>Electro phoretic deposition</i>	Must be conductive	<ul style="list-style-type: none"> - Easy scalable - Cost effective - Good uniformity - Dense packing - Controllable thickness - Deposition at RT 	<ul style="list-style-type: none"> - Limited thickness of insulating deposits (e.g. GO) - Possibility of side electrochemical reactions - Requires specific equipment 	164,165,166, 167,168.

4. Antimicrobial and biocompatible properties of GBMs

4.1. GBMs as antimicrobial materials

Antimicrobial materials can either prevent bacterial attachment or destroy bacteria on contact. Antibiofouling is the property possessed by some materials which prevent or limit the settlement of biological material on their surfaces. Agents that limit microbial growth through biocidal action should be referred to as bactericidal.^{169,170} There are also agents that prevent the growth of bacteria, keeping them in the stationary phase of growth, named as bacteriostatic agents.¹⁷¹

A newly emerging range of nanomaterials, GBMs, have been described as having more than one of the abovementioned antimicrobial mechanisms of action, therefore being a strong candidate for antimicrobial applications (Figure 4).¹⁷²

Investigating graphene as an antimicrobial material, Liu *et al.* compared the antibacterial activity of four types of GBMs in suspension, namely graphite (Gt), graphite oxide (GtO), graphene oxide (GO), and reduced graphene oxide (rGO), towards Gram-negative bacteria *Escherichia coli*.¹⁴ All of these GBMs showed some antibacterial activity using a colony counting method. Under similar concentrations (40 µg/mL) and incubation conditions, the antimicrobial potency of these materials followed this order: GO>rGO>Gt>GtO.

4.1.1. Antimicrobial mechanisms of immobilized GBMs

The development of novel biomaterials that can prevent infections and be used to produce medical devices is of great interest and it has been reported that GBMs have the described antibacterial properties and that their incorporation within polymer-based matrices or as applied coatings can improve the pristine polymer antimicrobial activity.¹⁵

Overall, direct contact of bacteria with GBMs at the surface (either with sharp edges or basal planes) is a requirement for GBMs-containing biomaterials to have antibacterial action, with no loss of bacteria viability being found when no contact is established. Nevertheless, antimicrobial mechanisms of action when GBMs are immobilized, rather than being free in solution, are less exploited and lack the comparative assessment studies as the aforementioned one.¹⁷³

Antibacterial properties are believed to be caused by chemical and physical interactions upon the direct contact of GBMs sheets with bacteria, in which the bacterial cell membrane seems to be the main target.¹⁷³ The key influencing factors in the antimicrobial performance of GBMs seem to be their exposure, hydrophobicity, size, oxidation degree and functionalization.¹⁵

Exposure of either GBMs sharp edges or basal planes has a major impact on the surface antibacterial properties. While GO-containing surfaces are antimicrobial when either basal planes or sharp edges are exposed, G-containing surfaces are mainly effective when sharp edges are protruding.¹⁵

As described in Figure 10, when bacteria are exposed only to basal planes, two possible actions have been reported to occur: electron transference between GBMs and bacteria membrane¹⁷⁴ and O₂ adsorption on defect sites and edges of the GBMs¹⁰, followed by electron transference. In both cases, the oxidative stress caused will lead to membrane disruption and bacterial death.

On the other hand, when sharp edges are exposed, both the aforementioned events can occur, as well as physical insertion of the GBMs sharp edges through the bacteria membrane (nano-knife effect),^{164,175} protein-protein bonding disruption and pore formation.¹⁷⁶ These events can have as consequences the induction of oxidative stress¹⁷⁷ and/or the direct disruption of the bacterial membrane.¹⁶⁴

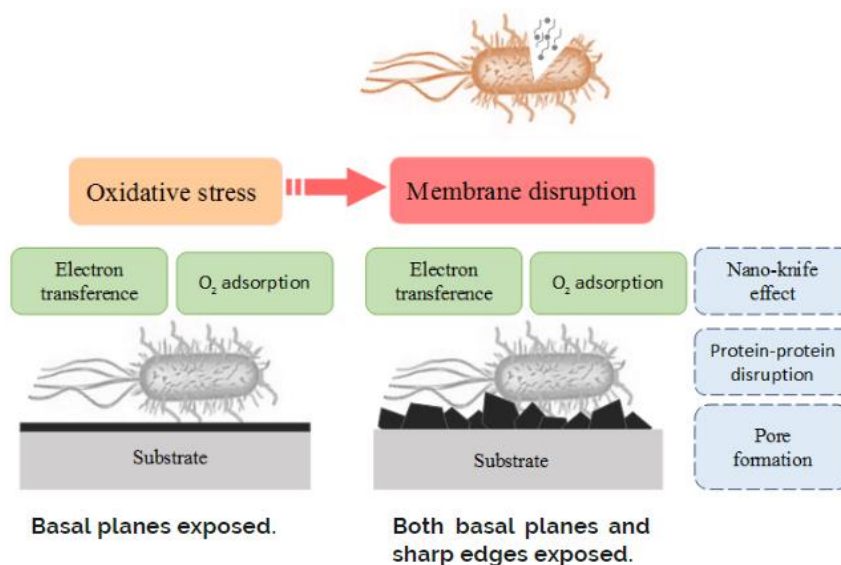


Figure 10. Antibacterial mechanisms of action of GBMs-containing surfaces, depending on basal planes/sharp edges exposure.

4.1.1.1. Antimicrobial effect of GO in composites

GO has been recurrently referred to as the most promising GBM when pursuing an antibacterial effect, although the majority of the studies assessed its effect in dispersions, rather than immobilized.^{7,14,15,178,179} Nevertheless, there are some papers regarding GO antibacterial activity when immobilized, namely in polymeric composite matrices.

Mazaheri and co-workers¹⁸⁰ found significant antibacterial activity on chitosan/GO composites against *S. aureus*, despite the inherent antibacterial effect of chitosan alone. More specifically, they concluded that the antibacterial performance and surface roughness increased with GO content, since chitosan alone presented a smooth surface¹⁸⁰ (Table 3).

A change in the surface morphology was also found for chitosan/polyvinylpyrrolidone/GO composites produced by Mahmoudi *et al.*¹⁸¹. With addition of 1 wt % GO, the surface became rougher, with nanosheets appearing to protrude from the polymer matrix; by increasing the GO concentration (3 wt %), more wrinkles and a more organized structure were found¹⁸¹ (Table 3).

Besides the described studies, there are several other examples of works in the literature which explored the antimicrobial potential of GO incorporated in polymeric matrixes, as displayed in Table 3.

Table 3. Antibacterial effect of non-functionalized GO-containing polymeric composites.

GBMs-containing composites	Bacteria	Antibacterial effect	References
<i>GO/CS/PVP</i>	<i>E. coli</i> <i>S. aureus</i>	After 12h <i>E. coli</i> and <i>S. aureus</i> : CS/PVP/GO (1, 2, 3 wt %)- improved bactericidal capacity, compared to CS/PVP	181
<i>GO/PLA/PU</i>	<i>E. coli</i> <i>S. aureus</i>	After 24h <i>E. coli</i> : PLA/PU-94%, PLA/PU/GO (5 wt%) -100%; <i>S. aureus</i> : PLA/PU-98%, PLA/PU/GO (5 wt%) - 100%	182
<i>GO/CS</i>	<i>S. aureus</i>	After 3h CS-77%, CS/GO (1.5 wt %)-78%, CS/GO (3 wt %)-82%, CS/GO (6 wt %)-87%	180
<i>GO/CS</i>	<i>E. coli</i> <i>Bacillus subtilis</i>	After 14h <i>E. coli</i> and <i>Bacillus subtilis</i> : d(zone of inhibition): CS-GO (2 wt%)> CS-GO (1 wt%)> CS or GO alone	183
<i>GO/PVDF</i>	<i>E. coli</i>	After 2h PVDF/GtO powder- 90.4%, PVDF/GO (0.1 wt%)- 93.3%, PVDF/GO (0.2 wt%)- 99.6%	184
<i>GO/pHEMA</i>	<i>E. coli</i>	After 3h Vertical-GO film - 44%, Random-GO film - 24.7%, Planar-GO film - 18.2%	185
<i>GO/Agar</i>	<i>E. coli</i> <i>S. aureus</i>	After 24h <i>E. coli</i> : Agar/GO - 40% <i>S. aureus</i> : Agar/GO - 53%	186

Abbreviations: CS - chitosan, PVP - polyvinylpyrrolidone, PLA - poly(lactic acid), PU - polyurethane, PVDF - polyvinylidene fluoride, pHEMA - poly(2-hydroxyethyl methacrylate).

As shown by the examples given in Table 3, GO-containing polymeric composites were described by many authors as being more antimicrobial, when compared to bulk polymer or even to GO alone. Several microorganisms appear to be susceptible to GO antimicrobial action, namely *E. coli*, *S. aureus* and *Bacillus subtilis*.

4.1.1.2. Antimicrobial effect of GO in coatings

Surface-modifying approaches have also largely focused on antimicrobial coating of devices and resulted in variable clinical success.²³ For GBMs-coated materials antimicrobial assessments, mainly GO was studied and evaluated.

Considering an existing controversy on the effect of the basal planes, Mangadlao *et al.*¹¹ produced GO films on PET substrates (non-conductive, with reduced antibacterial activity - 13%) and confirmed that neither contact with sharp edges nor conductive substrates are a requirement for the GO-coated surface to be antibacterial (Table 4). In this case, the antimicrobial effect might be arising from the oxygen-containing groups present on the basal planes of GO.¹¹

Krishnamoorthy *et al.*¹⁸⁷ reported a time-dependent antibacterial activity of a GO coating on cotton fabrics (non-conductive), where GO sharp edges were well exposed (Table 4). The antimicrobial effect seemed to arise from the sharp edges of the GO, with authors attributing the effect to the direct contact between the material and the bacteria or to the oxidative stress caused.¹⁸⁷

Several other studies which explored the antimicrobial potential of non-functionalized GO-coated polymers can be found in the literature, although few of them describe fibrous scaffolds coating (Table 4).

Table 4. Antibacterial effect of non-functionalized GO-coated polymers.

GBMs-containing coatings	Bacteria	Antibacterial effect	References
<i>GO-coated PET</i>	<i>E. coli</i>	After 2h: PET- 13%, 1 layer GO- 40%, 2 layers GO- 75%, 3 layers GO- 89%	11
<i>GO-coated cotton fabrics</i>	<i>S. iniae</i> <i>E. coli</i>	After 6h: <i>S. iniae</i> - 68%; <i>E. coli</i> - 46% After 12h: <i>S. iniae</i> - 86%; <i>E. coli</i> - 62% After 24h: <i>S. iniae</i> - 100%; <i>E. coli</i> - 74%	187
<i>GO-coated PS</i>	<i>E. coli</i> <i>S. aureus</i>	After 24h: <i>E. coli</i> - 36% at 60 µg, 90% at 150 µg, 100% at 180/200 µg <i>S. aureus</i> - 65% at 60 µg, 88% at 150 µg, 81% at 200 µg	9
<i>GO-coated PCU</i>	<i>S. aureus</i> <i>P. aeruginosa</i>	<i>S. aureus</i> : 85% <i>P. aeruginosa</i> : 64%	188

Abbreviations: PS - polystyrene, PCU - polycarbonate urethane.

GO-coated polymers were shown to have antimicrobial properties against several microorganisms, such as *E. coli*, *S. aureus*, *S. iniae* and *P. aeruginosa*.

Overall, the effectiveness of the antibacterial action depends on the amount of incorporated GO, as well as on the material production technique.

4.2. GBMs as biocompatible materials

When tissue integration is intended, rather than solely prevent bacteria adhesion and spreading, it is advantageous that biomaterials also promote mammalian cells' adhesion, migration and proliferation to allow the device integration in its biological environment.

The notion of biocompatibility has been restricted for a long time to inertia versus adverse events related to the implantable device or its biological surroundings. However, biocompatibility extends to the device's ability to function well while having an appropriate behavior in its environment. Extending beyond sole consideration of chemical toxicity, the biocompatibility concept includes all body responses to the biomaterial implantation.²⁸

GBMs toxicity towards mammalian cells is only observed when the particles are dispersed in suspension at high concentrations.⁶

Nevertheless, as in antimicrobial properties, the biocompatibility of GBMs may differ, depending on whether they are present in suspension or incorporated in polymeric surfaces.

Exploring the toxicity of GBMs immobilized in polymers, rather than in suspension, Pinto *et al.*¹⁸⁹ incorporated two GBMs - GO and GNPs - in PLA films and found that no variations in cell proliferation at the surface of the composite films were observed. An exception was found for GO-containing films, which presented higher cell proliferation than pristine PLA films, after 24h incubation. Furthermore, incorporation of GNP into PLA reduced platelet activation in the presence of plasma proteins. The results indicated that low concentrations (0.4 wt.%) of GO and GNP might be safely incorporated in PLA.¹⁸⁹

Several other studies are described in the literature using GBMs to ensure biocompatibility and even promote cell adhesion and growth.^{5,6,12,185,190} Focusing on GO-containing fibrous materials, for being the GBM and the polymeric structure used in this thesis, some examples are specified below.

Wang *et al.*¹⁹¹ fabricated electrospun silk fibroin (SF)/GO-blended nanofibers with a bioinspired nanostructure. The morphology, chemical structure, antibacterial activity and biocompatibility of the blending nanofibers were investigated and authors concluded that GO improved biocompatibility of SF nanofibers towards osteoblast precursors (MC3T3 cell line).¹⁹¹

Jalaja *et al.*¹⁹² incorporated GO in electrospun gelatin to form GO-decorated gelatin nanofibers. Cytocompatibility was assessed using mouse fibroblasts (L-929) and the results indicated that the GO-containing gelatin nanofibers support L-929 cell adhesion and proliferation.¹⁹²

Song *et al.*¹⁶ prepared biocomposite nanofiber scaffolds of PCL with different GO concentrations using electrospinning. To estimate the biocompatibility of PCL/GO composite scaffolds, mouse marrow mesenchymal stem cells (mMSCs) and low-differentiated rat pheochromocytoma (PC12-L) cells were cultured. Initial adhesion and spreading of mMSCs and PC12-L cells on PCL/GO scaffolds with moderate addition of GO (0.3 - 0.5 wt%) were significantly superior to those on pure PCL scaffolds.¹⁶

Chen *et al.*⁸ printed thermoplastic-PU (TPU)/PLA/GO nanocomposites (using FDM approach) and explored their potential application as biocompatible materials. The 3D-printed nanocomposites exhibited good cytocompatibility towards fibroblasts (NIH3T3 cells), since TPU/PLA/GO showed higher cell density when compared to TPU/PLA scaffolds.⁸

Thampi *et al.*¹⁸⁸ applied a GO coating onto electrospun polycarbonate urethane (PCU) porous fibers, using electrospraying. Studies using mammalian fibroblasts allowed to evaluate their metabolic activity (MTT assay). After 24 hours, a percentage of 82% metabolically active cells was found for PCU, against 86% for GO-coated PCU. After 72 hours, 87% was registered on PCU and 88% on GO-coated PCU.¹⁸⁸

Overall, the analysis of the literature reveals the great biocompatible potential of GO-containing polymeric fibers.

Long-term toxicity is still a poorly addressed but a crucial topic, since the available data on the biodegradation and metabolism of GBMs is still limited.¹⁹³ Furthermore, the incorporation of GBMs in biodegradable polymers arises additional concerns, since GBMs, although initially immobilized, will eventually end up being in suspension, when the entire polymeric matrix is degraded.

Chapter III: Materials and Methods

1. Materials production

1.1. Graphene Oxide

In this work, GO was chosen among GBMs to be incorporated into polymeric matrices and coatings. Carbon graphite micropowder, the starting material for GO production, was purchased from American Elements, Los Angeles, USA, with purity above 99% and a diameter between 7 and 11 μm .

1.1.1. Graphene Oxide production

GO was prepared according to the Modified Hummer's method¹¹³, adjusting reagents volume/mass for large scale production (2000 mL flask). Briefly, 320 mL of H_2SO_4 (VWR, Germany) were mixed with 80 mL of H_3PO_4 (Chem-Lab, Belgium) in a 4:1 ratio and stirred at RT, as proposed by Marcano¹¹⁴ for an improved oxidation. 8 g of graphite were added to this solution (Figure 11), then cooled down to 0 °C using an ice bath before gradual addition of 48 g of KMnO_4 (JMGS, Portugal), which renders a highly exothermic reaction.

At this point, when the solution gained a dark green/black color, it was heated up to 35 °C and stirred for 2 hours. Then, after lowering again the temperature to 0 °C with an ice bath, 1200 mL of distilled water were slowly added, and a brown solution was obtained. This was followed by careful addition of H₂O₂ 35% (to reduce KMnO₄ excess), until oxygen release stopped (approximately 30 mL were used). The brown solution turned yellow and finally became green, as displayed in the last picture in Figure 11.

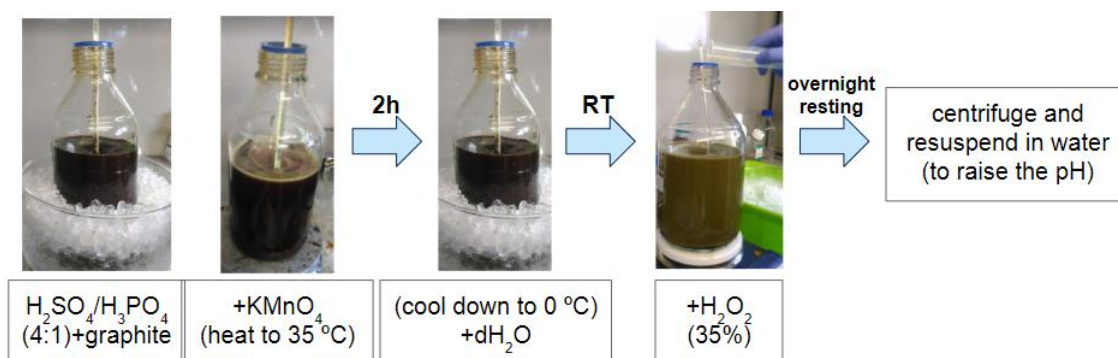


Figure 11. Modified Hummer's Method for GO production using commercial graphite.

After overnight resting, the resultant solution was decanted to separate the solid deposit from the acidic supernatant. The remaining product was washed with water and this aqueous solution centrifuged (Eppendorf 5810R) at 4000 rpm for 20 minutes (this process was repeated approximately ten times, until the washing water pH was equal to dH₂O pH).

By the end of this process, a 6-hour sonication was performed, in order to exfoliate oxidized graphite into single sheets. An ultrasound water bath was used, requiring frequent ice addition to avoid temperature increase. GO was stored at a final concentration of 10.6 mg/mL and briefly sonicated (approximately 20 minutes) whenever used. To determine this concentration, a known volume of GO/water suspension was dried in a vacuum oven at 60 °C overnight. The container was weighed before and after water evaporation and GO mass was calculated.

1.1.2. Graphene Oxide dispersions stability

The dispersion homogeneity and stability of the obtained GO was evaluated in different organic solvents, commonly considered potential solvents for the polymers explored in this thesis. For that, GO aqueous dispersion was centrifuged for 1h at RT and 15000 rpm speed (high performance SORVALL RC-5B centrifuge) and supernatant water was decanted. GO was resuspended in different solvents, namely chloroform (VWR, Germany), tetrahydrofuran (VWR, Germany), acetone (JMGS, Portugal) and trifluoroacetic acid/dichloromethane (1:2) (VWR, Germany/Merck, USA). Dispersions were left inside an ultrasonic water bath for several hours (approximately 3 hours), to dissociate aggregates and achieve homogeneity. To avoid solutions heating, ice was added every 30 minutes.

1.2. GO-containing fibrous scaffolds

1.2.1. PCL/GO fibrous scaffolds

GO-containing PCL solutions were prepared, to be used as an ink and loaded in the syringe during wet-spinning/AM process.

PCL (average M_n 80 000 g mol⁻¹) was purchased from Sigma-Aldrich in the form of dehydrated 3 mm pellets with less than 0.5% of water. PCL density is described as 1.145 g/mL at 25 °C and its melting point is approximately 60 °C.

1.2.1.1. Wet-spinning combined with additive manufacturing

Combining wet-spinning with AM (Figure 12) for scaffold production required several optimization steps. First, an effective PCL solvent that efficiently disperses GO had to be found. After solvent mixing, PCL non-solvents were screened, to select the best coagulation bath (a chemical bath that causes the fibers to precipitate, and then solidify). Printing parameters (namely flow rate and plotting speed) had to be adjusted for all tested PCL/GO concentrations. Lastly, 3D scaffolds design was optimized in terms of xyz inter-fiber distances, staggering and number of layers.

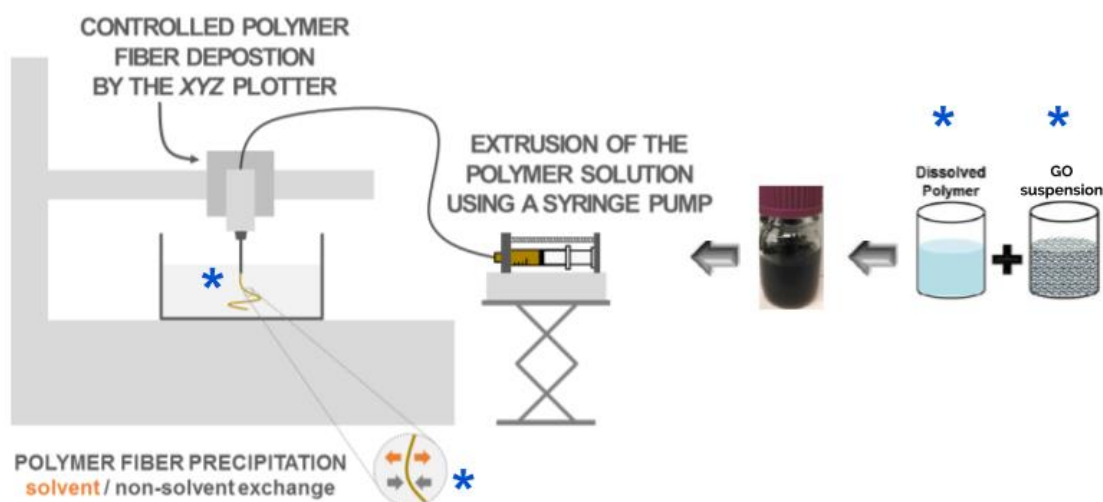


Figure 12. Wet-spinning+AM technique schematics. Asterisks represent optimizable parameters for a successful 3D printing. Adapted from Sara C Neves *et al.*, *Biofabrication* (2016).¹³³

Different reagents were screened as solvents for PCL: n-methyl-2-pyrrolidone (Sigma Aldrich, USA), dimethylformamide (DMF, Fisher Scientific, UK), chloroform (VWR, Germany), tetrahydrofuran (THF, VWR, Germany) and acetone (JMGS, Portugal). Dissolution conditions included a PCL concentration of 15% w/v in 5 mL of the tested solvents, with permanent magnetic stirring (300 rpm) at RT.

After PCL solvent selection, the mixture was loaded into a syringe and extruded into different coagulation baths, namely isopropanol (VWR, Germany) and ethanol (VWR, Germany). Wet-spinning is a solvent/non-solvent-exchange based technique. This exchanging rate is the most relevant influencing factor for the obtained fiber morphology, although other variables can also influence the process (e.g. temperature).

When the coagulation bath was selected, specific printing parameters were adjusted for each GO concentrations. Tested flow rates ranged from 0.5mL/h to 2.0mL/h, plotting speeds from 50% to 200%, xy distances from 200 μm to 400 μm , z-step from 20 μm to 80 μm , staggering between layers from 50 μm to 200 μm ; and the best fit was kept.

When printed, PCL/GO scaffolds were rinsed 3-5 times with ethanol, dried in the hotte and cut, using a 4 mm diameter stainless steel puncher (Integra® Miltex®).

1.2.2. PET/GO fibrous scaffolds

Two different approaches were pursued to obtain PET/GO fibrous scaffolds, namely the production of PET/GO fibers by wet-spinning combined with AM, and the use of commercially available PET fabrics and subsequent coating with GO.

1.2.2.1. Wet-spinning combined with additive manufacturing

GO-containing PET solutions were prepared, to be used as an ink and loaded in the syringe during wet-spinning/AM process, similarly to what was described for PCL. PET (250 g - granular) was purchased from Sigma-Aldrich in the form of dehydrated 1.5 mm (approximately) pellets. PET density is described as 1.680 g/mL at 25 °C and its melting point is approximately 250 °C.

Few working solvents are described in the literature for solid PET, hence solvent screening was exhaustively performed. Different solvents were screened for PET dissolution, namely chloroform (VWR, Germany), dimethylformamide (Fisher Scientific, UK), isopropanol (VWR, Germany), 1,2-dichloroethane (Sigma Aldrich, USA), o-xylene (AGA, Finland), nitrobenzene (Sigma Aldrich, USA), phenol (VWR, Germany), tetrachloroethane (Merck, USA), THF (VWR, Germany), ethyl acetate (VWR, Germany), dichloromethane (DCM; Merck, USA), dimethyl sulfoxide (DMSO; Merck, USA), DCM/1,4-dioxane (Merck, USA), acetone (JMGS, Portugal), n-methyl-2-pyrrolidone (Sigma Aldrich, USA), 1,1,1,3,3,3-hexafluoro-2-propanol (Sigma Aldrich, USA), ethylene glycol (J.T. Baker, USA), NaOH 0.1M (VWR, Germany)/ethylene glycol, trifluoroacetic acid (TFA; VWR, Germany) and TFA/DCM (1:2).

A PET concentration of 10% w/v was initially added to 5mL of each potential solvent and stirred (300 rpm) at RT. Whenever dissolution was not achieved, temperature was increased (25°C-80°C range), keeping all other parameters constant.

After PET solvent selection, injectability tests were performed with different PET concentrations (1% w/v - 5% w/v) and varying needles' diameter (ID range: 100-840 µm). Lastly, coagulation baths were tested, namely water, NaOH 1M (VWR, Germany), acetone, ethanol, ethyl ether (Sigma Aldrich, USA), ethylene glycol, dichloromethane and mixtures of TFA/water in different ratios.

Although the optimization steps were meticulously followed, PET/GO composite mixtures were not possible to continuously extrude (Figure 13).

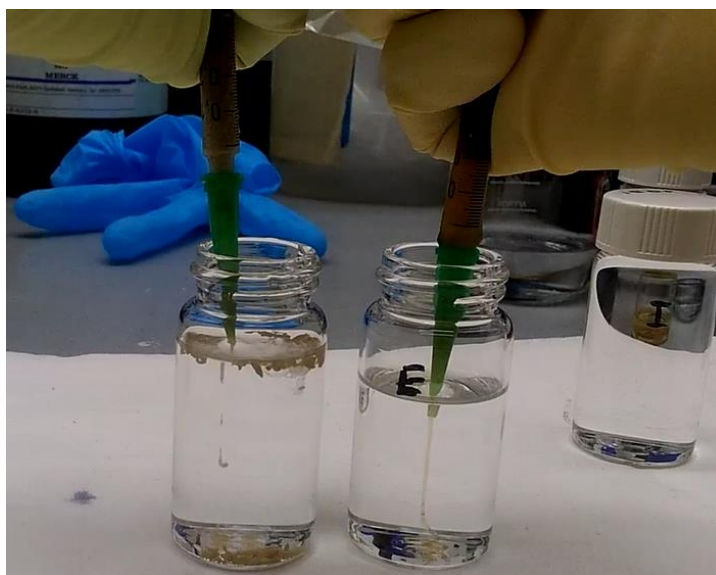


Figure 13. Solution printability comparison between PET/GO mixtures (left) and PCL/GO mixtures (right).

PET/GO extrusion in the selected coagulation bath led to the formation of intermittent fiber portions and beads, which is not suitable for wet-spinning. A continuous filament must be observed (as shown with PCL/GO) in order to successfully print a scaffold.

As such, plotting-related parameters were not assessed for PET/GO, and wet-spinning combined with additive manufacturing was no more pursued for PET/GO composite fibers production.

1.2.2.2. Spray coating

Since PET/GO composite fibers printing could not be performed using wet-spinning with the tested parameters, a different approach for GO incorporation was explored. GO-containing coating solutions were prepared and sprayed in commercially available PET randomly organized meshes.

Medical grade PET203 and PET305 felt fabrics were purchased from SurgicalMesh™, USA. PET203 and 305 differ in thickness, being 1.2 mm in the first case and 1.9 mm in the second, and therefore also in weight: 203 g/m² and 305 g/m², respectively. These fabrics were cut into 3 cm x 3 cm square samples and used as coating targets.

Using a previously optimized set-up, described in prior studies developed in our team¹³ and demonstrated in Figure 14 (B), an airbrush was fixed with a claw to a universal holder.

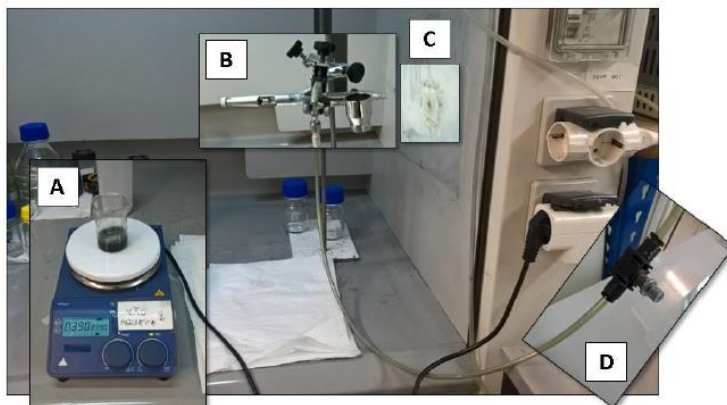


Figure 14. Spray coating set-up with a (A) magnetic stirrer, an (B) airbrush, (C) target polymeric mesh fixed to the hotte wall and (D) compressed air flux control valve.

The fixed positioning of the airbrush between tests guarantees reproducibility between coatings. The study of the relation between the distance of the airbrush to the wall and the area of the sprayed coating demonstrated that the nozzle end (0.2 mm) should be positioned 10 cm away from the target. The 3 cm x 3 cm PET samples were attached to the hotte wall with adhesive tape, keeping that ideal distance (Figure 14 C).

Coating dispersions were developed, by dispersing GO in different solvents (acetone, THF and water). GO dispersions in acetone and THF were prepared with a concentration of 0.5 mg/mL, whereas GO concentration in aqueous dispersions varied from 0.5 mg/mL to 2 mg/mL. These solutions were ultrasonicated (Hielsher UIP 1000 probe) three times for 90 seconds on an ice bath, to prevent solvent evaporation caused by the produced heat. Sonicated solutions were kept with magnetic stirring before use.

The dispersions' volume (6 mL) was added to the airbrush cup and, for this fixed airbrush set-up (as represented in Figure 14), the airbrush trigger was blocked (with tape) in "full open" mode, with the passage of compressed air being controlled solely by the valve opening (Figure 14 (D)). Compressed air was maintained at a pressure of 1.8 bar during all samples coating. Materials were dried in the hotte and cut with a 5 mm stainless steel puncher (Integra® Miltex®).

2. Materials characterization

2.1. GO characterization

2.1.1. X-ray photoelectron spectroscopy (XPS)

Graphite oxidation and consequent GO obtention was verified by X-ray photoelectron spectroscopy (XPS) analysis. This technique was performed at CEMUP (Centro de Materiais da Universidade do Porto) using Kratos Axis Ultra HSA. A monochromatic Al X-ray source (anode) operating at 15 kV (90 W) was used. A 300 μm x 700 μm square was the analyzed area.

80 eV was the energy used for survey spectra, whereas 40 eV were used for O 1s and C 1s high-resolution spectra acquisition. The effect of the electric charge was corrected by setting the reference of the C 1s peak to 285,0 eV. Spectral deconvolution was performed with CasaXPS software.

2.2. PCL/GO composite scaffolds characterization

2.2.1. Optical microscopy

Printed PCL/GO fibers were observed and photographed using a stereomicroscope (Olympus, Japan). This type of optical microscopy allowed a fast screening of preferable printing parameters, since printed scaffolds could be easily and rapidly observed, without the need for staining, sputtering or any type of sample fixation. This stereomicroscope allows a maximum magnification of 6.3x, which revealed enough to study fibers organization, diameter and possible printing defects.

2.2.2. Scanning electron microscopy (SEM)

SEM/EDS analysis of final PCL/GO scaffolds was performed using a high resolution (Schottky) environmental scanning electron microscope, with X-Ray microanalysis and backscattered electrons diffraction patterns analysis (Quanta 400 FEG ESEM/EDAX Genesis X4M), requiring a 15 kV voltage for the desired quality images. This analysis was performed at CEMUP (Centro de Materiais da Universidade do Porto).

Scaffolds were fixed on conductive carbon tape strips, both for top views and cross-section observations. Cross-section images acquisition required composite scaffolds' cryo-fracturing, which was possible by freezing them with liquid nitrogen.

All samples were coated with an Au/Pd thin film by sputtering, using the SPI Module Sputter Coater equipment for 100 seconds with a 15 mA current, to improve samples conductivity and consequent imaging quality.

2.3. GO-coated PET scaffolds characterization

2.3.1. Optical microscopy

PET203/305 meshes and GO-coated meshes were observed using the stereomicroscope (Olympus, Japan) described in section 2.2.1, and digital images were acquired.

2.3.2. Coating stability test

To determine spray coatings stability and verify GO adhesion to the fibers' surface, a washing test was performed. GO-coated PET scaffolds were placed in 15 mL Falcon tubes with 10 mL of dH₂O and vortex (maximum speed) was applied for 10 seconds.

Washing water was changed and its color observed, and the process was repeated for a total of three times.

2.3.3. Scanning electron microscopy (SEM)

PET and GO-coated PET meshes were observed before and after the stability test was performed, assessing possible fiber topography modifications and GO exposure/distribution differences promoted by washing. Phenom XL desktop SEM at UPTec (Parque de Ciência e Tecnologia, University of Porto) was used in this analysis, and the applied voltage varied between 10 and 15 kV. Samples were fixed with carbon tape and sputtered with Au, usually applied in non-conductive samples.

3. Antibacterial effect assessment

PCL/GO composite fibrous scaffolds and GO-coated PET meshes were analyzed to understand the mechanism of action of immobilized GO on bacteria. All samples were sterilized with ethylene oxide at Hospital de São João, Porto.

3.1. Bacteria strain and growth conditions

Antibacterial activity was evaluated towards *Staphylococcus epidermidis* (ATCC 35984). Bacteria were grown in Trypticase Soy Agar (TSA, Merck, USA) plates overnight at 37 °C, and colonies were hand-picked immediately after incubation or after plate storage at 4 °C (1-week shelf life).

Two colonies were collected, inoculated in 5 mL of Trypticase Soy Broth (TSB, Merck, USA) and cultured overnight at 37 °C in an orbital shaker oven (Raypa, Spain), at 150 rpm.

S. epidermidis overnight inoculum was centrifuged (2700 rpm for 10 minutes) and the pellet was washed with 5 mL of fresh TSB. This procedure was repeated for a total of three times.

3.2. Bacterial adhesion assays

The concentration of *S. epidermidis* overnight culture, which was in its exponential phase of the growth curve, was adjusted by optical density (OD) measurement at 600 nm, using an UV-Vis Spectrophotometer (Perkin Elmer, USA). Initial inoculum concentration was set at 1×10^7 Colony-Forming Units (CFUs)/mL for 2-hour adhesion assays and 6×10^5 CFUs/mL for 24-hour assays. The calculated volume needed to get the mentioned final concentrations was collected from the liquid culture and diluted in fresh TSB medium. TSB was further supplemented with 10% human plasma in some assays, to assess the influence of protein adsorption to the scaffolds on the antimicrobial properties.

3.2.1. PCL/GO composite scaffolds: drop assay

Given PCL and PCL/GO composite scaffolds hydrophobicity, an immersion assay, in which the sample is submerged in a considerable volume of medium, could not be performed, since scaffolds float.

Instead, a drop of 10 μL of bacterial suspension was placed on top of the sterilized PCL/GO scaffolds and incubation was performed for 2h or 24h at 37 $^{\circ}\text{C}$ under static conditions (Figure 15). In order to avoid drop evaporation, the remaining empty wells of the 48-well plate were filled with dH_2O or PBS, and the plate was placed into a container with humid tissues inside the incubator (Binder, Germany).

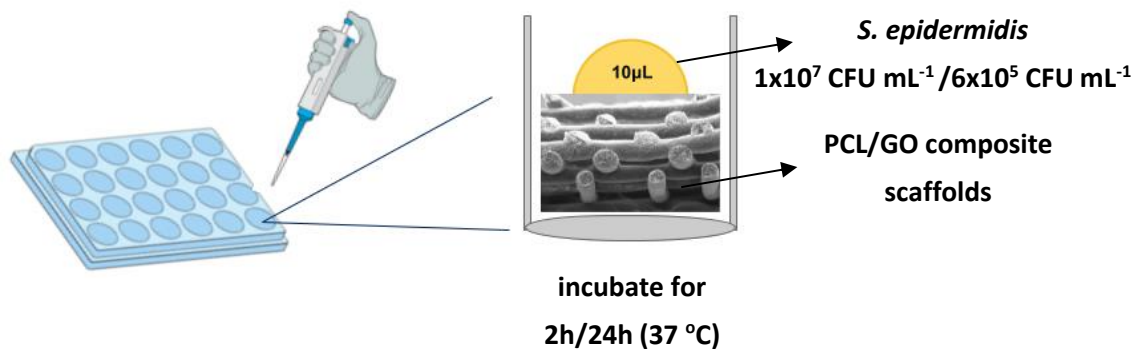


Figure 15. Bacterial adhesion assay schematics for PCL/GO composite scaffolds.

3.2.2. GO-coated PET scaffolds: immersion assay

PET hydrophilicity allowed the design of an immersion assay in this case, in which sterilized PET meshes were covered by 200 μL of bacterial suspension (Figure 16). 24-hour incubation assays were performed with PET fibers, under the aforementioned conditions.

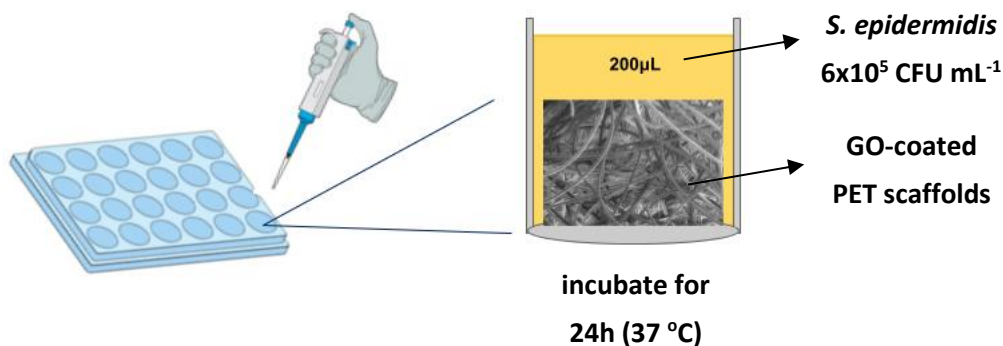


Figure 16. Bacterial adhesion assay schematics for GO-coated PET scaffolds.

3.3. Visualization of adherent bacteria

3.3.1. Live/Dead staining

After 2-hour or 24-hour incubation times, scaffolds with adherent bacteria were washed 3x with NaCl 0.85% to remove non-adherent bacteria, by sequential transfers between NaCl-filled wells (an approximate volume of 200 μ L was used in each well). Samples were stained with BacLight™ LIVE/DEAD® Kit (Molecular Probes, USA) to investigate adherent bacteria viability. This kit includes two dyes: SYTO9 (nucleic acid stain that labels in green all present bacteria) and propidium iodide (PI), which stains membrane-compromised bacteria in red.

SYTO9 and PI powders were dissolved in 5 mL of dH₂O to prepare 2x stock solutions, as recommended by the manufacturer. The dissolved dye solutions are described as being stable for up to a year, when stored frozen at -20 °C and protected from light. Then, both 2x stock solutions were mixed (1:1 ratio) and 10 μ L drops were placed on top of each scaffold, followed by a 15-minute incubation time, protected from light.

3.3.2. Confocal microscopy

After staining, the scaffolds were transferred to an imaging dish (Ibidi, Germany), ideal for high resolution microscopy on inverted microscopes, with the adherent bacteria-containing surface faced down. A Laser Scanning Confocal Microscope Leica TCS SP5 II (Leica Microsystems, Germany) was used with an HC PL APO Lbl. Blue 20x/0.70 objective. To properly detect red and green fluorescence conferred by staining (PI and SYTO9, respectively), one channel was programmed for DPSS 561nm laser photoexcitation and a second channel for Ar 488nm laser.

As displayed in Figure 17, besides laser power control, light trajectory settings and general acquisition configurations, the software allows a predefinition of a z-volume to be scanned. In these antimicrobial studies, a parallelepiped with an average depth of 150 μ m was set. A step size of 1.5 μ m was selected, given *S. epidermidis* dimensions (1-2 μ m), and its suitability was confirmed since bacteria localization varied progressively between two consecutive frames.

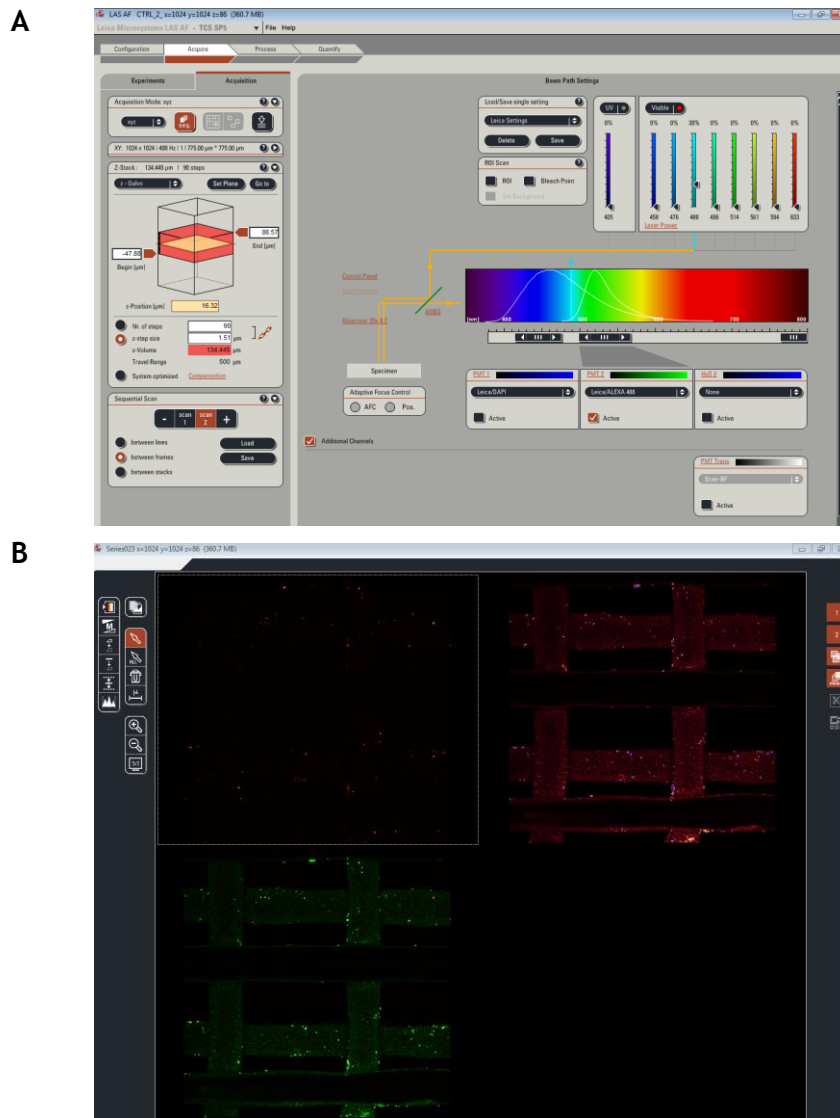


Figure 17. Confocal microscopy user interface (LAS AF software) screenshots. A: z-stack volume and step size, sequential scanning preferences and laser power can be adjusted, among several other parameters. B: Image acquisition, switching channels between frames.

3.3.3. Adherent bacteria quantification: ImageJ/Fiji

Confocal microscopy imaging files were processed with ImageJ (Fiji) software. For PCL scaffolds, a z-axis projection was built with all the z-stacks that captured a chosen fiber, in order to get the 3D reconstructed images. At least one fiber was fully analyzed in each acquired image, showing its entire z-dimension of approximately 100 μm , corresponding to its diameter. PCL fibers' area was measured, corresponding to the effectively available area for bacteria adhesion. Bacteria counts were displayed as “number of live/dead bacteria per μm^2 of fiber”.

For PET scaffolds, choosing the segment of stacks that captured a certain fiber was not necessary, since several fibers could be observed in the 150 μm depth acquired image. In this case, the number of stacks was preserved between different samples (100 μm z-volume) and all the bacteria present in the final 3D reconstruction were counted, regardless of their location. Therefore, fibers' area was not determined, and the bacteria counts were displayed as “number of live/dead bacteria per 100 μm z-stack”.

Contrast and brightness levels were adjusted, and some background noise was removed to improve projections' quality. Using “find maxima” ImageJ tool, it was possible to quantify live/dead adherent bacteria and further analyze these data.

4. *In vitro* biocompatibility assessment

In vitro biocompatibility assays were performed using human foreskin fibroblasts (HFF-1) cell line (ATCC, SCRC1041). Fibroblasts were selected to be cultured in the scaffolds since this cell type is the major constituent of connective tissue. Although cytocompatibility must be evaluated also towards different cell types, fibroblasts represent a particularly important target, given their frequent direct contact with implanted medical devices.

4.1. HFF-1 cell line and culture conditions

Human foreskin fibroblasts were grown in Dulbecco's modified Eagle's medium (DMEM+, Gibco, Thermo Fisher Scientific, USA) supplemented with 10% v/v fetal bovine serum (FBS, Gibco, Thermo Fisher Scientific, USA) and 1% v/v penicillin/streptomycin (Pen/Strep, Biowest, France) at 37 °C, in a fully humidified atmosphere, containing 5% CO₂. Media were replenished every 2 days.

When reaching 90% confluence, cells were rinsed with 5 mL of PBS (37 °C) and detached from culture flasks using 2 mL of 0.25% w/v trypsin solution (Sigma Aldrich, USA) in PBS. In all passages, HFF-1 cells were seeded at an approximate density of 15 000 cells/cm², as recommended by the supplier.

4.2. Adhesion and proliferation assay

Scaffolds were soaked on culture medium overnight, before cell seeding, to promote protein adsorption. Cells were then seeded on the polymeric scaffolds by placing a droplet of 10 µL on top of each scaffold, containing 20 000 cells. Based on previous studies, this concentration was chosen to avoid cell clustering upon seeding. As displayed in Figure 18, fibroblasts were allowed to adhere for 1h before adding 500 µL of supplemented DMEM+ medium per well.

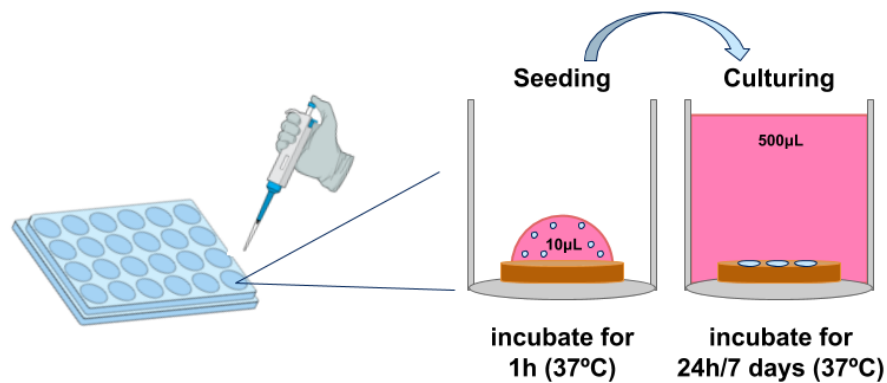


Figure 18. Cell adhesion assay schematics, showing a 1-hour seeding step and subsequent culturing conditions.

Media was refreshed every other day and fibroblasts were fixed at two different time points: after 24 hours and 7 days.

4.3. Visualization of adherent cells

4.3.1. Nuclei/F-actin staining

After the incubation times, scaffolds with adherent cells were rinsed with PBS. Then, fixation was performed with paraformaldehyde (PFA, Merck, USA) 4 wt.% in PBS for 15 minutes. PFA was removed, cells were rinsed with PBS (3x) and stored at 4 °C.

For microscopical observation, fibroblasts' cytoskeletal filamentous actin was bonded to green-fluorescent phalloidin (Alexa Fluor 488; Alfacene, Portugal) in a 1:100 dilution, and the nuclei were stained with a concentration of 3µg/mL of 6-diamidino-2-phenylindole dihydrochloride (DAPI, Merck, USA), which intercalates with nucleic acids.

For that, prior washing was done with PBS, incubation with phalloidin was performed in the dark, for 1 hour, under mild agitation, and afterwards cells were washed and kept at 4 °C in PBS until their observation, to avoid drying. DAPI was added approximately 10 minutes before confocal imaging was performed.

4.3.2. Confocal microscopy and LAS X software

After staining, scaffolds were transferred to an Ibidi dish and the same Leica SP5 confocal microscope was used with an HC PL APO CS 40x/1.10 objective. Diode 405nm and Ar 488nm lasers were used to detect DAPI stained nuclei (blue) and phalloidin stained cytoskeleton (green). As previously shown in Figure 17, lasers power, light trajectory settings, acquisition configurations and scanning preferences were set, as well as the z interval to be analyzed (approximately 150 μm). Despite cells being bigger than bacteria, a step size of 1.5 μm was kept, since it allowed superior quality and resolution of the final projected images.

Confocal microscopy imaging files were processed either using ImageJ (Fiji) or the equivalent LAS X processing software (Figure 19).

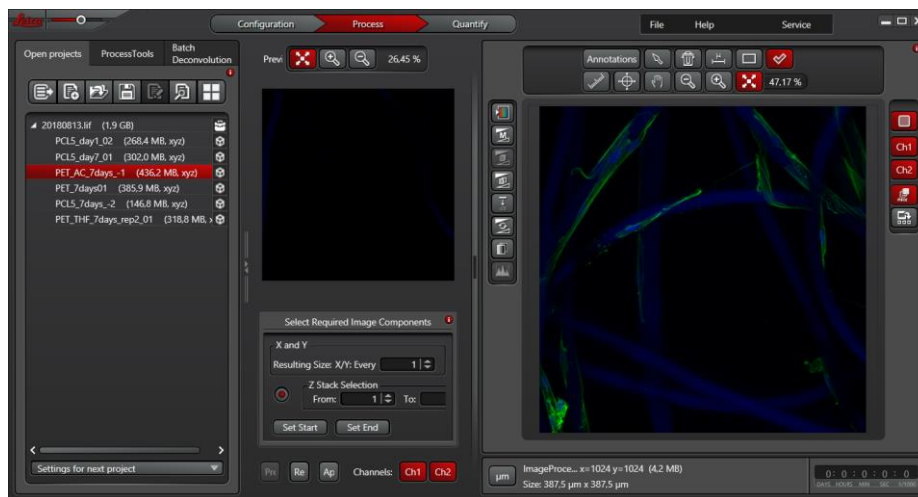


Figure 19. Image processing software (LAS X) screenshot. z-projections, orthogonal views decompositions and channel's color level tunings can be performed.

5. Statistical analysis

Statistical analysis and graphs construction were performed using GraphPad Prism 7.00 and SigmaPlot 12.5 software.

Normal distribution and homogeneity of variances criteria were evaluated with the Shapiro-Wilk normality test and using the Levene's or the Brown-Forsythe's test, respectively.

A parametric one-way ANOVA or an unpaired Welch's t test, depending on the number of groups being compared, were used when normality and homogeneity of variances were verified. When parametric one-way ANOVA was used, Holm-Šídák's multiple comparisons test allowed to find differences when analyzing every group against each other.

Non-parametric tests were used to compare groups that failed these criteria: non-parametric one-way ANOVA (Kruskal-Wallis), when three groups were compared, and Mann-Whitney test, when only two groups were compared. When non-parametric one-way ANOVA (Kruskal-Wallis) was performed, Dunn's multiple comparisons test was used to assess the statistical significance.

All selected tests were performed with a 95% confidence interval. Statistically significant differences are specified in the figure caption of the corresponding data, indicated with */# (p values ≤ 0.05), **/## (p values ≤ 0.01), ***/### (p values ≤ 0.001) and ****/#### (p values ≤ 0.0001).

Chapter IV: Results and Discussion

1. Graphene Oxide

Successful oxidation of graphite using Modified Hummer's Method (MHM) was verified by XPS analysis (Figure 20).

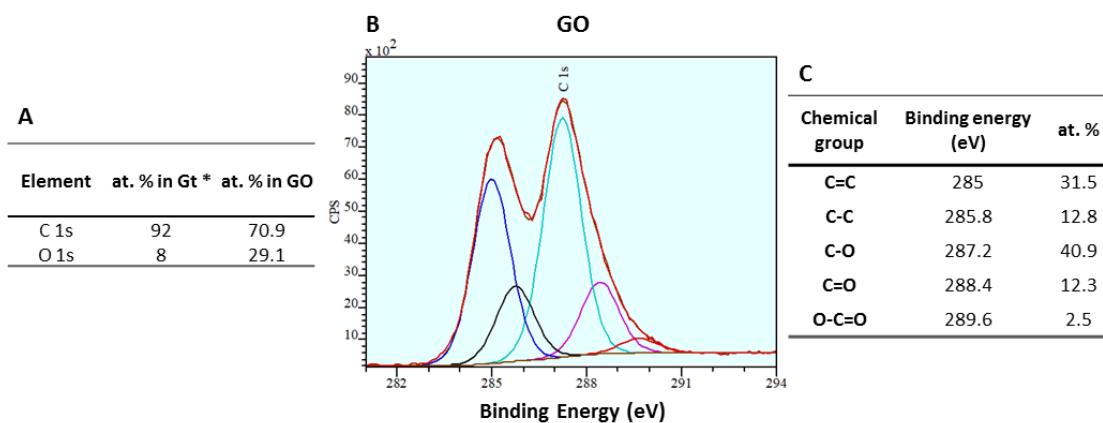


Figure 20. XPS analysis of GO. A: Differences in atomic percentages (at %) of Carbon 1s and Oxygen 1s between GO and commercial graphite. *XPS results for graphite were published by Pinto A *et. al.* (2013)¹⁹⁴; B: Carbon 1s high-resolution spectrum of GO; C: Contents of chemical groups resulting of C 1s spectra fitting.

XPS analysis revealed that GO is constituted by 70.9% of carbon atoms and 29.1% of oxygen atoms (Figure 20 A), confirming the oxidation of graphite, which typically has a much lower percentage of oxygen atoms (8% of O 1s was found in commercial pristine graphite by Pinto *et al.*¹⁹⁴). The percentage of Oxygen in GO (close to 30%) is in accordance to what is expected for oxidation through MHM.^{195,196}

After peak deconvolution (Figure 20 B), C-O groups, which emerge on the basal planes of GO sheets,¹⁹⁷ are the most prevalent oxygen-containing functional groups on GO structure, with an occurrence of 40.9% (Figure 20 C). Carbonyl (C=O) and carboxylic groups (O-C=O), which appear on GO edges,^{12,197} are less predominant, representing 12.3% and 2.5%, respectively (Figure 20C).

Overall, XPS results showed that, after performing MHM, graphite had been efficiently oxidized, with the introduction of various oxygenated groups.

GO was dispersed in some of the potential solvents for both polymers (PCL and PET), according to their performance. Chloroform, THF and Acetone were able to dissolve PCL, while a mixture of TFA and DCM (1:2) was the only solvent option for PET. GO dispersion in Chloroform was impossible, revealing large GO aggregates and an absence of GO affinity to this solvent (Figure 21). THF and Acetone exhibited analogous behavior, producing dispersions with perfectly dispersed GO, stable even after 10 days. TFA/DCM (1:2) allowed a fair dispersion of GO, although its stability was greatly limited, with GO deposition after 1 day. Therefore, storage of this dispersion was not viable, demanding preparation of fresh solutions whenever experiments with PET/GO composites were conducted.

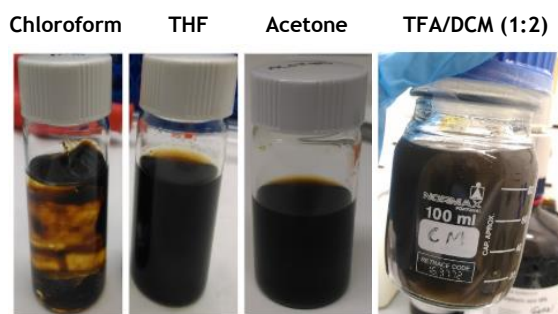


Figure 21. GO dispersions in: Chloroform, THF, Acetone and TFA/DCM (1:2).

Considering this GO dispersibility assessment, Chloroform was disregarded for further studies. THF, Acetone and TFA/DCM (1:2) were used to assess the printability of PCL and PET solutions, respectively.

2. PCL/GO fibrous scaffolds

2.1. Wet-spinning combined with additive manufacturing

Among the organic solvents tested, THF revealed to be the one in which the two key conditions were met: GO was well dispersed, and PCL was more efficiently dissolved (overnight at room temperature). This allowed the use of a small ID needle (170 μm) for plotting, avoiding the need of injectability tests, which are necessary when undissolved polymer is still present in the solution. When THF was used, wet-spinning combined with AM allowed the production of several layers composed by thin fibers (Figure 22).

On the other hand, when acetone was used, PCL started to precipitate in the syringe during plotting, hindering the deposition of more than two layers. Fiber diameter was also dramatically affected by the solvent used, with acetone leading to the production of fibers with undesired dimensions (diameters above 200 μm), despite the use of the same Gauge needle.

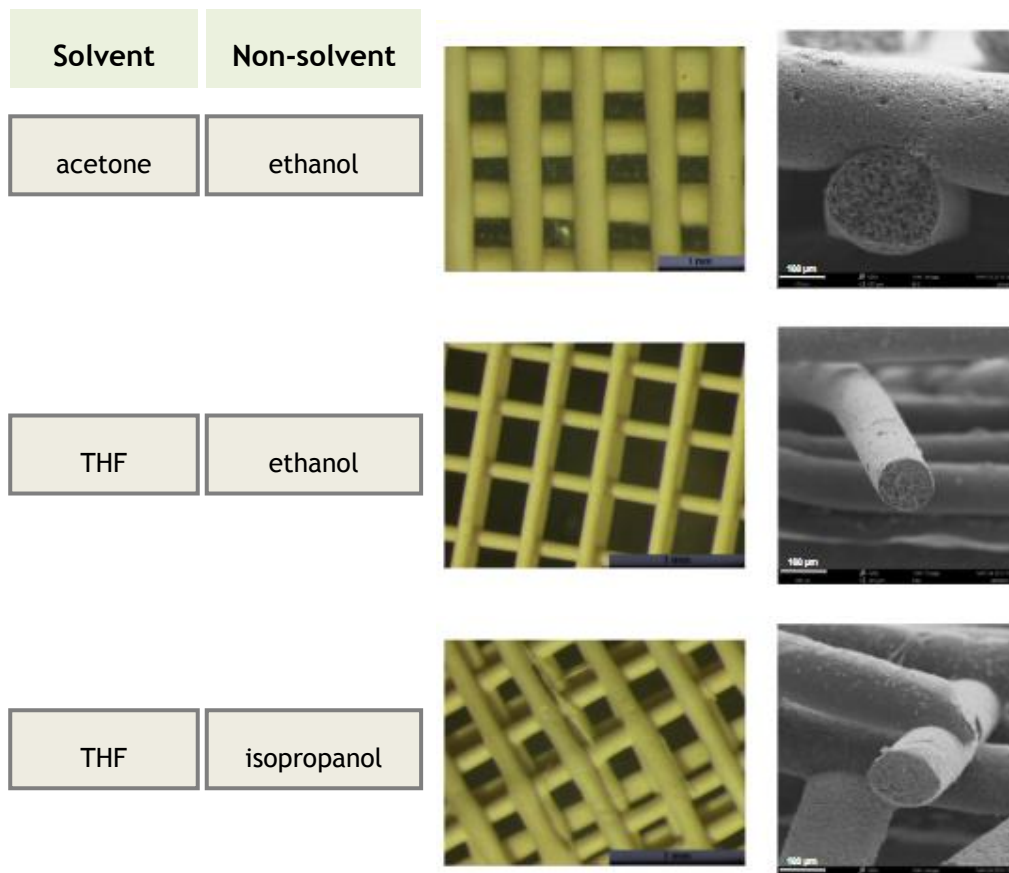


Figure 22. Screening for PCL solvents (acetone and THF) and non-solvents (ethanol and isopropanol). Left: stereomicroscope imaging; Right: SEM analysis (scale bar: 100 μm).

Regarding the coagulation baths, the use of ethanol showed compatibility with good design definition and relatively fast polymer fiber precipitation during solvent/non-solvent exchange. Moreover, ethanol excess is easy to eliminate from the scaffolds through evaporation. Nevertheless, isopropanol was also tested as a coagulation bath, keeping THF as solvent. Although a similar performance was observed when compared to ethanol, a slightly worse fiber definition was achieved (Figure 22). Taken this together, and as isopropanol is more expensive, ethanol was selected as the coagulation bath.

In these processes of solvent and coagulation bath evaluation, solutions of 15% (w/v) PCL with 5% (w/w) GO were used in all cases. Besides these concentrations, different amounts of both polymer and GO were incorporated in several solutions prepared (Figure 23). Regarding the 15% (w/v) PCL solution, GO concentration could not be increased above 5% (w/w), since higher concentrations affected the printing process due to constant clogging observed. For 7.5% (w/v) PCL solution, GO concentration ranged between 0% (w/w) and 10% (w/w), despite that the last one hindered the extrusion process, also causing clogging. Top views of the fibers surface showed GO exposure for all tested GO and PCL concentrations. Additionally, SEM images showed that an increase in the concentration of GO resulted in higher amounts exposed at the surface.

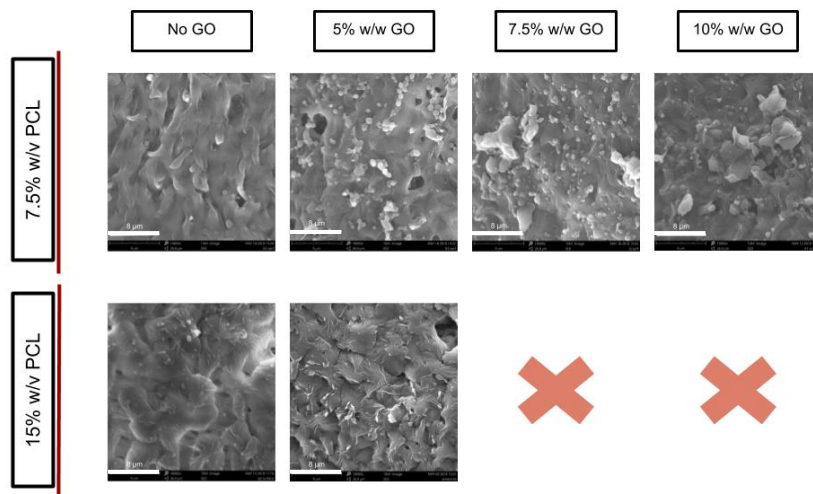


Figure 23. SEM images of the fiber surface of PCL and PCL/GO scaffolds, with different amounts of PCL and GO. Scale bar: 8 μm.

Furthermore, major effects in fiber porosity were observed through all concentrations (Figure 38 in ANNEXES: cross section, last column - scale bar: 8 μm). The decrease of PCL concentration increased surface porosity, with fibers being less dense and showing bigger combs in their cross-sections. Interestingly, the irregularity and the size of these combs increases in a direct proportion to the amount of GO present. Graphene oxide effect on non-solvent/solvent-induced phase separation seems to be considerable, and the distribution of more hydrophilic regions (GO) dispersed in a hydrophobic matrix (PCL) might be the key factor. In fact, heterogeneously arranged and highly interconnected pore formation caused by GO was described by Dinescu *et al.*¹⁹⁸ in CS/GO composite scaffolds, corroborating these results.

After solvent/non-solvent and PCL concentrations screening described, THF/ethanol and 7.5% (w/v) PCL concentration were the selected conditions, respectively. The 3D design of the scaffolds was the next step, for which several printing-related parameters were adjusted, namely plotting speed, flow rate, z-distance and xy-distance between fibers.

To evaluate the influence of those parameters, the first solution tested was 10% (w/w) GO, which would be the most challenging due to its higher viscosity. Fibers with the smallest diameters (around 100 μm) and best definition were obtained using lower flow rates (0.5 mL/h) and intermediate plotting speeds (75%), as displayed in Figure 24.

For higher flow rates (1-2 mL/h) and plotting speeds (100-200%), dragging of the fibers was observed upon deposition of the next fiber. This can be due to the short temporal gap between the deposition of two consecutive fibers, leading to the partial dissolution of PCL fibers that are already solidifying/solidified. Mota *et al.*¹⁹ vastly described the influence of several printing parameters, namely feed rate, and concluded that, for high solution feed rates, a filament may not be solidified enough when it reaches the previous layer, and a controlled fibrous deposition may be compromised, due to excessive fiber-fiber fusion.¹⁹

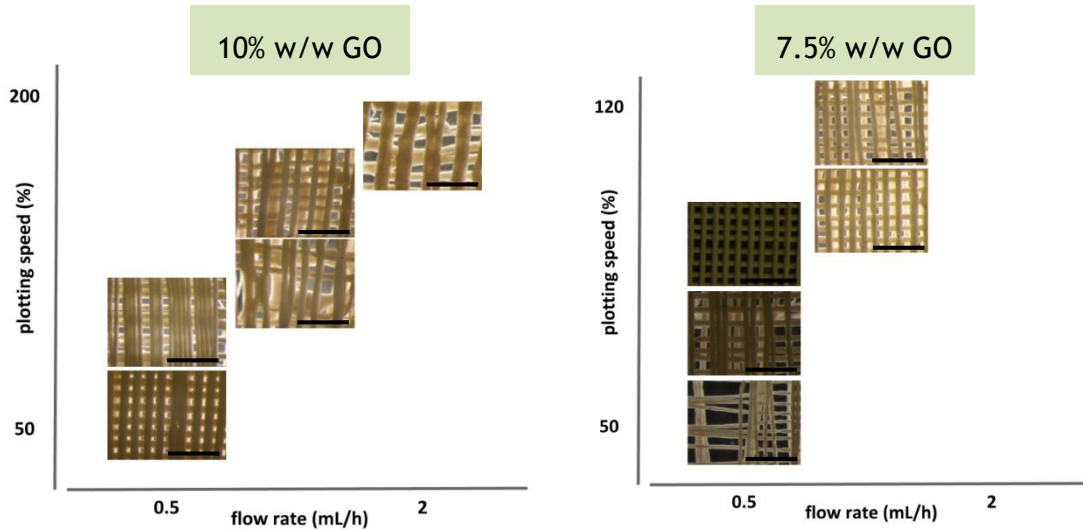


Figure 24. Flow rate and plotting speed adjustments for PCL/GO scaffolds prepared with 10% w/w GO (on the left) and 7.5% w/w GO (on the right). Images displayed were obtained by Stereomicroscopy (scale bar: 1 mm).

After this, 7.5% (w/w) GO solution printing was tested with the same parameters, to investigate if the previous conditions remained adequate for this lower GO concentration (Figure 24). The plotting speed window was narrowed down (50%-120%), similarly to what happened for flow rate range (2 mL/h was not tested). In this case, 0.5mL/h and an intermediate plotting speed (80%) showed again to be the best matching options.

Having the plotting speed and flow rate set in 80% and 0.5 mL/h, respectively, different x, y and z-distances were tested for the 5% (w/w) GO solution, to evaluate the best fit for a well-defined, precisely spaced structure. Although a small distance between fibers in the xy axis was preferable in order to close the squared pores and avoid a total permeability throughout the scaffold, the best design was achieved with bigger distances (400 μm) - Figure 25. When the space between two fibers was smaller, interference of THF in solidifying/solidified fibers was again verified. Therefore, to decrease inter-fiber spaces, staggering between layers was used (200 μm). Fibers in the “n” layer were placed right in the middle of the ones in the top layer (“n+2”). Concerning z-distance, the highest step tested (80 μm) resulted in well-separated layers, avoiding both collapsing of the structure and fiber crushing.

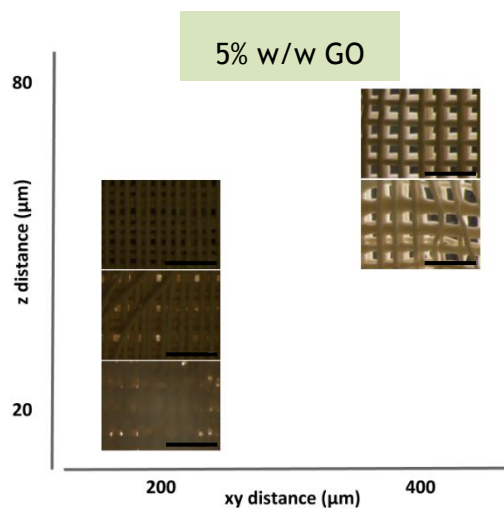


Figure 25. x, y and z distances adjustment for PCL/GO scaffolds prepared with 5% (w/w) GO . Images displayed were obtained by Stereomicroscopy (scale bar: 1 mm).

In conclusion, the referred parameters were fixed sequentially, using all different GO concentrations, starting with the most challenging one (10 % w/w) and ending in 5% w/w GO. After that, PCL scaffolds with 7.5% (w/v) PCL and without GO were successfully printed with these parameters. This may be due to the absence of GO, which facilitates the process.

For subsequent antimicrobial and biocompatibility tests, 10% w/w GO concentration was not used due to the technical difficulties during printing, namely the frequent needle clogging. More importantly, comparisons between the two lowest GO concentrations were considered more valuable, assuming a general preference in using the minimum amount of GO that ensures the desired antimicrobial effect, without compromising cell adhesion.

Final 3D structure of the scaffolds is shown in Figure 26, including top-view and cross-section schemes that represent the virtual CAD model used. The four-layer scaffold shown is representative of the entire real structure, which possesses 12 stacked layers.

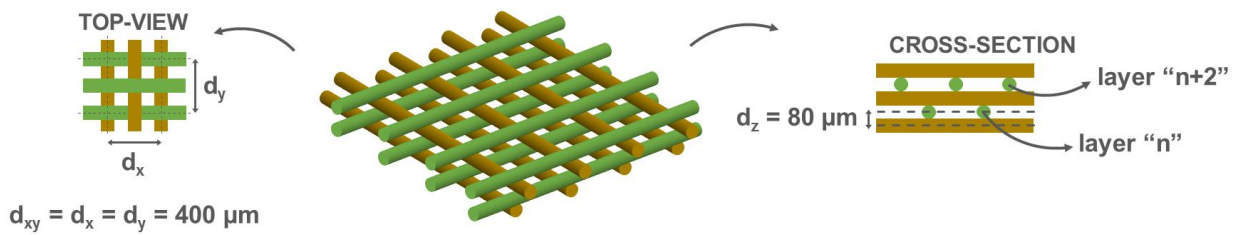


Figure 26. 3D model of the produced scaffolds, showing a top view, a cross-section view and x, y and z-axis distances.

Final materials were fabricated using this 3D model and 0.8cmx0.8cm squared PCL and PCL/GO scaffolds were printed (Figure 27). The meshes revealed great flexibility, although the fibers were extremely sensitive to deformation, demanding strict care during handling.

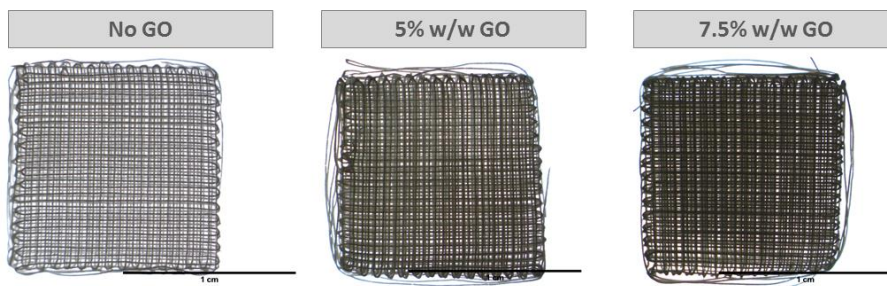


Figure 27. Stereomicroscope images of final optimized 3D printed PCL scaffolds with and without GO (scale bar: 1 cm).

SEM analysis of final produced materials was performed to confirm GO exposure at the fibers surface (top views in Figure 28) and the results were consistent with previous SEM analysis made during the optimization steps. Although GO sheets may vary in dimension, the acquired images indicated a regular size of approximately 8 μm . Smaller aggregates present at the fibers surfaces appeared to be accumulations of undissolved polymer. EDS analysis was performed, revealing that Carbon and Oxygen were the elements detected. Contamination hypothesis with other elements (namely Fe) was rejected, but the nature of those Carbon/Oxygen aggregates was not possible to verify, leaving their provenience unclear.

Differences in porosity were obvious in all cross-section images (Figure 28), confirming the presence of GO as an influencing factor, creating bigger and randomly shaped combs with the increase of GO concentration. SEM observation also demonstrated a precise plotting of the 3D configuration, showing the staggering between layers (visible in both top view and cross-section images, with lower magnifications (scale bar: 400 μm)).

Fibers' average diameter was also studied by several measurements along different fibers, with PCL scaffolds presenting diameters of $107 \pm 11 \mu\text{m}$, PCL/5% w/w GO scaffolds of $102 \pm 9 \mu\text{m}$ and PCL/7.5% w/w GO scaffolds of $103 \pm 13 \mu\text{m}$. The results show a cohesive resemblance independently of the GO concentrations, where fiber diameter was approximately 100 μm , although slight differences were registered. Song *et al.*¹⁶ also found that the diameter of PCL/GO composite fibers was smaller than that of pure PCL. In addition, it was described that the surface of composite fibers was coarser with grooves and protuberances, whereas that of pure PCL was relatively smooth,¹⁶ which is consonant with these results.

PCL/GO scaffolds with a 3D interconnected network of macropores and a local microporosity of the polymeric matrix, as a consequence of the phase inversion process governing material solidification, were successfully fabricated.

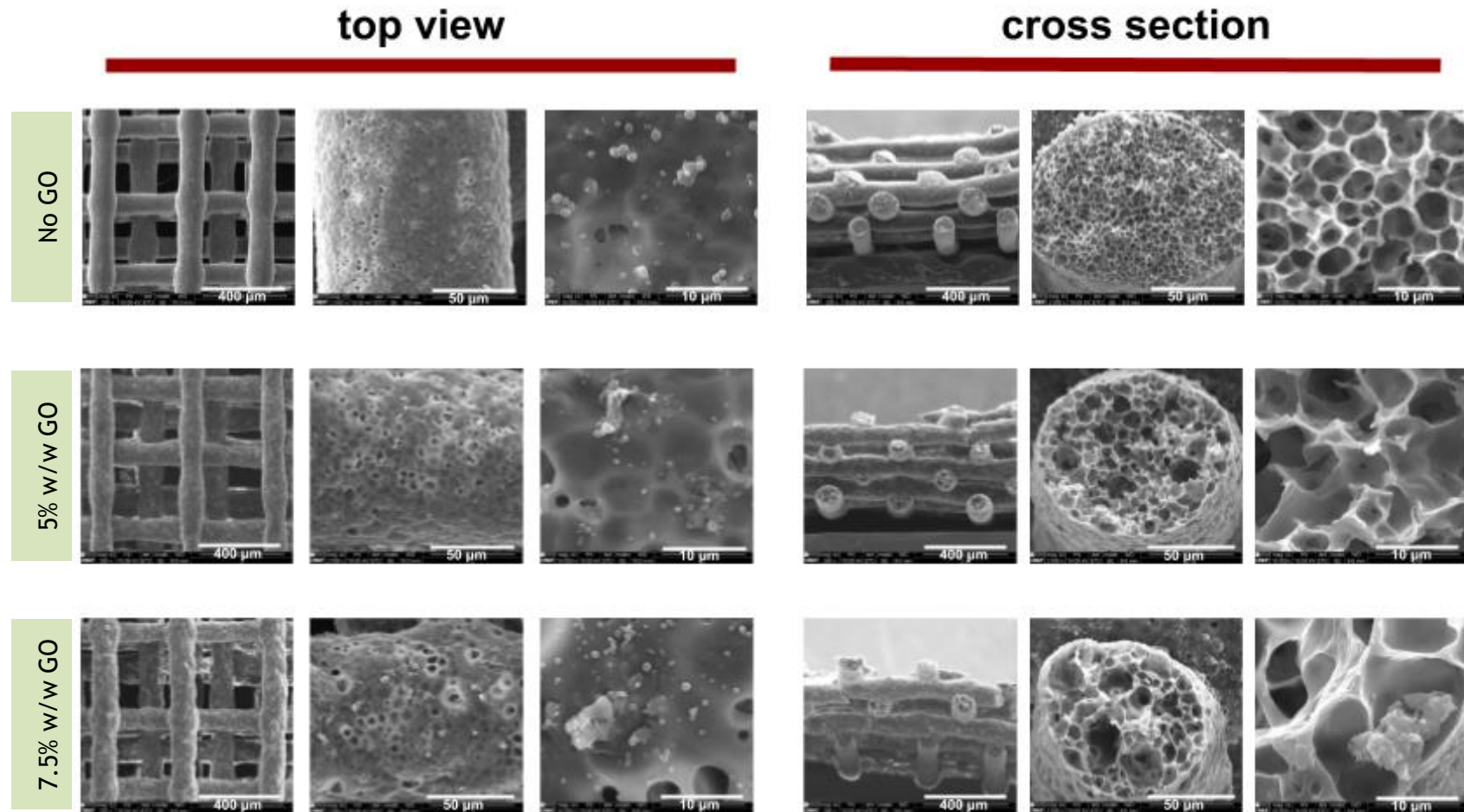


Figure 28. SEM analysis of the top views and cross-section views of final PCL scaffolds, with and without GO. Each row represents a different GO concentration. Scale bar, from left to right: 400 μm , 50 μm , 10 μm).

2.2. Antibacterial effect of PCL/GO scaffolds

To assess PCL/GO scaffolds bactericidal effect, adhesion assays were performed in two different time points: incubation of bacteria for 2 hours and 24 hours. In addition, assays were performed with only TSB as the growing media and TSB supplemented with 10% human plasma, to better mimic the contact with human body fluids that contain proteins, inevitably surrounding implanted medical devices. Adherent bacteria were stained and visualized by Confocal microscopy.

Images were acquired in two channels, using different lasers, so live and dead bacteria could be identified through green and red fluorescent emission, respectively. PCL and PCL/GO fibers were visible in both channels, revealing some autofluorescence, more evident in green wavelengths. Both live and dead bacteria were mostly present on the fibers' surface, where bacteria adhere.

For the 2-hour adhesion assay without human plasma in the culture media (Figure 29 A and B), the number of total bacteria found in the fibers was similar in all cases, independently of the presence of GO. However, slightly smaller amounts of live bacteria were found in GO-containing scaffolds comparing to PCL scaffolds without GO, whereas the number of dead bacteria was higher. The number of bacteria adhered to each fiber was counted and results are displayed in Figure 29 (B).

Regarding the number of dead bacteria in 5% w/w and 7.5% w/w GO concentrations, although it seems higher when compared with the control scaffold without GO, statistically significant differences were not found. Percentages of dead bacteria found were 23.3% and 34.7% for 5% w/w GO and 7.5% w/w GO, respectively, against 11.8% in the scaffolds without GO.

In this assay, GO effect was noticeable after only 2 hours, apparently being bactericidal and concentration-dependent. This surprisingly prompt action of GO was also described by Hong *et al.*,¹⁸⁴ who detected GO bactericidal effect towards *E. coli* after 2 hours in GO-containing PVDF fibers. In the highest GO concentration tested, 99.6% disinfection capacity was found.¹⁸⁴

Nevertheless, a similar assay was performed with 10% plasma supplemented TSB, to address the influence of proteins, their interaction with GO and bacteria, and to verify GO bactericidal effect after 2 hours in this condition.

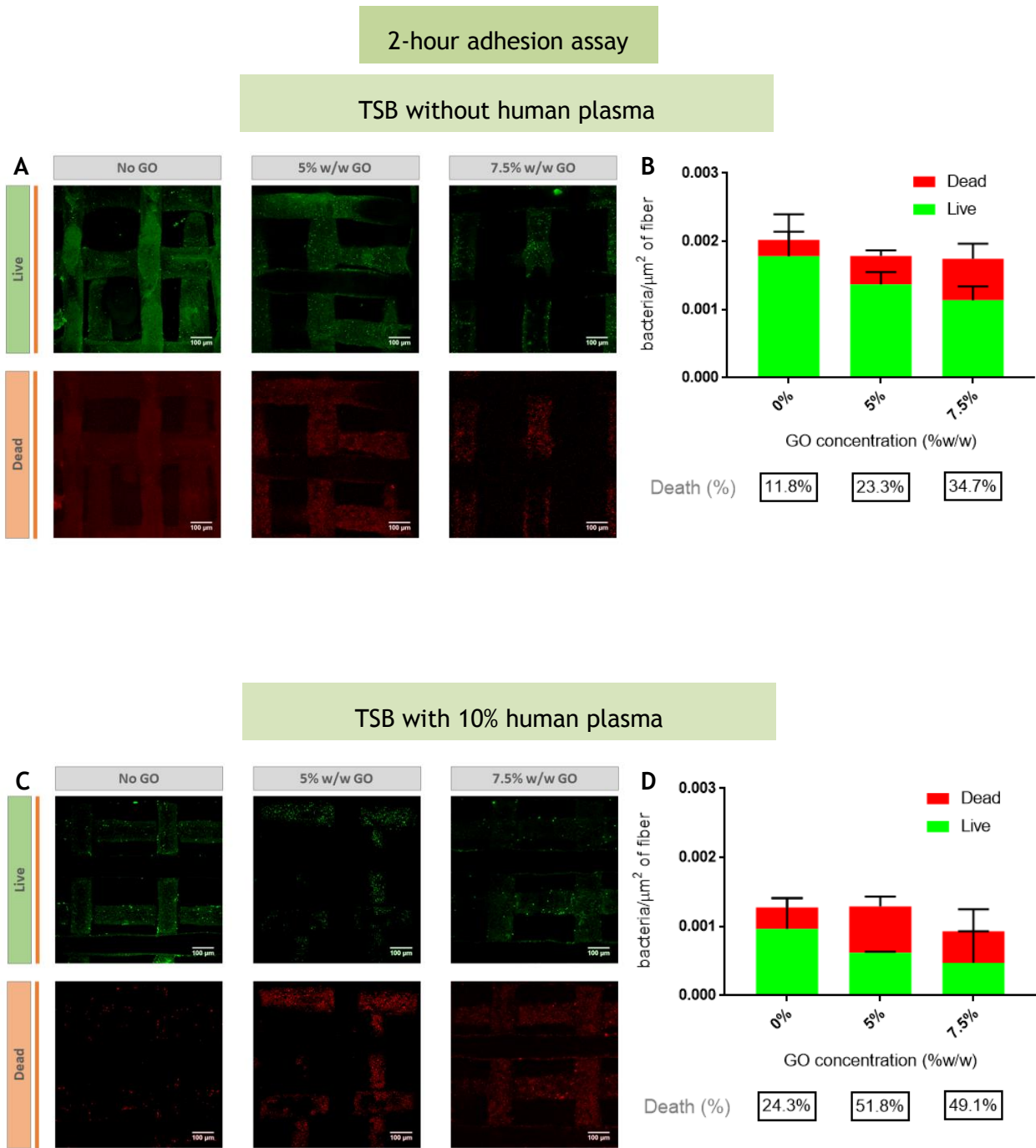


Figure 29. *S. epidermidis* adhesion to PCL/GO scaffolds after 2h incubation in plasma-free TSB (A) and 10% plasma supplemented TSB (C). Live and dead bacteria are stained in green and red, respectively. Scale bar: 100 μm . B, D: Grouped graphs with number of live bacteria per μm^2 of fiber displayed in green and number of dead bacteria per μm^2 of fiber displayed in red. Statistically significant differences are indicated with */# ($p \leq 0.05$), **/## ($p \leq 0.01$), ***/### ($p \leq 0.001$) and ****/#### ($p \leq 0.0001$).

Regarding the 2-hour adhesion assay with 10% human plasma supplemented TSB, confocal microscopy images are displayed in Figure 29 (C and D). The total number of bacteria counted in each scaffold was slightly reduced in comparison to the previous assay, which can be due either to plasma influence or to minor deviations in the initial *S. epidermidis* inoculum seeded.

PCL scaffolds without GO showed higher number of live bacteria (75.7%), whereas few dead bacteria were found (24.3%).

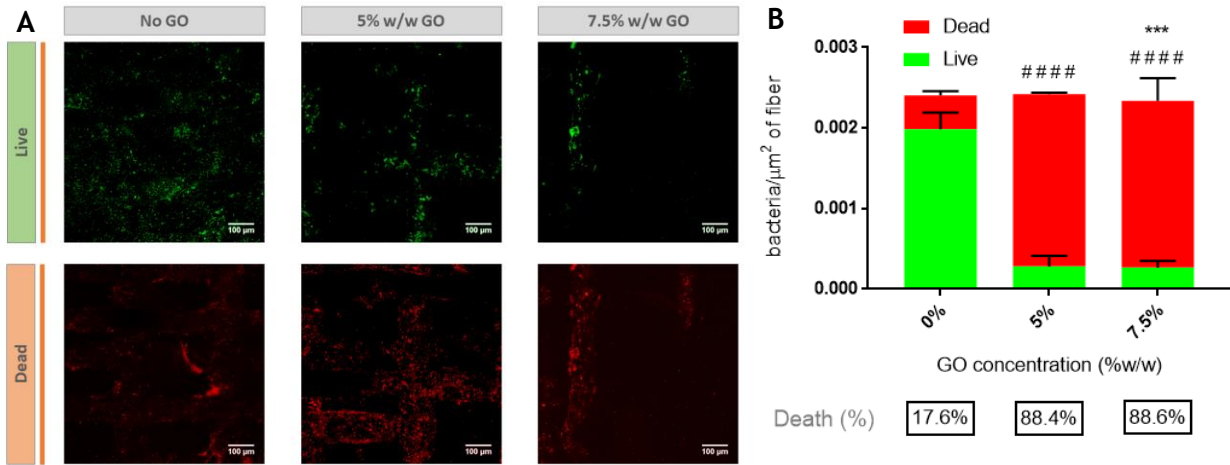
Quantitative analysis for GO-containing scaffolds confirms the results obtained for the previous plasma-free TSB assay, concerning the number of dead bacteria: an increase in both 5% w/w and 7.5% w/w GO concentrations, when compared to the PCL scaffolds without GO. Percentages of dead bacteria were around 50% for 5% w/w and 7.5% w/w GO. Again, statistically significant differences were not found. The presence of human plasma appears to potentiate GO bactericidal effect, since equal concentrations of GO (7.5% w/w, for instance) provoked different death percentages depending on the supplementation with 10% human plasma. In plasma-free TSB, this GO concentration caused 35% bacterial death after 2 hours, whereas in supplemented TSB 49% of the adherent bacteria were dead. Effects of plasma proteins on *S. epidermidis* initial adhesion to biomaterials were explored by Xu *et al.*¹⁹⁹, unravelling important influence of proteins such as fibronectin in promoting bacterial attachment.¹⁹⁹ On the other hand, molecular interactions between GO and plasma were described by Kenry *et al.*,²⁰⁰ demonstrating a significant dependence on the lateral size distribution and mean lateral sizes of the GO nanosheets.²⁰⁰ However, there is a lack of studies that integrate the presence of plasma proteins and GO, assessing their combined effect on bacteria adhesion and survival. From the obtained results, it seems that the presence of plasma proteins enhanced GO bactericidal potential, however this issue should be further addressed and confirmed.

Although the mortality was relatively higher than expected in the PCL scaffolds without GO, it was still the group with more live bacteria present.

To investigate GO effect on bacterial adhesion with a longer contact period, 24-hour incubation assays were performed (Figure 30) with and without plasma supplementation.

24-hour adhesion assay

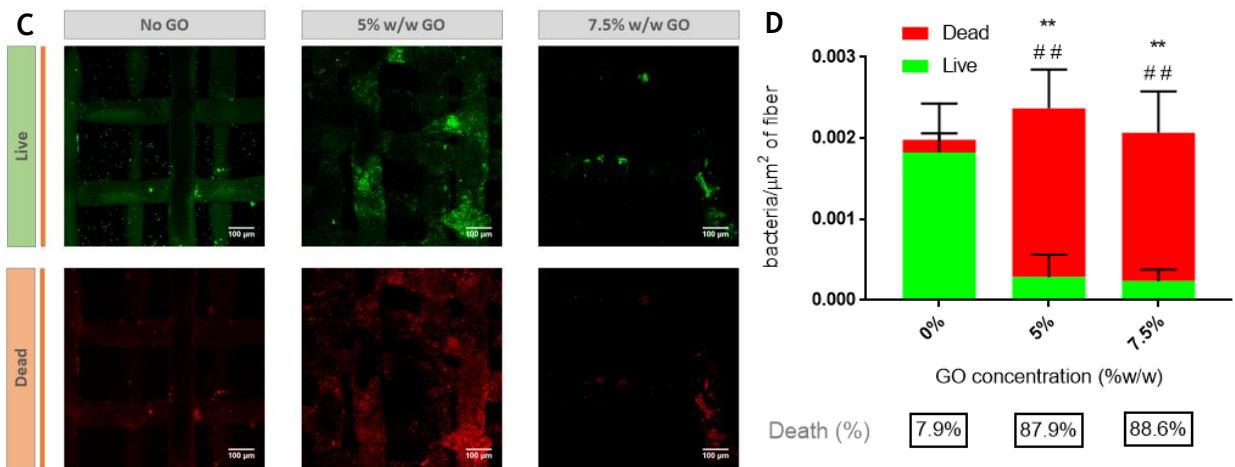
TSB without human plasma



* Differences in "Dead" bacteria, compared with control group (0%)

Differences in "Live" bacteria, compared with control group (0%)

TSB with 10% human plasma



* Differences in "Dead" bacteria, compared with control group (0%)

Differences in "Live" bacteria, compared with control group (0%)

Figure 30. *S. epidermidis* adhesion to PCL/GO scaffolds after 24h incubation in plasma-free TSB (A) and 10% plasma supplemented TSB (C). Live and dead bacteria are stained in green and red, respectively. Scale bar: 100 μm. B, D: Grouped graphs with number of live bacteria per μm² of fiber displayed in green and number of dead bacteria per μm² of fiber displayed in red. Statistically significant differences are indicated with */# (p ≤ 0.05), **/## (p ≤ 0.01), ***/### (p ≤ 0.001) and ****/#### (p ≤ 0.0001).

Graphs in Figure 30 (B and D) display consonant bacteria counting results in both assays, regardless of the medium supplementation. In the experiment using plasma-free TSB (B), percentages of dead bacteria found were close to 90% for both GO concentrations. Statistically significant differences in dead bacteria numbers were found only for 7.5% w/w GO (**), when compared to PCL without GO. On the other hand, statistical analysis revealed important variations in live bacteria numbers for both GO concentrations (####). Graph D (Figure 30) reflects that, for live and dead bacteria counts, statistically significant differences were present (** ##) concerning both GO concentrations when compared to PCL without GO. Percentages of dead bacteria were again approximately 90% for 5% w/w GO and 7.5% w/w GO.

When both plasma-free and supplemented TSB medium were used, death rates when GO was present were higher compared to PCL without GO and substantially higher than the ones found for same conditions in the 2-hour assays. These results allowed to conclude that the presence of GO has a noticeable time-dependent effect on bacterial activity, as bacteria are mostly dead after 24h of contact with GO-containing scaffolds. Confocal images supported this hypothesis, particularly when looking at the dead bacteria pictures, where their number drastically increased after 24h incubation with the presence of GO. Several authors described GO antibacterial effect as being time-dependent, particularly when GO is incorporated in a composite polymeric matrix. An *et al.*¹⁸² found significant differences in the antibacterial effect of GO in a PU/PLA/GO composite against *E. coli* and *S. aureus*, when comparing incubation times of 4 hours and 24 hours. In 4-hour incubation assays, 54% - 91% growth inhibition percentages were found, depending on GO concentration; whereas in 24-hour assays, 99% - 100% of inhibition was found for both bacterial species. GO antibacterial effects have been associated with either induced oxidative stress or bacteria physical disruption.¹⁸²

Noteworthy, some fluorescent (in both channels) aggregates were found in GO-containing scaffolds, with 5% w/w GO and 10% human plasma (Figure 30 C) being the condition in which this aspect was more noticeable. Firstly, GO autofluorescence was thought to be the reason, but given the size of these fluorescent aggregates, the hypothesis of a fiber defect or hole that retained staining dyes during washing steps was considered. As stated by Song *et al.*,¹⁶ GO-containing fibers are more prone to show protuberances and a rougher surface than pristine polymer fibers.

Considering 2-hour and 24-hour assays' results, GO-containing scaffolds revealed capable of causing substantial bacterial death in a contact time-dependent manner. This effect did not seem to be immediate, since 2-hour adhesion assessments showed low bacterial death percentages. Moreover, a GO concentration of 5% w/w seemed to be enough to produce the desired effects in all the performed assays.

All the experiments showed similar total bacteria concentrations in all groups, independently of GO presence. Therefore, a supposition of an anti-adherent effect promoted by GO was discarded. Graphene oxide appeared to act as a killing agent, rather than creating an antifouling surface.

Supplementation of bacterial growing media with human plasma did not affect experimental readouts, since the acquired images and sequential bacteria counts were similar, particularly in 24-hour adhesion assays.

2.3. *In vitro* biocompatibility of PCL/GO scaffolds

To evaluate PCL/GO scaffolds ability to promote mammalian cells attachment and growth, HFF-1 cells were seeded on the materials and fixed at two different time points: after 1 day and 7 days. Cells were stained and observed using Confocal microscopy.

Representative images of the scaffolds are presented in Figure 31, where it is possible to perceive cell growing and stretching between the 1st and the 7th day of culture, for all tested conditions. It is important to mention that fibroblasts are attached and projected along PCL fibers, not visible in these channels with the laser intensities used for cell visualization.

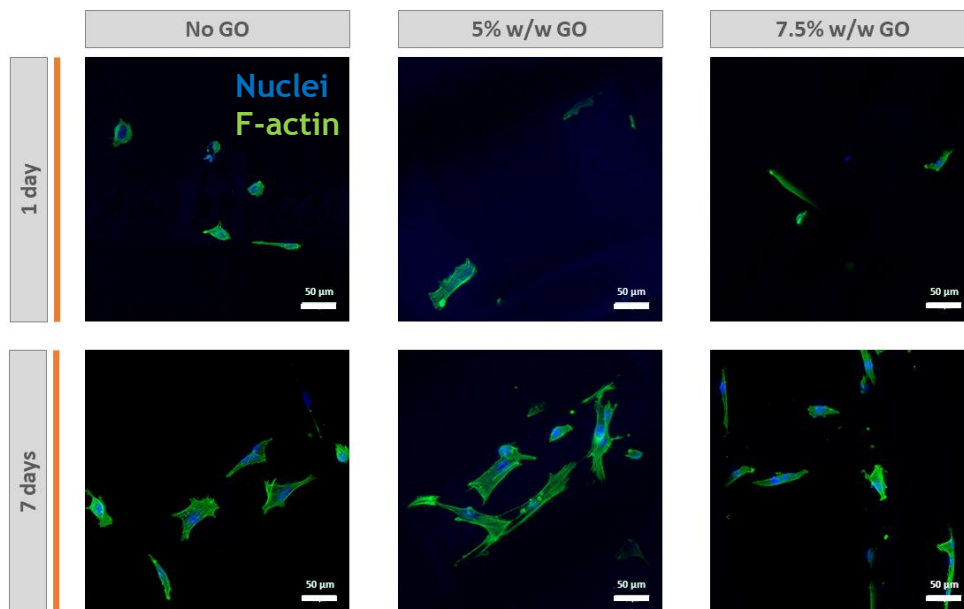


Figure 31. HFF-1 adhesion and growth in PCL scaffolds after 1 day and 7 days. DNA was stained with DAPI (3 μ g/mL) and F-actin was stained with Phalloidin (1:100). Images represent a 150 μ m volume z-stack projection. Scale bar: 50 μ m.

F-actin filaments' spreading after 7 days indicated cytoskeleton functionality, which plays an important role in cell mobility and contraction during division processes, with cells presenting a typical fibroblast-like morphology.¹⁶ 5% w/w GO seemed to be the condition in which adhesion and subsequent stretching were more accentuated, although all the scaffolds (PCL without GO and GO-containing PCL) allowed cell survival and growth.

In 7.5% w/w GO fibers, F-actin was less outstretched in some cells, although the difference was slight. Apparent toxicity effects were not perceived in any condition, which is supported by presumed stable incorporation of GO in this composite polymeric matrix, where GO release, and possible cytotoxicity, were not expected.

When combined with PCL, the hydrophilic nature of GO probably enhanced its wettability, its interaction with proteins of the supplemented medium and, therefore, its biocompatibility, as concluded by Yoon *et al.*²⁰¹ regarding PLGA/GO nanocomposite fibers biocompatibility. However, if the loading level of GO is too high, the GO may not 'lay' flat in the polymer matrix and thus the enhancement in cellular growth is not afforded.²⁰¹

Puppi *et al.*¹³⁶ observed that, at final phases of culturing (after 28 days), PCL scaffolds exhibited a nearly full cellular colonization of the available fiber surface by a wide continuous cell culture net. This behavior would be expectable in this case, if HFF-1 cells were cultured for longer periods in PCL and PCL/GO scaffolds, which could be further explored. Similar observations concerning cellular colonization were found in several studies with cells being cultured for relatively long periods (14 - 28 days).^{20,21,134,136}

3. PET/GO fibrous scaffolds

3.1. Wet-spinning combined with additive manufacturing

3.1.1. Parameters optimization

Table 5 depicts the results from solvent screening for PET, showing unsuccessful solvents in grey, moderately effective ones in yellow, reasonably good in light green and the best results in dark green.

In the presence of NaOH, the pH of ethylene glycol solution increased, and PET started to dissolve. However, since this process was extremely slow, temperature had to be increased to approximately 60°C. Even in these conditions, polymer complete dissolution was only observed after several days.

Regarding trifluoroacetic acid (TFA), a structural analogue of acetic acid (although stronger than acetic acid), it caused immediate pellet disintegration, with an observed effervescent effect, which might indicate an instant degradation rather than polymer dissolution.

Therefore, an increase of the pH, reducing the acidic character of the solvent, was tested by adding DCM. A mixture of TFA/DCM (proportion of 1:2) was able to apparently dissolve PET within approximately 12 hours at room temperature.

Table 5. Solvent screening for PET. Solubility was scored between (-), which represents total lack of solubility, and (++), which represents fast solubility. The solvents with best performances are displayed in green.


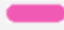





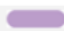
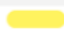
Solvents	PET solubility
chloroform	-
dimethylformamide	-
2-propanol	-
1,2-dichloroethane	-
o-xilene	-
nitrobenzene	-
phenol	-
tetrachlorethane	-
tetrahydrofuran	-
ethyl acetate	-
dichloromethane (DCM)	-
dimethyl sulfoxide	-
DCM + 1,4-dioxane	-
acetone	-
N-methyl-2-pyrrolidone	-
1,1,1,3,3,3-Hexafluoro-2-propanol	-
ethylene glycol	-
NaOH in ethylene glycol	+/-
trifluoroacetic acid (TFA)	+
TFA + DCM (1:2)	++

This TFA/DCM (1:2) solution was also suitable to fairly disperse graphene oxide (GO), as shown above in Graphene Oxide results section (Figure 21). After solvent selection, injectability tests were performed with different PET concentrations and varying needle internal diameter (ID range: 100-840 μm), as described in Table 6, since clogging was observed when the parameters previously set for PCL were tried. A solution of 7.5% w/v PET was completely impossible to pass through the previously chosen 170 μm needle. Consequently, PET concentration was substantially decreased until 1% w/v, and a large spectrum of IDs were tried.

A solution of 5 mg/mL GO without PET was firstly tested, to confirm that clogging was not being caused by graphene oxide sheets. Validating this assumption, it was observed that this GO solution flowed through all tips. A constant GO concentration of 10% w/w was fixed (representing 5 mg/mL of GO in 5% w/v PET solution) for further tested PET-containing solutions.

For the lowest polymer concentrations (1% and 2% w/v), despite the good injectability observed with both solutions flowing easily through a 200 μm tip, fiber formation was not possible, as PET concentration was insufficient to ensure fibers consistency, which instantly collapsed when injected in a coagulation bath.

Table 6. Injectability assessment for PET/GO dispersions with increasing amounts of PET. First column, without PET: a solution of 5 mg/mL GO was used. Last 5 columns: [GO]=10% w/w. Green boxes represent continuous flow; yellow boxes mean occasional clogging events; red boxes report total clogging.

G	Color	ID	No PET [GO]= 5mg/mL	[PET]= 1%w/v	[PET]= 2%w/v	[PET]= 3%w/v	[PET]= 4%w/v	[PET]= 5%w/v
18	 Green	840 μm	Green	White	White	White	White	White
20	 Pink	610 μm	Green	White	White	White	Green	Green
21	 Purple	510 μm	Green	White	White	White	Green	Green
22	 Blue	410 μm	Green	White	White	Green	Yellow	Yellow
23	 Orange	330 μm	Green	White	White	Yellow	White	White
25	 Red	250 μm	Green	White	White	White	Yellow	White
27	 Clear	200 μm	Green	Green	Green	White	Yellow	White
30	 Lavender	150 μm	Green	Green	Yellow	White	White	White
32	 Yellow	100 μm	Green	Yellow	Red	White	White	White

Among the highest (fiber-forming) PET concentrations (3-5% w/v), the best combination was found with 3% w/v PET and an ID of 410 μm (22G), using the established 10% w/w GO concentration.

Lastly, coagulation baths of PET non-solvents were tested. As illustrated in Table 7, water and NaOH 1M produced similar results, with an immediate solidification process that led to constant clogging. On the other hand, acetone, ethanol and ethyl ether revealed inability in keeping original fiber shape, partially dispersing the composite. Ethylene glycol, DCM and TFA/water (1:1) failed, since those are partial solvents for PET and, therefore, did not promote solidification.

TFA/water (1:2) and (1:3) allowed fast solidification without constant clogging, representing the best choices. Nevertheless, 1:3 ratio seemed more adequate, given that less solvent fraction (TFA) was present.

Table 7. Coagulation bath screening for PET. Light grey boxes (-): described behavior was not observed; grey boxes (+/-): described behavior was occasionally observed; dark grey (+) boxes: described behavior was frequently observed.

Coagulation baths (10 mL)	Immediate solidification (leads to clogging)	Original form maintenance (allows drawing)	Composite dissolution (leads to liquid dispersion)
water	+	+/-	-
NaOH 1M	+	+/-	-
acetone	-	-	+/-
ethanol	-	-	+/-
ethyl ether	-	-	+/-
ethylene glycol	-	-	+
dichloromethane	-	-	+
TFA/water (1:1)	-	-	+
TFA/water (1:2)	+/-	+	-
TFA/water (1:3)	+/-	+	-

A trial using a syringe pump and applying all the above mentioned fixed conditions, including TFA/water (1:3) as the coagulation bath, allowed the formation of “fiber-like” shapes, although their definition and diameter could not be compared to the ones obtained with polycaprolactone (Figure 32).



Figure 32. Printing trial of the 3% w/v PET and 10% w/w GO solution using TFA/water (1:3) as coagulation bath, a 410 μ m dispensing tip and a flow rate of 0.5mL/h.

Despite all the optimization process, the attempt to precisely deposit the composite fibers using a XYZ plotter failed, since proper design and consistency were not obtained.

Overall, additive manufacturing/wet-spinning was considered an inappropriate method for 3D printing of PET fibers. A different approach was therefore explored to incorporate GO in PET meshes, namely spraying a GO coating in commercially available fibers, rather than developing scaffold *de novo* fabrication techniques.

3.2. Spray coating

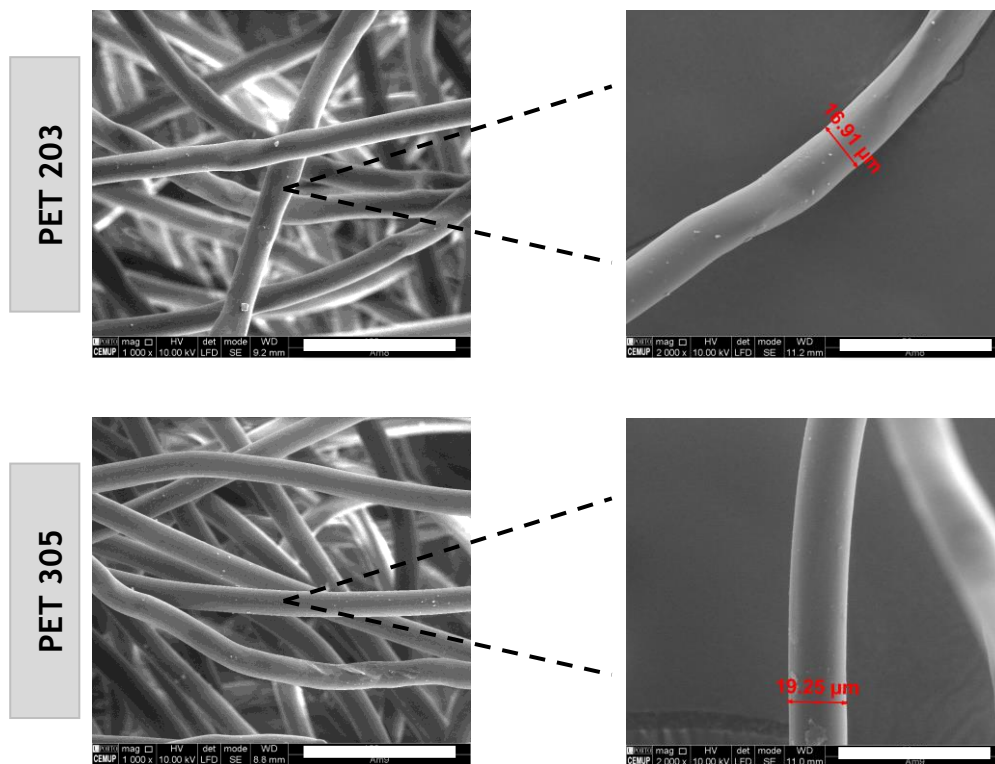


Figure 33. SEM images of commercially available electrospun PET meshes. Top: PET203; Bottom: PET305. Scale bar: 100 μm (on the left) and 50 μm (on the right).

Two different medical grade PET meshes were purchased: PET203 and PET305. These nonwoven fabrics with several biomedical applications were used as control materials and characterized by SEM (Figure 33) and Stereomicroscopy (Figure 34 - first column). SEM images showed randomly organized PET fibers, with approximate diameters of 17-19 μm.

After spray coating of these fabrics with GO-containing solutions, changes in materials' color (initially white) were macroscopically visible, since GO attributed them a light brown shade (Figure 34). PET meshes appeared to be homogeneously coated after drying. Nevertheless, circular samples were collected from the centered area with a 5 mm puncher.

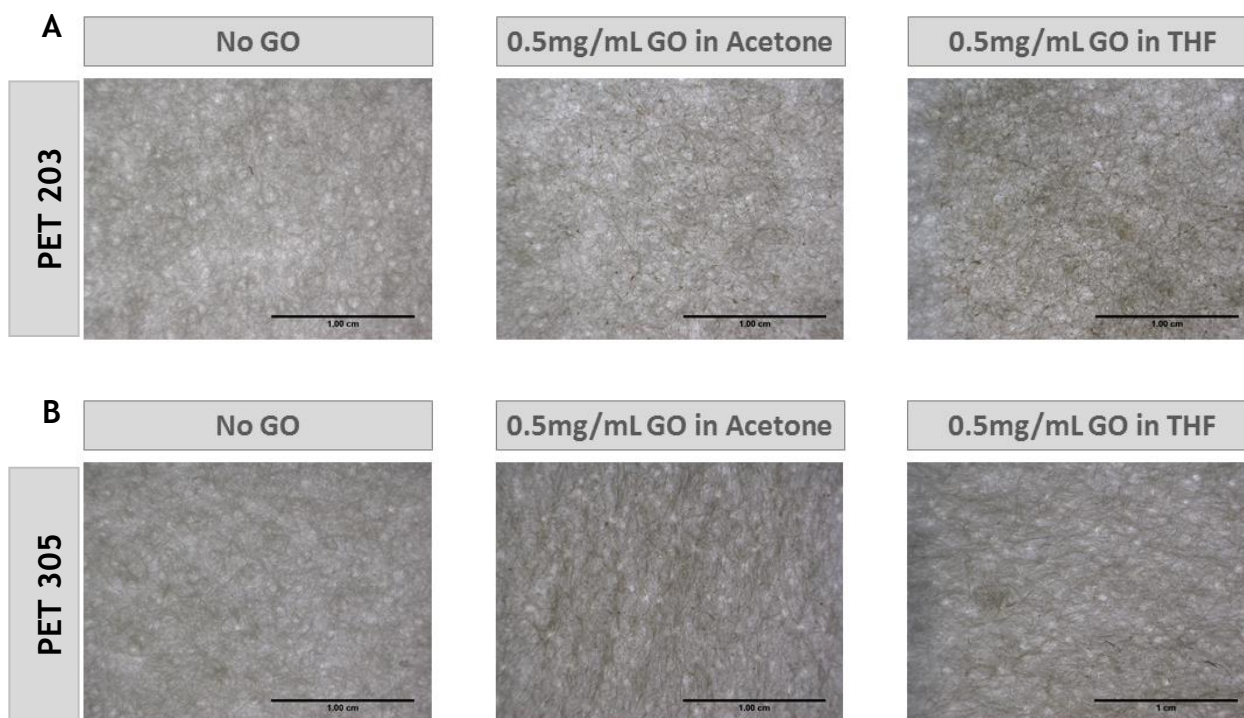


Figure 34. Stereomicroscope images of commercially available electrospun PET meshes before (left) and after spray coating with 0.5mg/mL of GO dispersed in acetone and THF. Row A: PET203; row B: PET305. Scale bar: 1cm.

To evaluate coating stability, coated scaffolds were washed as described in Chapter III and SEM images of the fibers were collected before and after washing (Figure 35). Both PET203 and PET305 exhibited GO exposure on the fibers surface before washing, confirming that GO-containing coating dispersions were properly sprayed on PET meshes.

After washing, PET203 fibers preserved their GO-coating regardless of the solvent used in its dispersion (acetone or THF) - Figure 35 (A). GO deposition was verified, and its distribution was similar before and after washing. Moreover, it was possible to trustingly conclude that the washing step was not removing the coating, since fibers displayed the same features after washing was performed. Few GO sheets or aggregates were found bonded to the fibers, creating a discontinuous and heterogeneously spread coating layer.

SEM analysis of PET305 is also shown in Figure 35 (B), and exhibits two distinct types of coated fibers: in some cases, GO deposition occurred similarly to what was described for PET203, with GO sheets landed on the fibers in a heterogeneous manner (e.g. after washing pictures for both acetone and THF solutions). In other cases, namely with 0.5 mg/mL of GO in THF before washing, a typically literature-described GO wrinkled layer was observed. Wrinkling occurs in GO sheets in the form of undulation as a consequence of the interactions between the adjacent individual GO sheets.²⁰²

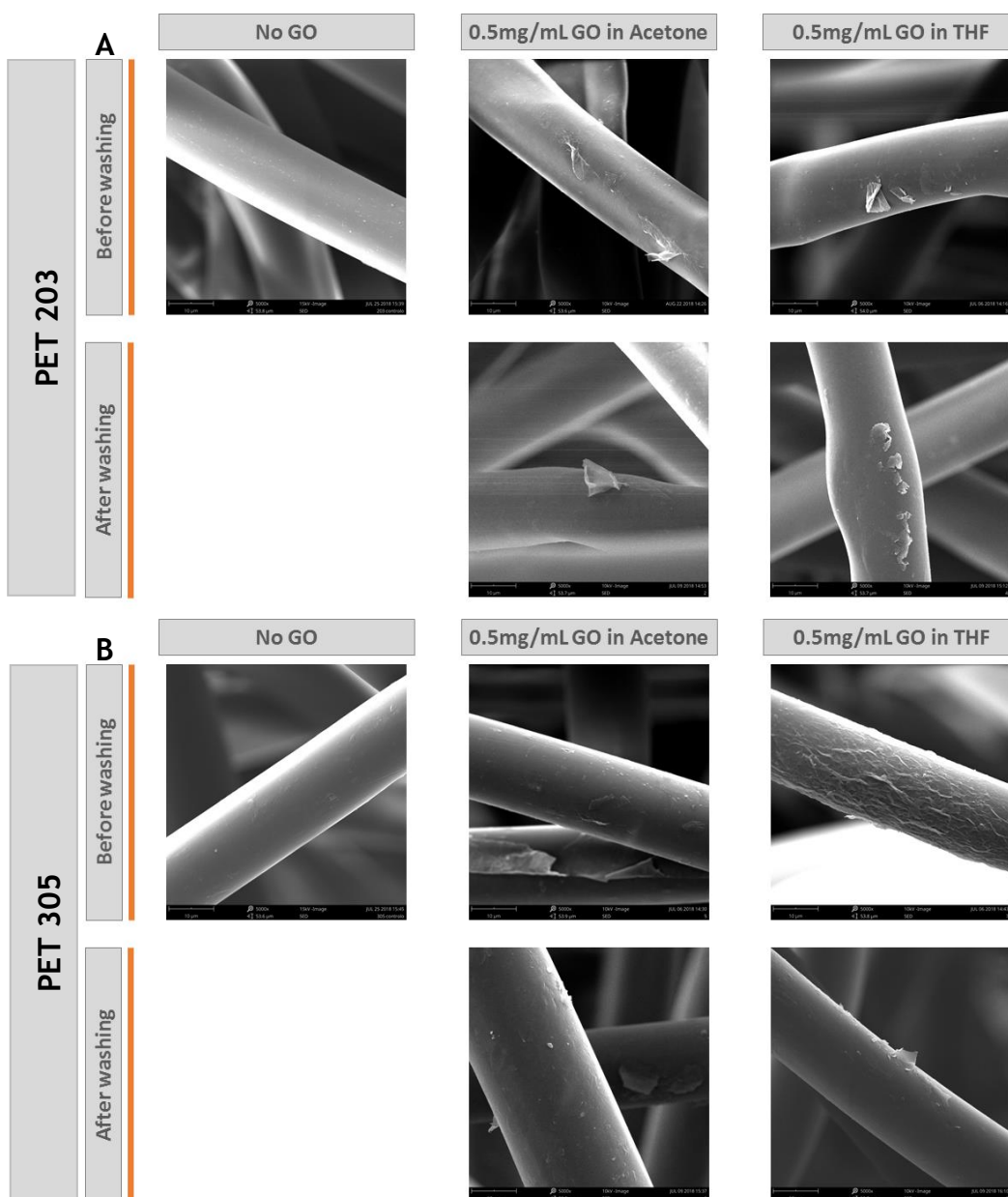


Figure 35. SEM images of PET without GO and GO-coated PET fibers before and after washing. Top panel A: PET203; bottom panel B: PET305. Scale bar: 10 μ m.

3.3. Antibacterial effect of GO-coated PET scaffolds

To explore the bactericidal effect of GO (in acetone/THF)-coated PET203/305 scaffolds, surface adhesion assays were performed for 24 hours using 10% human plasma supplemented TSB as bacterial growth media. Bacteria counting was performed through fibers' surface imaging using Confocal microscopy (Figure 36).

Regarding PET203, total bacteria number in the 0.5 mg/mL GO in THF scaffold was approximately 5 times lower than this number in the control. An anti-adhesive effect promoted by GO was observed, although this effect seemed to be solvent-dependent, as three times more bacteria were found in a coated scaffold with the same GO concentration dispersed in acetone. The theory of THF-caused toxicity was considered, but cell proliferation assays refuted it, as presented forward in this Chapter.

Regarding live/dead counts, most of the bacteria found in the PET scaffolds without GO were alive. Considering 0.5 mg/mL GO in acetone coating, the number of live bacteria lowered, accompanied by an increase in the number of dead bacteria. When the coating solution contained GO dispersed in THF, the number of dead bacteria was larger than the number found in uncoated fibers. On the other hand, very few live bacteria were found in this condition.

Death percentages of 5.1%, 43.8% and 65.4% were the calculated values for the uncoated, GO in acetone and GO in THF coated samples, respectively. The incorporation of graphene oxide in spray coatings proved to be a powerful way to kill adherent bacteria, with THF-containing coating causing the highest mortality rate.

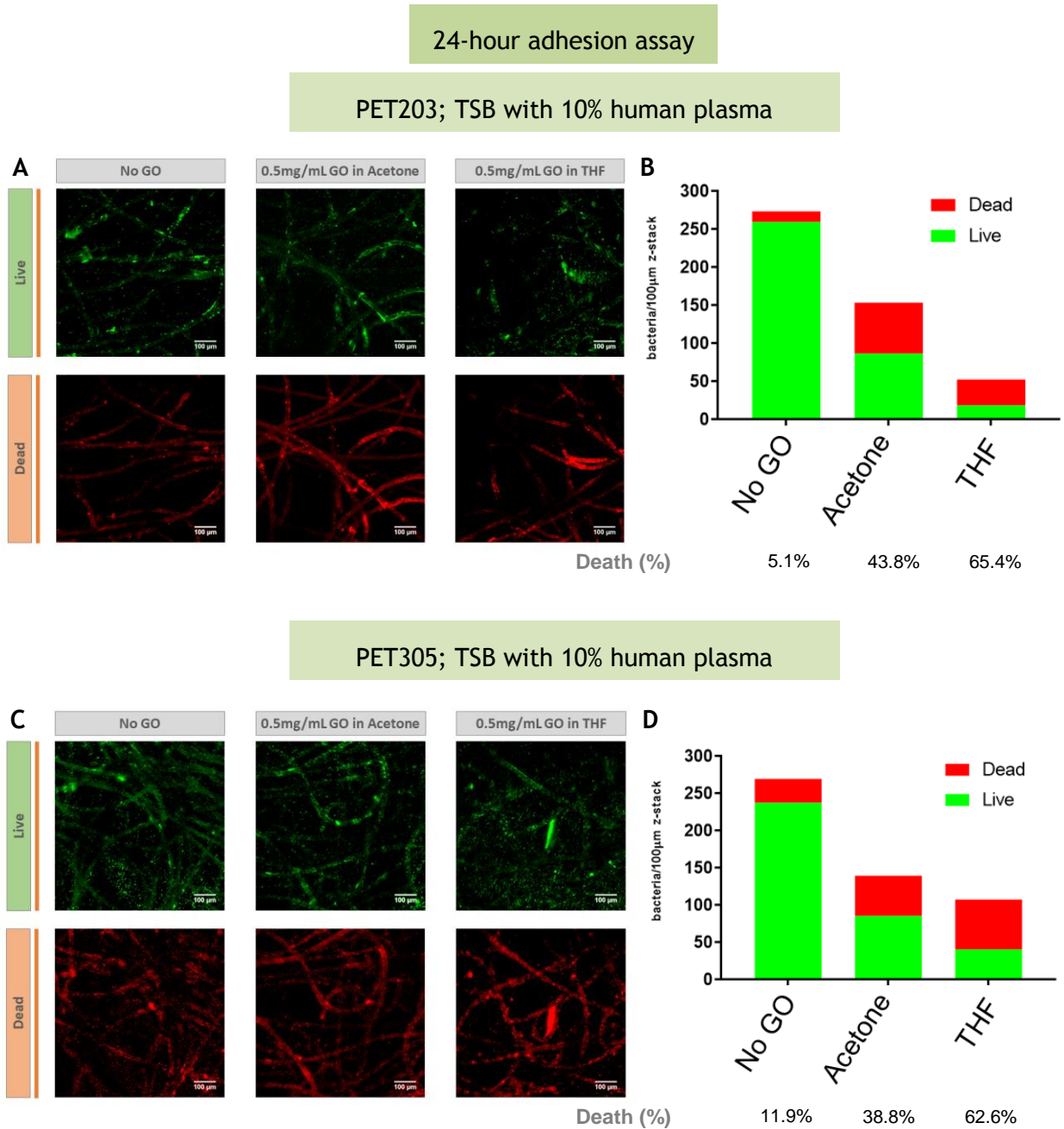


Figure 36. *S. epidermidis* adhesion to PET and GO-coated PET scaffolds (PET203 - A; PET305 - C) after 24h incubation in 10% plasma supplemented TSB. Live and dead bacteria are stained in green and red, respectively. Scale bar: 100 μm . B, D: Grouped graphs with number of live bacteria per μm^2 of fiber displayed in green and number of dead bacteria per μm^2 of fiber displayed in red.

Similar adhesion assay was performed in PET305 fibers - uncoated and GO-coated - (Figure 36 C and D), showing similar results. Tendencies regarding the number of live and dead bacteria in coated and uncoated fibers were maintained. Although the percentage of death in the uncoated PET305 was slightly higher (11.9%) when compared to uncoated PET203, treated PET305 scaffolds presented extremely resembling mortality (38.8% for GO in acetone and 62.6% for GO in THF) when compared to coated PET203 scaffolds. Total bacteria numbers also followed the same bias, except for 0.5 mg/mL GO in THF condition, in which the total count doubled, compared to PET203 equivalent result.

Mangadlao and co-workers¹¹ also found a higher death percentage (40%) concerning *E. coli* in contact with GO-coated PET (1 layer), when compared to pristine PET, which caused only 13% of bacterial death. These percentages correspond to an exposure time of 2 hours and coated PET was produced by Langmuir-Blodgett (LB) technique.¹¹ Despite these differences in protocol, Mangadlao and other authors^{9,187,188} have described GO coatings as antimicrobial agents.

Comparing these results with the ones obtained for PCL/GO composite scaffolds, although the composites showed higher bacterial death, GO coatings exhibited a combination of anti-adherent and killing effects. Surfaces with the ability to switch reversibly between possessing bactericidal and anti-biofouling properties have been already reported in the literature.²⁰³

In fact, GO concentration included in these coatings (0.5 mg/mL) is considerably lower, when compared to 7.5% w/w (e.g.) used in the composites. On the other hand, controlling the GO concentration that is exposed at the fibers surface, thus directly contacting with bacteria and cells, is only possible with spray coating. When a composite is 3D printed, although the GO concentration in the initial solution is known, the amount that becomes exposed is difficult to tune.

Spray coating of GO in acetone/THF dispersions in PET203 and PET305 showed similar results in coating stability tests and antimicrobial activity assessments. Therefore, PET203 was the selected material for further cytocompatibility testing. Besides being the most used material in Health Facilities, PET203 caused lower percentage of bacterial death in the uncoated scaffolds.

3.4. *In vitro* biocompatibility of GO-coated PET scaffolds

To assess PET fibers ability to promote cell attachment, HFF-1 cells were seeded and fixed at two different time points: after 1 day and 7 days. Cells were stained, and representative images are displayed in Figure 37, qualitatively showing a higher cell number after 7 days for both coated and uncoated fibers.

PET's autofluorescence at lower wavelengths interfered with the identification of DNA by DAPI, reducing nuclei contrast. However, it was still possible to distinguish cells nuclei from the fibers. Phalloidin staining was successful, allowing to observe F-actin projections along the fibers.

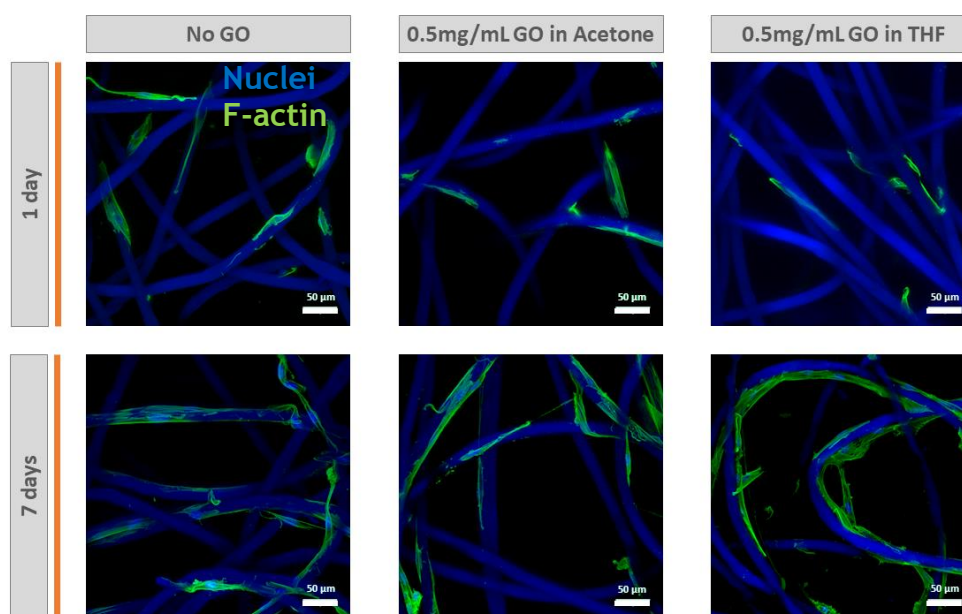


Figure 37. HFF-1 adhesion and growth in PET203 fibers after 1 day and 7 days. DNA was stained with DAPI (3 μ g/mL) and F-actin was stained with Phalloidin (1:100). Images represent a 150 μ m volume z-stack projection. Scale bar: 50 μ m.

In the first day after seeding, cells cytoskeleton was shrunken, equally in uncoated and GO-coated PET fibers. The following 6 days were marked by a notorious actin filaments' stretching, hence indicating scaffolds propensity to adhere cells and support colonization. Electrospun fibers offer topological structure features similar to the native extracellular matrix (ECM), thus providing an excellent environment for cell growth.²⁰⁴ This was in fact observed, since fibroblasts were notoriously stretched along PET fibers, uncoated and GO-coated, after 7 days.

Even though fibroblasts spreading was observed after 7 days in all cases, THF-dispersed GO-coated PET fibers sheltered the most widely spread cells. Therefore, former suspicions of THF toxicity were refuted. Additionally, the presence of GO did not inhibit HFF-1 attachment, reaffirming GO cytocompatibility and its cell adhesion facilitator character.

Despite being commonly described as cytocompatible in several papers, lack of biocompatibility of PET velour (Dacron®) has been reported, evoking an inflammatory response rather than supporting tissue ingrowth.³⁴ However, such discouragement in cellular growth caused by uncoated PET was not observed in this work.

Facing an uncertain GO distribution disclosed by previously shown SEM analysis, new spray coating conditions were studied: GO concentration was incremented, and water was used as the GO dispersive agent.

For that, solutions of 0,5 mg/mL (for comparison), 1 mg/mL and 2 mg/mL GO concentrations were prepared. These solutions were sprayed in PET203 and PET305 meshes, although PET203 was the selected material for further coating stability testing (Figure 39 Annexes). Using water holds an important advantage, representing a more innocuous alternative, compared to harmful solvents such as acetone and THF.

Chapter V: Conclusion and Future Considerations

1. Conclusion

Pristine graphite was successfully oxidized to GO using MHM, confirmed by an increase in the atomic percentage of O 1s (from 8% to 30%), with the introduction of several Oxygen-containing chemical groups, revealed by XPS analysis.

Acetone, THF, water and TFA/DCM (1:2) were able to disperse GO, producing homogeneous dispersions after ultrasonication, contrarily to chloroform, which was not suitable to disperse GO.

Wet-spinning combined with additive manufacturing allowed the production of well-defined PCL/GO composite fibers with average diameters of 100 μm . SEM analysis of the produced fibers revealed that a concentration of 5% w/w of GO was apparently sufficient to expose GO sheets at the surface of the composite fibers.

Antimicrobial properties of PCL/GO composite 3D-organized fibrous scaffolds were assessed for the first time, revealing GO time-dependent bactericidal effect. Moreover, the presence of human plasma did not cause relevant changes on the results regarding bactericidal potential after 24 hours.

In vitro biocompatibility evaluation showed that PCL/GO scaffolds allowed cell adhesion and spreading along the fibers during 7 days of culture.

Wet-spinning combined with AM was not suitable to produce PET/GO composite fibers, as printing conditions were inappropriate, despite optimization.

Spray coating of PET commercial scaffolds with GO dispersions revealed to be an efficient approach for GO incorporation in fibers. Although GO coatings showed heterogeneous distribution along the fibers, coatings stability was ensured.

Antimicrobial effect of GO-coated PET scaffolds was found to be derived from a combination of anti-adherent and bactericidal surface properties, leading to decreased amounts of adherent bacteria and increased bacterial death in GO-containing fibers.

HFF-1 adhesion and stretching was observed along the studied PET fibers, uncoated and GO-coated, with F-actin production being visually confirmed.

Globally, GO-containing fibrous scaffolds developed in this work promoted bacteria death, while inducing cell adhesion. These features demonstrate the potential of GO incorporation in polymer fibrous scaffolds for medical implantation purposes.

2. Future Considerations

The study developed in this thesis clarified several aspects regarding scaffolds fabrication techniques, GO antimicrobial potential and GO biocompatible character. However, a lot of questions still need to be answered and future work can be suggested.

Particularly regarding the assays performed and the methods used in this work, other studies would be interesting to explore. Different concentrations of GO could be incorporated in the scaffolds, increasing the range of tested GO loadings and assessing its influence on antimicrobial/biocompatible behavior.

Bacteria staining and counting could be complemented with metabolic activity assessments or by culturing bacteria detached from the scaffolds and investigating their viability.

Concerning wet-spinning combined with AM for scaffolds production, patterns (3D models) and fiber diameters could be varied, and their influence in antimicrobial/biocompatible properties assessed.

The spray-coating method performed could be further improved, since coatings were not uniform, with areas showing GO aggregation and different roughness being observed between fibers coated in similar conditions. Together with GO concentration, the applied coating volume (currently 6 mL) can be increased. The use of water as dispersing agent of GO for PET203 coatings showed to be very promising, and therefore the antibacterial properties and cytocompatibility of these scaffolds should be explored.

Besides the aforementioned specific improvements and optimization for the techniques described in this thesis, broader future perspectives can be proposed.

2.1. Exploring different GBMs

To deeper explore the importance of the selected GBM in the observed antimicrobial and cytocompatible behaviors, other GBMs can be tested, namely rGO, GNP and GNPOx. Thus, the influence of GBMs oxidation degree and exfoliation level would be investigated. Moreover, particularly regarding GNP and GNPOx, the lateral size of the materials can also be varied, as GNPs with diverse dimensions are commercially available (e.g. 5 μm and 15 μm).

2.2. Testing on different bacteria

Besides *S. epidermidis*, it would be interesting to test GO-containing scaffolds effects towards several other bacteria involved in implantable device-related infections, namely *S. aureus*, *E. coli* or *P. aeruginosa*.

2.3. Melt-Electro-Writing to produce PET/GO fibrous scaffolds

Since wet spinning combined with AM revealed unsuitable for the production of PET/GO composite 3D-oriented scaffolds, MEW could be envisaged as a technique to produce micrometric-range fibers. Although recent, this method has shown promising results in the production of 3D-organized fibrous structures from an initial composite melt. A collaboration has been initiated with a group with expertise on MEW in UMC Utrecht, in the Netherlands, for the production of these scaffolds, which will then be evaluated in our group regarding antibacterial properties and biocompatibility.

References

1. Novoselov, K. S. *et al.* Electric Field Effect in Atomically Thin Carbon Films. *Science* (80-.). **306**, 666-669 (2004).
2. Feng, R. *et al.* In situ synthesis of poly(ethylene terephthalate)/graphene composites using a catalyst supported on graphite oxide. *J. Mater. Chem.* **21**, 3931 (2011).
3. Jakus, A. E. *et al.* Three-dimensional printing of high-content graphene scaffolds for electronic and biomedical applications. *ACS Nano* **9**, 4636-4648 (2015).
4. Das, T. K. & Prusty, S. Graphene-Based Polymer Composites and Their Applications. *Polym. Plast. Technol. Eng.* **52**, 319-331 (2013).
5. Yang, Y., Asiri, A. M., Tang, Z., Du, D. & Lin, Y. Graphene based materials for biomedical applications. *Mater. Today* **16**, 365-373 (2013).
6. Pinto, A. M., Gonçalves, I. C. & Magalhães, F. D. Graphene-based materials biocompatibility: A review. *Colloids Surfaces B Biointerfaces* **111**, 188-202 (2013).
7. Pang, L., Dai, C., Bi, L., Guo, Z. & Fan, J. Biosafety and Antibacterial Ability of Graphene and Graphene Oxide In Vitro and In Vivo. *Nanoscale Res. Lett.* **12**, 564 (2017).
8. Chen, Q. *et al.* 3D printing biocompatible polyurethane/poly(lactic acid)/graphene oxide nanocomposites: Anisotropic properties. *ACS Appl. Mater. Interfaces* **9**, 4015-4023 (2017).
9. Yadav, N. *et al.* Graphene Oxide-Coated Surface: Inhibition of Bacterial Biofilm Formation due to Specific Surface-Interface Interactions. *ACS Omega* **2**, 3070-3082 (2017).
10. Perreault, F., De Faria, A. F., Nejati, S. & Elimelech, M. Antimicrobial Properties of Graphene Oxide Nanosheets: Why Size Matters. *ACS Nano* **9**, 7226-7236 (2015).
11. Mangadla, J. D. *et al.* On the antibacterial mechanism of graphene oxide (GO) Langmuir-Blodgett films. *Chem. Commun.* **51**, 2886-2889 (2015).
12. Pinto, A. M. *et al.* Smaller particle size and higher oxidation improves biocompatibility of graphene-based materials. *Carbon N. Y.* **99**, 318-329 (2016).
13. Gomes, R. N. *et al.* Antimicrobial graphene nanoplatelets coatings for silicone catheters. *Carbon N. Y.* **139**, 635-647 (2018).
14. Liu, S. *et al.* Antibacterial Activity of Graphite, Graphite Oxide, Graphene Oxide, and Reduced Graphene Oxide: Membrane and Oxidative Stress. *ACS Nano* **5**, 6971-6980 (2011).
15. Henriques, P. C., Borges, I., Pinto, A. M., Magalhães, F. D. & Gonçalves, I. C. Fabrication and antimicrobial performance of surfaces integrating graphene-based materials. *Carbon N. Y.* **132**, 709-732 (2018).
16. Song, J. *et al.* The preparation and characterization of polycaprolactone/graphene oxide biocomposite nanofiber scaffolds and their application for directing cell behaviors. *Carbon N. Y.* **95**, 1039-1050 (2015).
17. Wei, X. *et al.* 3D Printable Graphene Composite. *Sci. Rep.* **5**, 1-7 (2015).
18. Wang, W. *et al.* Enhancing the Hydrophilicity and Cell Attachment of 3D Printed PCL/Graphene Scaffolds for Bone Tissue Engineering. *Mater. (Basel, Switzerland)* **9**, (2016).

19. Mota, C., Puppi, D., Dinucci, D., Gazzarri, M. & Chiellini, F. Additive manufacturing of star poly(ϵ -caprolactone) wet-spun scaffolds for bone tissue engineering applications. *J. Bioact. Compat. Polym.* **28**, 320-340.
20. Dini, F. *et al.* Tailored star poly (ϵ -caprolactone) wet-spun scaffolds for in vivo regeneration of long bone critical size defects. *J. Bioact. Compat. Polym.* **31**, 15-30 (2016).
21. Puppi, D. *et al.* Additive manufacturing of wet-spun polymeric scaffolds for bone tissue engineering. *Biomed. Microdevices* **14**, 1115-1127 (2012).
22. Francolini, I. *et al.* Antifouling polyurethanes to fight device-related staphylococcal infections: synthesis, characterization, and antibiofilm efficacy. *Pathog. Dis.* **70**, 401-407 (2014).
23. Darouiche, R. O. & Darouiche, R. O. Device-Associated Infections: A Macroproblem that Starts with Microadherence. *Clin. Infect. Dis.* **33**, 1567-1572 (2001).
24. Rimondini, L., Fini, M. & Giardino, R. The microbial infection of biomaterials: A challenge for clinicians and researchers. A short review. *J. Appl. Biomater. Biomech.* **3**, 1-10.
25. Gristina, A. G. Biomaterial-centered infection: microbial adhesion versus tissue integration. *Science* **237**, 1588-95 (1987).
26. Subbiahdoss, G., Grijpma, D. W., Van Der Mei, H. C., Busscher, H. J. & Kuijper, R. Microbial biofilm growth versus tissue integration on biomaterials with different wettabilities and a polymer-brush coating. *J. Biomed. Mater. Res. - Part A* **94**, 533-538 (2010).
27. Illingworth, B. L., Tweden, K., Schroeder, R. F. & Cameron, J. D. In vivo efficacy of silver-coated (Silzone) infection-resistant polyester fabric against a biofilm-producing bacteria, *Staphylococcus epidermidis*. *J. Heart Valve Dis.* **7**, 524-30 (1998).
28. Durand, B. & Marchand, C. *Smart features in fibrous implantable medical devices. Smart Textiles and their Applications* 257-307 (2016).
29. Yoshimoto, H., Shin, Y. M., Terai, H. & Vacanti, J. P. A biodegradable nanofiber scaffold by electrospinning and its potential for bone tissue engineering. *Biomaterials* **24**, 2077-2082 (2003).
30. Koepsell, L., Zhang, L., Neufeld, D., Fong, H. & Deng, Y. Electrospun Nanofibrous Polycaprolactone Scaffolds for Tissue Engineering of Annulus Fibrosus. *Macromol. Biosci.* **11**, 391-399 (2011).
31. Panseri, S. *et al.* Electrospun micro- and nanofiber tubes for functional nervous regeneration in sciatic nerve transections. *BMC Biotechnol.* **8**, 39 (2008).
32. Veleirinho, B. *et al.* Foreign Body Reaction Associated with PET and PET/Chitosan Electrospun Nanofibrous Abdominal Meshes. *PLoS One* **9**, e95293 (2014).
33. Schreuders, P. D., Salthouse, T. N. & von Recum, A. F. Normal wound healing compared to healing within porous Dacron implants. *J. Biomed. Mater. Res.* **22**, 121-135 (1988).
34. Walboomers, F., Paquay, Y. C. G. J. & Jansen, J. A. *Perit. Dial. Int.* **21**, 254-262.
35. Stratton, S., Shelke, N. B., Hoshino, K., Rudraiah, S. & Kumbar, S. G. Bioactive polymeric scaffolds for tissue engineering. *Bioact. Mater.* **1**, 93-108 (2016).
36. Xie, J. *et al.* Nerve Guidance Conduits Based on Double-Layered Scaffolds of Electrospun Nanofibers for Repairing the Peripheral Nervous System. *ACS Appl. Mater. Interfaces* **6**, 9472-9480 (2014).
37. Zhang, W. *et al.* Porous Silk Scaffolds for Delivery of Growth Factors and Stem Cells to Enhance Bone Regeneration. *PLoS One* **9**, e102371 (2014).
38. Venugopal, J., Ma, L., Yong, T. & Ramakeishna, S. In vitro study of smooth muscle cells on polycaprolactone and collagen nanofibrous matrices. *Cell Biol. Int.* **29**, 861-867 (2005).
39. Moncrief, J. W. *et al.* Reduction in peritonitis incidence in continuous ambulatory peritoneal dialysis with a new catheter and implantation technique. *Perit. Dial. Int.* **13 Suppl 2**, S329-31 (1993).

40. Metzger, A. Polyethylene Terephthalate and the Pillar™ Palatal Implant: Its Historical Usage and Durability in Medical Applications. *Biomed Eng* 11:301-306 (1976).
41. Falagas, M. E. & Kasiakou, S. K. Mesh-related infections after hernia repair surgery. *Clin. Microbiol. Infect.* **11**, 3-8 (2005).
42. O'Toole, G., Kaplan, H. B. & Kolter, R. Biofilm Formation as Microbial Development. *Annu. Rev. Microbiol.* **54**, 49-79 (2000).
43. Büttner, H., Mack, D. & Rohde, H. Structural basis of Staphylococcus epidermidis biofilm formation: mechanisms and molecular interactions. *Front. Cell. Infect. Microbiol.* **5**, 14 (2015).
44. Vuong, C. & Otto, M. Staphylococcus epidermidis infections. *Microbes Infect.* **4**, 481-9 (2002).
45. Rupp, M. E. & Archer, G. L. Coagulase-negative staphylococci: pathogens associated with medical progress. *Clin. Infect. Dis.* **19**, 231-43; quiz 244-5 (1994).
46. Ratner, B. D. *Biomaterials science: an introduction to materials in medicine*. Elsevier Academic Press (2004).
47. Rupp, M. E., Ulphani, J. S., Fey, P. D., Bartscht, K. & Mack, D. Characterization of the importance of polysaccharide intercellular adhesin/hemagglutinin of Staphylococcus epidermidis in the pathogenesis of biomaterial-based infection in a mouse foreign body infection model. *Infect. Immun.* **67**, 2627-32 (1999).
48. Galdbart, J., Allignet, J., Tung, H., Rydén, C. & El Solh, N. Screening for *Staphylococcus epidermidis* Markers Discriminating between Skin-Flora Strains and Those Responsible for Infections of Joint Prostheses. *J. Infect. Dis.* **182**, 351-355 (2000).
49. Azimi, B., Nourpanah, P., Rabiee, M. & Arbab, S. Poly (ϵ -caprolactone) Fiber: An Overview. *J. Eng. Fiber. Fabr.* **9**, (2014).
50. Sousa, I., Mendes, A., Pereira, R. F. & Bártolo, P. J. Collagen surface modified poly(ϵ -caprolactone) scaffolds with improved hydrophilicity and cell adhesion properties. *Mater. Lett.* **134**, 263-267 (2014).
51. Mondal, D., Griffith, M. & Venkatraman, S. S. Polycaprolactone-based biomaterials for tissue engineering and drug delivery: Current scenario and challenges. *Int. J. Polym. Mater. Polym. Biomater.* **65**, 255-265 (2016).
52. Labet, M. & Thielemans, W. Synthesis of polycaprolactone: a review. *Chem. Soc. Rev.* **38**, 3484 (2009).
53. Woodruff, M. A. & Hutmacher, D. W. The return of a forgotten polymer—Polycaprolactone in the 21st century. *Prog. Polym. Sci.* **35**, 1217-1256 (2010).
54. Sarasam, A. & Madihally, S. Characterization of chitosan-polycaprolactone blends for tissue engineering applications. *Biomaterials* **26**, 5500-5508 (2005).
55. Malikmammadov, E., Tanir, T. E., Kiziltay, A., Hasirci, V. & Hasirci, N. PCL and PCL-based materials in biomedical applications. *J. Biomater. Sci. Polym. Ed.* **29**, 863-893 (2018).
56. Sun, H., Mei, L., Song, C., Cui, X. & Wang, P. The in vivo degradation, absorption and excretion of PCL-based implant. *Biomaterials* **27**, 1735-1740 (2006).
57. Peña, J., Corrales, T., Izquierdo-Barba, I., Doadrio, A. L. & Vallet-Regí, M. Long term degradation of poly(ϵ -caprolactone) films in biologically related fluids. *Polym. Degrad. Stab.* **91**, 1424-1432 (2006).
58. Joshi, P. & Madras, G. Degradation of polycaprolactone in supercritical fluids. *Polym. Degrad. Stab.* **93**, 1901-1908 (2008).
59. De Kesel, C., Wauven, C. V. & David, C. Biodegradation of polycaprolactone and its blends with poly(vinylalcohol) by micro-organisms from a compost of house-hold refuse. *Polym. Degrad. Stab.* **55**, 107-113 (1997).
60. Chen, D. ., Bei, J. . & Wang, S. . Polycaprolactone microparticles and their biodegradation. *Polym. Degrad. Stab.* **67**, 455-459 (2000).
61. Chandra, R. & Rustgi, R. Biodegradable polymers. *Prog. Polym. Sci.* **23**, 1273-1335 (1998).
62. Lam, C. X., Teoh, S. H. & Hutmacher, D. W. Comparison of the degradation of polycaprolactone and polycaprolactone-(β -tricalcium phosphate) scaffolds in alkaline medium. *Polym. Int.* **56**, 718-728 (2007).

63. Ikada, Y. & Tsuji, H. Biodegradable polyesters for medical and ecological applications. *Macromol. Rapid Commun.* **21**, 117-132 (2000).
64. Sinha, V. R., Bansal, K., Kaushik, R., Kumria, R. & Trehan, A. Poly- ϵ -caprolactone microspheres and nanospheres: an overview. *Int. J. Pharm.* **278**, 1-23 (2004).
65. Gross, R. A. & Kalra, B. Biodegradable polymers for the environment. *Science* **297**, 803-7 (2002).
66. Woodward, S. C., Brewer, P. S., Moatamed, F., Schindler, A. & Pitt, C. G. The intracellular degradation of poly(ϵ -caprolactone). *J. Biomed. Mater. Res.* **19**, 437-444 (1985).
67. Guarino, V., Gentile, G., Sorrentino, L. & Ambrosio, L. in *Encyclopedia of Polymer Science and Technology* 1-36 (2017).
68. Manea, L. R., Hristian, L., Leon, A. L. & Popa, A. Recent advances of basic materials to obtain electrospun polymeric nanofibers for medical applications. *IOP Conf. Ser. Mater. Sci. Eng.* **145**, 032006 (2016).
69. Jensen, J. *et al.* Surface-modified functionalized polycaprolactone scaffolds for bone repair: *In vitro* and *in vivo* experiments. *J. Biomed. Mater. Res. Part A* **102**, 2993-3003 (2014).
70. Bassi, A. K., Gough, J. E., Zakikhani, M. & Downes, S. The Chemical and Physical Properties of Poly(ϵ -caprolactone) Scaffolds Functionalised with Poly(vinyl phosphonic acid-co-acrylic acid). *J. Tissue Eng.* **2011**, 615328 (2011).
71. Hutmacher, D. W. *et al.* Mechanical properties and cell cultural response of polycaprolactone scaffolds designed and fabricated via fused deposition modeling. *J. Biomed. Mater. Res.* **55**, 203-216 (2001).
72. Ceretti, E., Ginestra, P., Neto, P. I., Fiorentino, A. & Silva, D. Multi-layered scaffolds production via Fused Deposition Modeling (FDM) using an open source 3D printer: process parameters optimization for dimensional accuracy and design reproducibility. *Procedia CIRP* **65**, 13-18 (2017).
73. Powell, H. M. & Boyce, S. T. Engineered Human Skin Fabricated Using Electrospun Collagen-PCL Blends: Morphogenesis and Mechanical Properties. *Tissue Eng. Part A* **15**, 2177-2187 (2009).
74. Venugopal, J. & Ramakrishna, S. Biocompatible Nanofiber Matrices for the Engineering of a Dermal Substitute for Skin Regeneration. *Tissue Eng.* **11**, 847-854 (2005).
75. Li, W.-J. *et al.* A three-dimensional nanofibrous scaffold for cartilage tissue engineering using human mesenchymal stem cells. *Biomaterials* **26**, 599-609 (2005).
76. Baker, S. R., Banerjee, S., Bonin, K. & Guthold, M. Determining the mechanical properties of electrospun poly- ϵ -caprolactone (PCL) nanofibers using AFM and a novel fiber anchoring technique. *Mater. Sci. Eng. C* **59**, 203-212 (2016).
77. Scaffaro, R. *et al.* Combining in the melt physical and biological properties of poly(caprolactone) and chlorhexidine to obtain antimicrobial surgical monofilaments. *Appl. Microbiol. Biotechnol.* **97**, 99-109 (2013).
78. Xiang, P., Li, M., Zhang, C., Chen, D. & Zhou, Z. Cytocompatibility of electrospun nanofiber tubular scaffolds for small diameter tissue engineering blood vessels. *Int. J. Biol. Macromol.* **49**, 281-288 (2011).
79. Lee, S. J. *et al.* Development of a composite vascular scaffolding system that withstands physiological vascular conditions. *Biomaterials* **29**, 2891-2898 (2008).
80. Ramírez-Agudelo, R. *et al.* Hybrid nanofibers based on poly-caprolactone/ gelatin/ hydroxyapatite nanoparticles-loaded Doxycycline: Effective anti-tumoral and antibacterial activity. *Mater. Sci. Eng. C* **83**, 25-34 (2018).
81. Ladd, M. R., Lee, S. J., Stitzel, J. D., Atala, A. & Yoo, J. J. Co-electrospun dual scaffolding system with potential for muscle-tendon junction tissue engineering. *Biomaterials* **32**, 1549-1559 (2011).
82. Ciardelli, G. *et al.* Blends of Poly-(ϵ -caprolactone) and Polysaccharides in Tissue Engineering Applications. *Biomacromolecules* **6**, 1961-1976 (2005).
83. Puskas, J. E. & Chen, Y. Biomedical Application of Commercial Polymers and Novel Polyisobutylene-Based Thermoplastic Elastomers for Soft Tissue Replacement. *Biomacromolecules* **5**(4), 1141-54 (2004).

84. Bronzino, J. D. *The Biomedical Engineering Handbook* (2000).
85. Harper, C. A. *Modern Plastics Handbook*. (2000).
86. PET Resin Association. About PET | PETRA: Information on the Use, Benefits & Safety of PET Plastic. Available at: <http://www.petresin.org/aboutpet.asp>. (Accessed: 29th January 2018).
87. Khan, W. *et al. Implantable Medical Devices*. **2**.
88. Greenwald, D., Shumway, S., Albear, P. & Gottlieb, L. Mechanical comparison of 10 suture materials before and after in vivo incubation. *J. Surg. Res.* **56**, 372-377 (1994).
89. Feldman, D. S., Hultman, S. M., Colaizzo, R. S. & von Recum, A. F. Electron microscope investigation of soft tissue ingrowth into Dacron® velour with dogs. *Biomaterials* **4**, 105-111 (1983).
90. Tilney, N. L. & Boor, P. J. Host Response to Implanted Dacron Grafts: A Comparison Between Mesh and Velour. *Arch. Surg.* **110**, 1469-1472 (1975).
91. Rahman, M. Degradation of Polyesters in Medical Applications. (2012).
92. Homsy, C. A., McDonald, K. E., Akers, W. W., Short, C. & Freeman, B. S. Surgical suture-Canine tissue interaction for six common suture types. *J. Biomed. Mater. Res.* **2**, 215-230 (1968).
93. Gassner, R. Wound closure materials. *Oral Maxillofac. Surg. Clin. North Am.* **14**, 95-104 (2002).
94. Klinge, U. *et al.* Modified mesh for hernia repair that is adapted to the physiology of the abdominal wall. *Eur. J. Surg.* **164**, 951-960 (1998).
95. Soares, B. M. *et al.* In vivo characterization of a fluoropassivated gelatin-impregnated polyester mesh for hernia repair. *J. Biomed. Mater. Res.* **32**, 293-305 (1996).
96. Francioni, G. *et al.* The use of prosthesis in abdominal and thoracic wall defect, 15 year experience: evaluation of tissue reactions and complications. *Chir Ital* **51**, 21-30 (1999).
97. Vinard, E. *et al.* Stability of performances of vascular prostheses retrospective study of 22 cases of human implanted prostheses. *J. Biomed. Mater. Res.* **22**, 633-648 (1988).
98. Riepe, G. *et al.* Long-term in vivo alterations of polyester vascular grafts in humans. *Eur. J. Vasc. Endovasc. Surg.* **13**, 540-548 (1997).
99. Tweden, K. S., Cameron, J. D., Razzouk, A. J., Holmberg, W. R. & Kelly, S. J. Biocompatibility of silver-modified polyester for antimicrobial protection of prosthetic valves. *J. Hear. Valve Dis* **6**, 553-561 (1997).
100. von Recum, A. F. Applications and failure modes of percutaneous devices: A review. *J. Biomed. Mater. Res.* **18**, 323-336 (1984).
101. Yan, J. Y. J., Cooke, F. W., Vaskelis, P. S. & von Recum, A. F. Titanium-coated dacron® velour: A study of interfacial connective tissue formation. *J. Biomed. Mater. Res.* **23**, 171-189 (1989).
102. Lambooi, E., De Groot, P. H. S., Molenbeek, R. F. & Gruys, E. Subcutaneous tissue reaction to polyethylene terephthalate-covered electronic identification transponders in pigs. *Vet. Q.* **14**, 145-7 (1992).
103. Al Meslmani, B. M., Mahmoud, G. F., Sommer, F. O., Lohoff, M. D. & Bakowsky, U. Multifunctional network-structured film coating for woven and knitted polyethylene terephthalate against cardiovascular graft-associated infections. *Int. J. Pharm.* **485**, 270-276 (2015).
104. Rodrigues, L. R. 351-367 *Springer, Dordrecht*. (2011).
105. Geim, A. K. Graphene: Status and prospects. *Science* **324**, 1530-1534 (2009).
106. Bhuyan, M. S. A., Uddin, M. N., Bipasha, F. A., Islam, M. M. & Hossain, S. S. A Review of Functionalized Graphene properties and its application. *Int. J. Innov. Sci. Res.* **17**, 303-315 (2015).
107. Scaffaro, R., Botta, L., Maio, A., Mistretta, M. & La Mantia, F. Effect of Graphene Nanoplatelets on the Physical and Antimicrobial Properties of Biopolymer-Based Nanocomposites. *Materials (Basel)*. **9**, 351 (2016).
108. Mohan, V. B., Lau, K. tak, Hui, D. & Bhattacharyya, D. Graphene-based materials and their composites: A review on production, applications and product limitations. *Composites Part B: Engineering* **142**, 200-220 (2018).

109. Potts, J. R., Dreyer, D. R., Bielawski, C. W. & Ruoff, R. S. Graphene-based polymer nanocomposites. *Polymer (Guildf)*. **52**, 5-25 (2011).
110. Singh, V. *et al.* Graphene based materials: Past, present and future. *Prog. Mater. Sci.* **56**, 1178-1271 (2011).
111. Staudenmaier, L. Verfahren zur Darstellung der Graphitsäure. *Berichte der Dtsch. Chem. Gesellschaft* **31**, 1481-1487 (1898).
112. Hofmann, U. & König, E. Untersuchungen über Graphitoxyd. *Zeitschrift für Anorg. und Allg. Chemie* **234**, 311-336 (1937).
113. Hummers, W. S. & Offeman, R. E. Preparation of Graphitic Oxide. *J. Am. Chem. Soc.* **80**, 1339 (1958).
114. Marcano, D. C. *et al.* Improved Synthesis of Graphene Oxide. *ACS Nano* **4**, 4806-4814 (2010).
115. Cristina Gómez-Navarro, † *et al.* Electronic transport properties of individual chemically reduced graphene oxide sheets. *Nano Lett.* **7**, 3499-3503 (2007).
116. Kim, H., Abdala, A. A. & Macosko, C. W. Graphene/polymer nanocomposites. *Macromolecules* **43**, 6515-6530 (2010).
117. Chee, W. K., Lim, H. N., Huang, N. M. & Harrison, I. Nanocomposites of graphene/polymers: a review. *RSC Adv.* **5**, 68014-68051 (2015).
118. Silva, C. *et al.* Nanostructured Biopolymer/Few-Layer Graphene Freestanding Films with Enhanced Mechanical and Electrical Properties. *Macromol. Mater. Eng.* **303**, 1700316 (2018).
119. Zhang, H. Bin *et al.* Electrically conductive polyethylene terephthalate/graphene nanocomposites prepared by melt compounding. *Polymer (Guildf)*. **51**, 1191-1196 (2010).
120. Papageorgiou, D. G., Kinloch, I. A. & Young, R. J. Graphene/elastomer nanocomposites. *Carbon* **95**, 460-484 (2015).
121. Kim, H., Miura, Y. & Macosko, C. W. Graphene/Polyurethane Nanocomposites for Improved Gas Barrier and Electrical Conductivity. *Chem. Mater.* **22**, 3441-3450 (2010).
122. Li, D. & Xia, Y. Electrospinning of Nanofibers: Reinventing the Wheel? *Adv. Mater.* **16**, 1151-1170 (2004).
123. Ghorani, B. & Tucker, N. Fundamentals of electrospinning as a novel delivery vehicle for bioactive compounds in food nanotechnology. *Food Hydrocoll.* **51**, 227-240 (2015).
124. Silva, C. S. R. *et al.* Poly(ϵ -caprolactone) Electrospun Scaffolds Filled with Nanoparticles. Production and Optimization According to Taguchi's Methodology. *J. Macromol. Sci. Part B* **53**, 781-799 (2014).
125. Dalton, P. D. *et al.* Electrospinning and additive manufacturing: converging technologies. *Biomater. Sci.* **1**, 171-185 (2013).
126. Lu, W., Sun, J. & Jiang, X. Recent advances in electrospinning technology and biomedical applications of electrospun fibers. *J. Mater. Chem. B* **2**, 2369 (2014).
127. Wang, C., Lee, M.-F. & Wu, Y.-J. Solution-Electrospun Poly(ethylene terephthalate) Fibers: Processing and Characterization. *Macromolecules* **45**, 7939-7947 (2012).
128. Holmes, B., Castro, N. J., Zhang, L. G. & Zussman, E. Electrospun fibrous scaffolds for bone and cartilage tissue generation: recent progress and future developments. *Tissue Eng. Part B. Rev.* **18**, 478-86 (2012).
129. Zhang, D. & Chang, J. Patterning of Electrospun Fibers Using Electroconductive Templates. *Adv. Mater.* **19**, 3664-3667 (2007).
130. Neves, N. M. *et al.* Patterning of polymer nanofiber meshes by electrospinning for biomedical applications. *Int. J. Nanomedicine* **2**, 433-48 (2007).
131. Imura, Y., Hogan, R. M. C. & Jaffe, M. Dry spinning of synthetic polymer fibers. *Adv. Filam. Yarn Spinn. Text. Polym.* 187-202 (2014).
132. Neves, S. C. *et al.* Chitosan/Poly(ϵ -caprolactone) blend scaffolds for cartilage repair. *Biomaterials* **32**, 1068-1079 (2011).
133. Neves, S. C. *et al.* Additive manufactured polymeric 3D scaffolds with tailored surface topography influence mesenchymal stromal cells activity. *Biofabrication* **8**, 1-15 (2016).
134. Mota, C., Puppi, D., Dinucci, D., Gazzarri, M. & Chiellini, F. Additive manufacturing of star poly(ϵ -caprolactone) wet-spun scaffolds for bone tissue engineering applications. *J. Bioact. Compat. Polym.* **28**, 320-340 (2013).

135. Leonor, I. B., Rodrigues, M. T., Gomes, M. E. & Reis, R. L. In situ functionalization of wet-spun fibre meshes for bone tissue engineering. *J. Tissue Eng. Regen. Med.* **5**, 104-111 (2011).
136. Puppi, D., Morelli, A. & Chiellini, F. Additive Manufacturing of Poly(3-hydroxybutyrate-co-3-hydroxyhexanoate)/poly(ϵ -caprolactone) Blend Scaffolds for Tissue Engineering. *Bioeng. (Basel, Switzerland)* **4**, (2017).
137. Nagy, Z. K. *et al.* Solvent-Free Melt Electrospinning for Preparation of Fast Dissolving Drug Delivery System and Comparison with Solvent-Based Electrospun and Melt Extruded Systems. *J. Pharm. Sci.* **102**, 508-517 (2013).
138. Hutmacher, D. W. & Dalton, P. D. Melt Electrospinning. *Chem. - An Asian J.* **6**, 44-56 (2011).
139. Zaiss, S., Brown, T. D., Reichert, J. C. & Berner, A. Poly(ϵ -caprolactone) Scaffolds Fabricated by Melt Electrospinning for Bone Tissue Engineering. *Mater. (Basel, Switzerland)* **9**, (2016).
140. Castilho, M. *et al.* Melt Electrowriting Allows Tailored Microstructural and Mechanical Design of Scaffolds to Advance Functional Human Myocardial Tissue Formation. *Adv. Funct. Mater.* 1803151 (2018).
141. Brown, T. D., Dalton, P. D. & Hutmacher, D. W. Direct Writing By Way of Melt Electrospinning. *Adv. Mater.* **23**, 5651-5657 (2011).
142. Khan, U., Young, K., O'Neill, A. & Coleman, J. N. High strength composite fibres from polyester filled with nanotubes and graphene. *J. Mater. Chem.* **22**, 12907 (2012).
143. Ning, F., Cong, W., Qiu, J., Wei, J. & Wang, S. Additive manufacturing of carbon fiber reinforced thermoplastic composites using fused deposition modeling. *Compos. Part B Eng.* **80**, 369-378 (2015).
144. Sayyar, S. *et al.* Extrusion Printed Graphene/Polycaprolactone/Composites for Tissue Engineering. *Mater. Sci. Forum* **773-774**, 496-502 (2013).
145. Dul, S., Fambri, L. & Pegoretti, A. Fused deposition modelling with ABS-graphene nanocomposites. *Compos. Part A Appl. Sci. Manuf.* **85**, 181-191 (2016).
146. Polschikov, S. V. *et al.* Composite materials of graphene nanoplatelets and polypropylene, prepared by in situ polymerization. *J. Appl. Polym. Sci.* **127**, 904-911 (2013).
147. 3D printers - how do they work? *3D printing* 1-23 Available at: http://3dprintingforbeginners.com/wp-content/uploads/2014/04/3D-Printing-Technology_Download.pdf. (Accessed: 31st January 2018).
148. Zhang, W. *et al.* Use of graphene as protection film in biological environments. *Sci. Rep.* **4**, 4097 (2015).
149. Chen, S. *et al.* Oxidation Resistance of Graphene-Coated Cu and Cu/Ni Alloy. *ACS Nano* **5**, 1321-1327 (2011).
150. Cho, J. *et al.* Atomic-Scale Investigation of Graphene Grown on Cu Foil and the Effects of Thermal Annealing. *ACS Nano* **5**, 3607-3613 (2011).
151. Li, J. *et al.* Antibacterial activity of large-area monolayer graphene film manipulated by charge transfer. *Sci. Rep.* **4**, 4359 (2015).
152. Xuan Wang, Linjie Zhi, * and & Müllen*, K. Transparent, Conductive Graphene Electrodes for Dye-Sensitized Solar Cells. (2007).
153. Sun, H. B., Yang, J., Zhou, Y. Z., Zhao, N. & Li, D. Preparation of reduced graphene oxide films by dip coating technique and their electrical conductivity. *Mater. Technol.* **29**, 14-20 (2014).
154. Li, D., Müller, M. B., Gilje, S., Kaner, R. B. & Wallace, G. G. Processable aqueous dispersions of graphene nanosheets. *Nat. Nanotechnol.* **3**, 101-105 (2008).
155. Scott Gilje, Song Han, Minsheng Wang, Kang L. Wang, & Richard B. Kaner*, A Chemical Route to Graphene for Device Applications. (2007).
156. Pham, V. H. *et al.* Fast and simple fabrication of a large transparent chemically-converted graphene film by spray-coating. *Carbon N. Y.* **48**, 1945-1951 (2010).

157. Dybowska-Sarapuk, Ł. *et al.* Graphene Nanolayers as a New Method for Bacterial Biofilm Prevention: Preliminary Results. *J. AOAC Int.* **100**, 900-904 (2017).
158. Becerril, H. A. *et al.* Evaluation of Solution-Processed Reduced Graphene Oxide Films as Transparent Conductors. *ACS Nano* **2**, 463-470 (2008).
159. Kim, T. I. *et al.* Antibacterial Activities of Graphene Oxide-Molybdenum Disulfide Nanocomposite Films. *ACS Appl. Mater. Interfaces* **9**, 7908-7917 (2017).
160. Kotsilkova, R. *et al.* Mechanical properties investigation of bilayer graphene/poly(methyl methacrylate) thin films at macro, micro and nanoscale. *Carbon N. Y.* **100**, 355-366 (2016).
161. Bonaccorso, F., Bartolotta, A., Coleman, J. N. & Backes, C. 2D-Crystal-Based Functional Inks. *Adv. Mater.* **28**, 6136-6166 (2016).
162. Zhao, C. *et al.* Formation of uniform reduced graphene oxide films on modified PET substrates using drop-casting method. *Particuology* **17**, 66-73 (2014).
163. Zhao, C. *et al.* Graphene oxide based coatings on nitinol for biomedical implant applications: effectively promote mammalian cell growth but kill bacteria. *RSC Adv.* **6**, 38124-38134 (2016).
164. Akhavan, O. & Ghaderi, E. Toxicity of Graphene and Graphene Oxide Nanowalls Against Bacteria. *ACS Nano* **4**, 5731-5736 (2010).
165. Besra, L. & Liu, M. A review on fundamentals and applications of electrophoretic deposition (EPD). *Prog. Mater. Sci.* **52**, 1-61 (2007).
166. Wu, Z.-S. *et al.* Field Emission of Single-Layer Graphene Films Prepared by Electrophoretic Deposition. *Adv. Mater.* **21**, 1756-1760 (2009).
167. Diba, M., Fam, D. W. H., Boccaccini, A. R. & Shaffer, M. S. P. Electrophoretic deposition of graphene-related materials: A review of the fundamentals. *Prog. Mater. Sci.* **82**, 83-117 (2016).
168. Ishikawa, R., Ko, P. J., Kurokawa, Y., Konagai, M. & Sandhu, A. Electrophoretic deposition of high quality transparent conductive graphene films on insulating glass substrates. *J. Phys. Conf. Ser.* **352**, 012003 (2012).
169. Ivanova, E. P. *et al.* Natural Bactericidal Surfaces: Mechanical Rupture of *Pseudomonas aeruginosa* Cells by Cicada Wings. *Small* **8**, 2489-2494 (2012).
170. Hasan, J., Crawford, R. J. & Ivanova, E. P. Antibacterial surfaces: The quest for a new generation of biomaterials. *Trends Biotechnol.* **31**, 295-304 (2013).
171. Pankey, G. A. & Sabath, L. D. Clinical Relevance of Bacteriostatic versus Bactericidal Mechanisms of Action in the Treatment of Gram-Positive Bacterial Infections. *Clin. Infect. Dis.* **38**, 864-870 (2004).
172. Kumar, S. & Chatterjee, K. Comprehensive Review on the Use of Graphene-Based Substrates for Regenerative Medicine and Biomedical Devices. *ACS Appl. Mater. Interfaces* **8**, 26431-26457 (2016).
173. Hegab, H. M. *et al.* The controversial antibacterial activity of graphene-based materials. *Carbon N. Y.* **105**, 362-376 (2016).
174. Lu, B. *et al.* Graphene-based composite materials beneficial to wound healing. *Nanoscale* **4**, 2978 (2012).
175. Zou, F. *et al.* Wrinkled Surface-Mediated Antibacterial Activity of Graphene Oxide Nanosheets. *ACS Appl. Mater. Interfaces* **9**, 1343-1351 (2017).
176. Pham, V. T. H. *et al.* Graphene Induces Formation of Pores That Kill Spherical and Rod-Shaped Bacteria. *ACS Nano* **9**, 8458-8467 (2015).
177. Oberdörster, G., Oberdörster, E. & Oberdörster, J. Nanotoxicology: an emerging discipline evolving from studies of ultrafine particles. *Environ. Health Perspect.* **113**, 823-39 (2005).
178. Gurunathan, S., Woong Han, J., Abdal Daye, A., Eppakayala, V. & Kim, J. Oxidative stress-mediated antibacterial activity of graphene oxide and reduced graphene oxide in *Pseudomonas aeruginosa*. *Int. J. Nanomedicine* **7**, 5901 (2012).
179. Karahan, H. E. *et al.* Graphene Materials in Antimicrobial Nanomedicine: Current Status and Future Perspectives. *Adv. Healthc. Mater.* **7**, 1701406 (2018).
180. Mazaheri, M., Akhavan, O. & Simchi, A. Flexible bactericidal graphene oxide-chitosan layers for stem cell proliferation. *Appl. Surf. Sci.* **301**, 456-462 (2014).

181. Mahmoudi, N., Ostadhosseini, F. & Simchi, A. Physicochemical and antibacterial properties of chitosan-polyvinylpyrrolidone films containing self-organized graphene oxide nanolayers. *J. Appl. Polym. Sci.* **133**, (2016).
182. An, X., Ma, H., Liu, B. & Wang, J. Graphene Oxide Reinforced Polylactic Acid/Polyurethane Antibacterial Composites. *J. Nanomater.* **2013**, 1-7 (2013).
183. Sundar, K., Harikarthick, V., Karthika, V. S. & Ravindran, A. Preparation of Chitosan-Graphene Oxide Nanocomposite and Evaluation of Its Antimicrobial Activity. *J. Bionanoscience* **8**, 207-212 (2014).
184. Hong, B., Jung, H. & Byun, H. Preparation of Polyvinylidene Fluoride Nanofiber Membrane and Its Antibacterial Characteristics with Nanosilver or Graphene Oxide. *J. Nanosci. Nanotechnol.* **13**, 6269-6274 (2013).
185. Gurunathan, S. & Kim, J.-H. Synthesis, toxicity, biocompatibility, and biomedical applications of graphene and graphene-related materials. *Int. J. Nanomedicine* **11**, 1927 (2016).
186. Papi, M. *et al.* Biomimetic antimicrobial cloak by graphene-oxide agar hydrogel. *Sci. Rep.* **6**, 12 (2016).
187. Krishnamoorthy, K., Navaneethaiyer, U., Mohan, R., Lee, J. & Kim, S.-J. Graphene oxide nanostructures modified multifunctional cotton fabrics. *Appl. Nanosci.* **2**, 119-126 (2012).
188. Thampi, S., Nandkumar, A. M., Muthuvijayan, V. & Parameswaran, R. Differential Adhesive and Bioactive Properties of the Polymeric Surface Coated with Graphene Oxide Thin Film. *ACS Appl. Mater. Interfaces* **9**, 4498-4508 (2017).
189. Pinto, A. M. *et al.* Biocompatibility of poly(lactic acid) with incorporated graphene-based materials. *Colloids Surfaces B Biointerfaces* **104**, 229-238 (2013).
190. Sayyar, S., Murray, E., Thompson, B. C., Gambhir, S. & Officer, D. L. Covalently linked biocompatible graphene/polycaprolactone composites for tissue engineering. *Carbon* (2013).
191. Wang, S.-D., Ma, Q., Wang, K. & Chen, H.-W. Improving Antibacterial Activity and Biocompatibility of Bioinspired Electrospinning Silk Fibroin Nanofibers Modified by Graphene Oxide. *ACS Omega* **3**, 406-413 (2018).
192. Jalaja, K., Sreehari, V. S., Kumar, P. R. A. & Nirmala, R. J. Graphene oxide decorated electrospun gelatin nanofibers: Fabrication, properties and applications. *Mater. Sci. Eng. C* **64**, 11-19 (2016).
193. Zhang, B., Wei, P., Zhou, Z. & Wei, T. Interactions of graphene with mammalian cells: Molecular mechanisms and biomedical insights. *Adv. Drug Deliv. Rev.* **105**, 145-162 (2016).
194. Pinto, A. M., Cabral, J., Tanaka, D. A. P., Mendes, A. M. & Magalhães, F. D. Effect of incorporation of graphene oxide and graphene nanoplatelets on mechanical and gas permeability properties of poly(lactic acid) films. *Polym. Int.* **62**, 33-40 (2013).
195. Stobinski, L. *et al.* Graphene oxide and reduced graphene oxide studied by the XRD, TEM and electron spectroscopy methods. *J. Electron Spectros. Relat. Phenomena* **195**, 145-154 (2014).
196. Geng, Y., Wang, S. J. & Kim, J.-K. Preparation of graphite nanoplatelets and graphene sheets. *J. Colloid Interface Sci.* **336**, 592-598 (2009).
197. Dreyer, D. R., Park, S., Bielawski, C. W. & Ruoff, R. S. The chemistry of graphene oxide. *Chem. Soc. Rev.* **39**, 228-240 (2010).
198. Dinescu, S. *et al.* In vitro cytocompatibility evaluation of chitosan/graphene oxide 3D scaffold composites designed for bone tissue engineering. *Biomed. Mater. Eng.* **24**, 2249-56 (2014).
199. Xu, L.-C. & Siedlecki, C. A. Effects of Plasma Proteins on Staphylococcus epidermidis RP62A Adhesion and Interaction with Platelets on Polyurethane Biomaterial Surfaces. *J. Biomater. Nanobiotechnol.* **3**, 487-498 (2012).
200. Kenry, K., Loh, K. P. & Lim, C. T. Molecular interactions of graphene oxide with human blood plasma proteins. *Nanoscale* **8**, 9425-9441 (2016).
201. Yoon, O. J. *et al.* Nanocomposite nanofibers of poly(D, L-lactic-co-glycolic acid) and graphene oxide nanosheets. *Compos. Part A Appl. Sci. Manuf.* **42**, 1978-1984 (2011).
202. Shen, X., Lin, X., Yousefi, N., Jia, J. & Kim, J.-K. Wrinkling in graphene sheets and graphene oxide papers. *Carbon N. Y.* **66**, 84-92 (2014).

203. Cao, Z. *et al.* Reversibly Switching the Function of a Surface between Attacking and Defending against Bacteria. *Angew. Chemie Int. Ed.* **51**, 2602-2605 (2012).
204. Scaffaro, R. *et al.* Electrospun PCL/GO-g-PEG structures: Processing-morphology-properties relationships. *Compos. Part A Appl. Sci. Manuf.* **92**, 97-107 (2017).

Annexes

Table 8. XPS analysis: effects on the oxidation degree of graphene oxide caused by TFA and TFA+DCM (1:2), unusually found as chosen solvents for GO dispersion.

	<i>Control</i>	<i>Effects of the acid (TFA) alone</i>		<i>Effects of TFA+DCM</i>	
ELEMENT	GO in water	GO in TFA	GO in TFA (10 days exposure)	GO in TFA+DCM	GO in TFA+DCM (10 days exposure)
C 1s	70.6	68.5	76.3	67.8	72.8
O 1s	28.7	30.0	20.4	30.0	22.5
N 1s	-	-	-	1.0	0.7
F 1s	-	0.6	3.2	0.8	1.1
S 2p	0.6	0.9	-	0.5	2.9

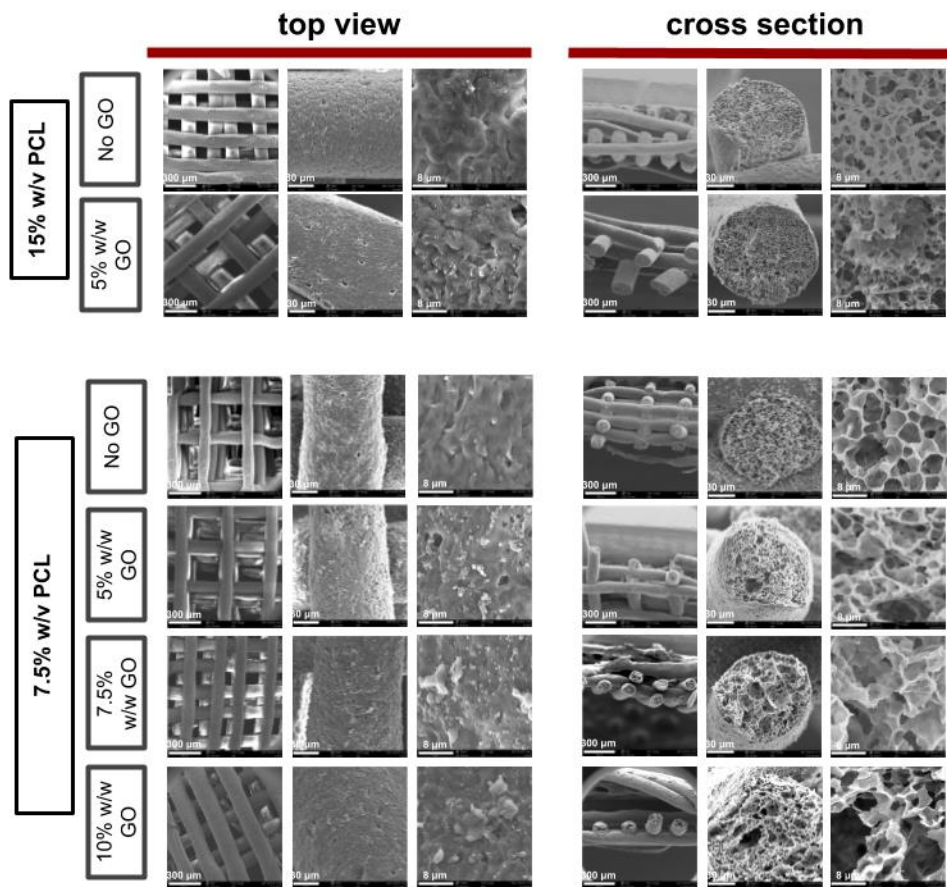


Figure 38. Detailed top and cross section views of different produced materials. GO exposure is visible in all cases (top view, last column - scale bar: 8 μm). Effects in porosity are observed for all concentrations (cross section, last column - scale bar: 8 μm).

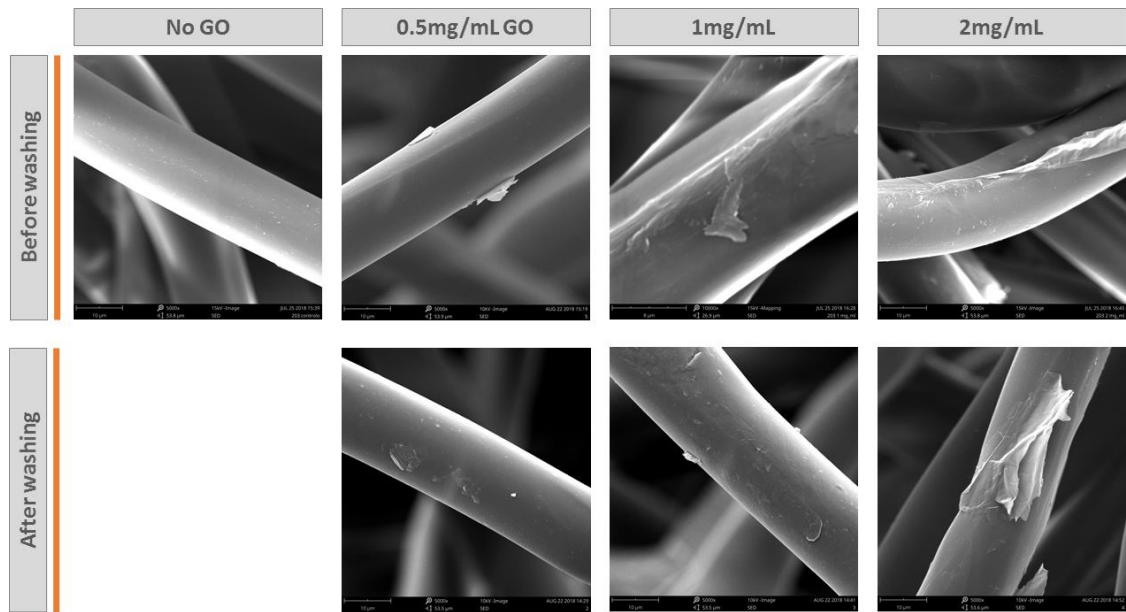


Figure 39. SEM images of PET203 control and GO in water-coated (0.5 mg/mL-2 mg/mL) fibers before and after washing. Scale bar: 10 μ m.

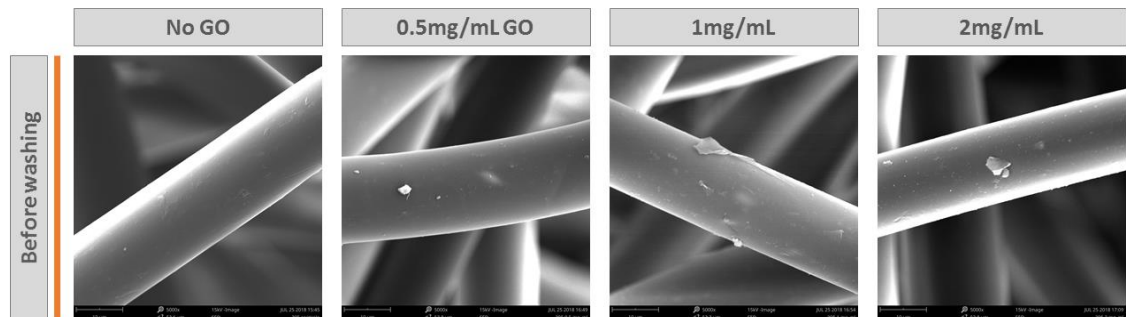


Figure 40. SEM images of PET305 control and GO in water-coated fibers before washing. Scale bar: 10 μ m.